Investigating a Perceptual Approach for Optimizing Geometric Distortions of Progressive Addition Lenses

Dissertation

der Mathematisch-Naturwissenschaftlichen Fakultät

der Eberhard Karls Universität Tübingen

zur Erlangung des Grades eines

Doktors der Naturwissenschaften

(Dr. rer. nat.)

vorgelegt von

Yannick Sauer

aus Aalen

Tübingen

2024

Gedruckt mit Genehmigung der Mathematisch-Naturwissenschaftlichen Fakultät der Eberhard Karls Universität Tübingen.

Tag der mündlichen Qualifikation:	04.07.2025
Dekan:	Prof. Dr. Thilo Stehle
1. Berichterstatter/-in:	Prof. Dr. Siegfried Wahl
2. Berichterstatter/-in:	Prof. Dr. Volker Franz

Acknowledgments

First and foremost, I would like to express my deep gratitude for the support of my supervisors, Siegfried Wahl and Felix Wichmann. I am very thankful for their continuous guidance and reassurance, which was invaluable for the completion of this thesis. Their mentorship has been indispensable, not only for my research but also for my personal development.

I am grateful to my collaborators and co-authors, Katharina Rifai, Markus Lappe, Malte Scherf, and Niklas Stein. Our collaborative work was an essential part of my research. I enjoyed our extensive scientific discussions and could learn a lot from all of them. After working together only online for an extended period, meeting in person and presenting our research together was an unforgettable experience.

Furthermore, I would like to express my gratitude to my collaborator from the University of Tübingen, David-Elias Künstle. I have not encountered any other researcher with whom our work was so wonderfully complementary and enjoyable. It was a pleasure working with him.

Special thanks to the optics design team of Carl Zeiss Vision GmbH for supporting me with optical design data that I could use for the simulation and analysis of my research.

Lastly, I would like to thank all my colleagues at the ZEISS Vision Science Lab who have supported me throughout this time. Our shared experience and mutual support have made this journey more enjoyable and rewarding. It makes me happy to have found friends for life.

Despite this irreplaceable support from colleagues and collaborators, this thesis would not have been possible without the continuous encouragement of my friends and family. I am deeply thankful for everyone who accompanied me during the ups and downs of the last few years.

Contents

Abstract

Presbyopia is the age-related decrease in the eye's capability to focus close objects. Everyone is affected by this process, with most people experiencing their first problems with blurry near vision in their forties. Presbyopes often wear glasses with Progressive Addition Lenses (PALs) that enable clear vision at multiple distances through a gradual change of optical power throughout the lens. This gradient in power inevitably leads to optical aberrations: geometric distortions impact visual perception by unevenly magnifying and curving the wearer's image of the environment. Especially during dynamic situations, distortions cause unnatural and uncomfortable perception of the environment. This so-called "swim effect" is not well understood. To improve new spectacle lenses for reduced discomfort, it is necessary to study the relationship between perception and the shape or strength of distortions. This thesis investigates approaches for objectively quantifying the perceptual effects of distortions during natural behavior. A key focus lies in employing a distortion simulation for psychophysical experiments and mathematical modeling.

In the first study, I present results demonstrating that the visual system can adapt to distortions, even when these geometric distortions vary across the visual field, as seen with PALs. However, the perceived distortion pattern of spectacle lenses is not fixed, since eye movements constantly change the part of the lens through which the gaze is directed. The second study tested how perception changes with different viewing directions. We used a model for heading estimation from optic flow (the motion vector field perceived during self-motion), to estimate the influence of distortions and gaze direction. The model estimation was validated in a psychophysical experiment using a virtual simulation of PAL distortions.

To extend the analysis to a broader spectrum of perceptual effects, the thesis concludes with a virtual reality experiment testing distortion perception during free behavior in a natural environment. Using a triplet paradigm with ordinal embedding we derived psychophysical scaling functions, which objectively quantify the relationship between perception and tested distortions.

The investigated methods introduce a new, perception-oriented, approach for im-

proving distortions of optical imaging systems. Simulating optical aberrations for applying psychophysical paradigms is a key concept for future research and development, with potential applications beyond spectacle lenses.

Zusammenfassung

Als Teil des natürlichen Alterungsprozesses des Auges wird das Fokussieren naher Objekte mit zunehmendem Alter schwieriger. Jeder ist von dieser Alterssichtigkeit (Presbyopie) betroffen, wobei die ersten Probleme von unscharfer Sicht in der Nähe in unseren Vierzigern auftreten. Viele alterssichtige Menschen tragen Gleitsichtbrillen, die scharfes Sehen in unterschiedlichen Entfernungen ermöglichen. Dies wird durch eine allmähliche Zunahme der optischen Brechkraft zum unteren Teil der Linse erreicht. Eine solche Änderung der Brechkraft führt jedoch zu optischen Aberrationen: Geometrische Verzeichnungen beeinträchtigen die visuelle Wahrnehmung des Brillenträgers durch ungleichmäßige Vergrößerung und Krümmung des Bildes. Besonders während dynamischer Situationen führt dies zu einem unnatürlichen und unangenehmen Seheindruck. Dieser sogenannte “Swim Effect” ist nicht ausreichend verstanden. Die Optimierung neuer Brillengläser hin zu einem weniger unangenehmen Seheindruck erfordert es, den Zusammenhang zwischen Wahrnehmung und dem Verlauf der Verzeichnungen im Brillenglas zu untersuchen. Diese Thesis befasst sich mit Ansätzen der objektiven Quantifizierung der durch Verzeichnungen hervorgerufenen perzeptuellen Effekte während natürlichen Verhaltens. Ein Fokus liegt dabei auf der Anwendung einer Verzeichnungssimulation, sowohl für psychophysische Experimente als auch für mathematische Modellierung.

In der ersten Studie präsentiere ich Ergebnisse, die die Fähigkeit unseres visuellen Systems zur Adaptation an Verzeichnungen zeigen, selbst wenn diese, wie bei Gleitsichtbrillen, räumlich variieren. Brillenträger nehmen jedoch nicht ein konstantes Verzeichnungsmuster wahr, da Augenbewegungen die Verzeichnungen ständig innerhalb des visuellen Feldes verschieben. Die zweite Studie untersuchte, wie sich diese Unterschiede in der Blickrichtung auf die Wahrnehmung von Eigenbewegung ausüben. Durch ein Modell, das die wahrgenommene Bewegungsrichtung anhand des optischen Flusses schätzt, simulierten wir zunächst den Einfluss von Verzeichnungen und Blickrichtung. Anschließend wurde die Modellschätzung in einem psychophysische Experiment mit einer Verzeichnungssimulation in Virtual Reality validiert.

Um die Untersuchung auf ein breiteres Spektrum möglicher perzeptueller Effekte zu

erweitern, erlaubte die dritte Studie den Versuchsteilnehmern freies Verhalten in einer realistischen virtuellen Umgebung. Die Verwendung eines Triplet-Paradigmas und Anwendung von ordinaler Einbettung erlaubte die Schätzung einer psychophysischen Skalierungsfunktion, die die relative wahrgenommene Verzeichnung in Relation zu den getesteten Verzeichnungsstimuli quantifiziert.

Die untersuchten Methoden ermöglichen einen neuen, auf die Wahrnehmung ausgerichteten Ansatz der Optimierung optischer Abbildungssysteme. Dabei ist die virtuelle Simulation optischer Aberrationen zur Anwendung psychophysischer Methoden ein zentrales Konzept für zukünftige Forschung und Entwicklung, mit möglichen Anwendungen auch außerhalb von Brillengläsern.

Abbreviations

3D	three-dimensional
Add	addition power (near correction)
AR	augmented reality
FOE	focus of expansion
FoV	field of view
HMD	head-mounted display
PAL	progressive addition lens
PSE	point of subjective equality
Sph	spherical power (far correction)
VR	virtual reality

List of publications

The main results of this thesis are based on the research presented in the following publications:

Sauer, Y., Wahl, S., Rifai, K. (2020). Parallel adaptation to spatially distinct distortions. Frontiers in Psychology, 11, 544867.

Sauer, Y., Scherff, M., Lappe, M., Rifai, K., Stein, N., Wahl, S. (2022). Self-motion illusions from distorted optic flow in multifocal glasses. Iscience, 25(1).

Sauer, Y., Künstle, D. E., Wichmann, F., Wahl, S. (2024). An objective measurement approach to quantify the perceived distortions of spectacle lenses. Scientific Reports, 14(1), 3967.

Other publications

The work for the following publications was performed during my time as doctoral student, but the studies are not directly connected to the objectives of this thesis:

Sauer, Y., Sipatchin, A., Wahl, S., García García, M. (2022). Assessment of consumer VR-headsets' objective and subjective field of view (FoV) and its feasibility for visual field testing. Virtual Reality, 26(3), 1089-1101.

Sauer, Y., Wahl, S., Habtegiorgis, S. W. (2022). Realtime blur simulation of varifocal spectacle lenses in virtual reality. In SIGGRAPH Asia 2022 Technical Communications (pp. 1-4).

Conference contributions

Sauer, Y., Wahl, S., Rifai, K. (2019). Simultaneous retinotopic adaptation to opposing distortions [Poster presentation]. ECVP, Leuven (Belgium).

Sauer, Y., Wahl, S., Rifai K. (2020). Interocular transfer of distortion adaptation [Poster presentation]. VSS, Virtual meeting.

Sauer, Y., Scherff, M., Lappe, M., Wahl, S., Rifai, K. (2020). Misestimations in heading from distorted optic flow in a VR-based optics simulation of a progressive addition lens [Poster presentation]. MueTueZue, Tuebingen (Germany).

Sauer, Y., Wahl, S., Rifai, K. (2021). Spatiotopic skew distortion adaptation with simultaneously present opposing stimuli [Poster presentation]. VSS, Virtual meeting.

Sauer, Y., Scherff, M., Stein, N., Habtegiorgis, S. W., Lappe, M., Wahl, S. (2022). Inconsistent self-motion perception between hemifields from optic flow distorted by progressive addition lenses [Poster presentation]. VSS, St. Pete Beach (Florida, USA)

Sauer, Y., Künstle, D. E., Wichmann, F. A., Wahl, S. (2023). Psychophysical scale of optical distortions of multifocal spectacle lenses [Poster presentation]. VSS, St. Pete Beach (Florida, USA)

Other contributions

Publications

Essig, P., **Sauer, Y.**, Wahl, S. (2021). Contrast sensitivity testing in healthy and blurred vision conditions using a novel optokinetic nystagmus live-detection method. Translational Vision Science & Technology, 10(12), 12-12.

Essig, P., **Sauer, Y.**, Wahl, S. (2021). OKN-onset is influenced by the contrast level of a visual stimulus. Investigative Ophthalmology & Visual Science, 62(8), 3330-3330.

Neumann, A., Leube, A., Nabawi, N., **Sauer, Y.**, Essig, P., Breher, K., Wahl, S. (2022). Short-Term Peripheral Contrast Reduction Affects Central Chromatic and Achromatic Contrast Sensitivity. Photonics 2022, 9, 123.

Essig, P., **Sauer, Y.**, Wahl, S. (2022). Reflexive Saccades Used for Objective and Automated Measurements of Contrast Sensitivity in Selected Areas of Visual Field. Translational Vision Science & Technology, 11(5), 29-29.

Sipatchin, A., García García, M., **Sauer, Y.**, Wahl, S. (2022). Application of Spatial Cues and Optical Distortions as Augmentations during Virtual Reality (VR) Gaming: The Multifaceted Effects of Assistance for Eccentric Viewing Training. International Journal of Environmental Research and Public Health 2022, 19(15): 9571.

García García, M., **Sauer, Y.**, Watson, T., Wahl, S. (2024). Virtual reality (VR) as a testing bench for consumer optical solutions: A machine learning approach (GBR) to visual comfort under simulated progressive addition lenses (PALS) distortions. Virtual Reality, 28(1), 36.

Conference contribution

Scherff, M., **Sauer, Y.**, Lappe, M., Rifai, K., Stein, N., Wahl, S., (2022) The effects of distorted optic flow in multifocal glasses on self-motion perception [Poster presentation]. VSS, St. Pete Beach, Florida (USA). s

Essig, P., **Sauer, Y.**, Wahl, S. (2022) The latency of reflexive saccades is influenced by contrast and correlates over the horizontal and vertical visual field plane [Poster presentation]. VSS, St. Pete Beach, Florida (USA).

Agarwala, R., Dechant, M., **Sauer, Y.**, Wahl, S. (2023). Feasibility of eye tracking to control a prototype for presbyopia correction with focus tunable lenses [Poster presentation]. Investigative Ophthalmology & Visual Science, 64(8), 2503-2503.

Contributions

Individual contributions of all authors for the three main publications:

> Sauer, Y., Wahl, S., Rifai, K. (2020). Parallel adaptation to spatially distinct distortions. Frontiers in Psychology, 11, 544867.

All authors contributed to the conceptualization of the study and helped with defining the methodology. Implementation and conduction of the experiment as well as data analysis was performed by myself. Results were interpreted by all authors. I wrote a first draft of the manuscript, which was improved and finalized by all authors.

> Sauer, Y., Scherff, M., Lappe, M., Rifai, K., Stein, N., Wahl, S. (2022). Self-motion illusions from distorted optic flow in multifocal glasses. Iscience, 25(1).

Malte Scherff, Markus Lappe, Katharina Rifai, and I contributed to the conceptualization of the study. The methodology was discussed between all authors. After initial simulations performed by Malte Scherff, I implemented the experiment and performed the measurements. Further optic flow simulations, data analysis as well as writing the original manuscript draft were performed by Malte Scherff and myself. All authors contributed to reviewing and editing the manuscript.

> Sauer, Y., Künstle, D. E., Wichmann, F. A., Wahl, S. (2023). An objective measurement approach to quantify the perceived distortions of spectacle lenses. Scientific Reports, 14(1), 3967.

All authors contributed to the conceptualization of the study. I implemented an initial version of the VR experiment and, in collaboration with David-Elias Künstle, conducted preliminary testing before finalizing the implementation and experimental procedure. The experiment was conducted by me. Subsequently, David-Elias Künstle and I performed the data analysis. The interpretation of results and further analysis were deliberated among all authors. I wrote the initial manuscript draft together with David-Elias Künstle. All authors contributed to reviewing and editing the manuscript.

1. Introduction

1.1. Progressive addition lenses

1.1.1. Optical correction of presbyopia

A fundamental part of our visual perception is to naturally adjust focus when looking at objects at different distances. This process requires an optical system that can dynamically change its optical power. The human eye achieves this process, called accommodation, by changing the shape of the crystalline lens [1, 2].

Unfortunately, this physiological functionality declines with age. While children can focus on objects closer than $10\,\mathrm{cm}$, starting in early adulthood, the accommodative capabilities continuously decrease, until it is not sufficient to focus comfortably on close objects [3]. Most adults experience blurry near vision for the first time in their early to mid-forties, when the accommodative functionality becomes too low for typical reading distance [4]. This condition is called Presbyopia, which translates to “old eye”. The aging of society in combination with increased life expectancy will lead to a growth of the number of presbyopes in the next decades, with more than two billion expected worldwide by the year 2030 [5].

The exact functionality of the accommodative system and the reason for its strong decline have been a matter of research for centuries. Thomas Young was able to show that the eye’s focusing mechanism was not based on changes in the cornea curvature or length of the eye, but on the changes in the shape of the lens [6]. To focus on close objects, the ciliary muscle, which is located around the lens, contracts. This allows the lens to assume a more curved shape, which refracts incoming light more and focuses the image on the retina [7, 4, 2]. Two different contributions have been considered for influencing the functional regression leading to presbyopia: stiffening of the lens, and decline of the ciliary muscle. Current research suggests that mainly lens stiffening is responsible for the loss of accommodation [8, 2, 9], which leads to a mismatch between the lens curvature and object distance causing blurry close vision.

For the treatment of presbyopia, near vision can be corrected by helping the eye

with additional optical power. A spectacle lens with a convex shape refracts the light before it reaches the eye and helps to focus the image on the retina. First versions of such reading glasses existed as early as the 13th century [10] and are still widely used today but only work for close distances. Many presbyopes need two different spectacle lenses, correcting either far or near vision, which requires constant switching between glasses. Efforts to solve this problem started in the 19th century.

Benjamin Franklin is often credited with inventing bifocals, spectacles that combine two lenses with different optical powers in a single frame for both near and far correction [11]. Franklin's approach was to cut the different lenses for far and near correction in half and place them into one frame, as illustrated in Fig. 1.1A.

Glasses with a similar principle are still used today. However, the near area is not a half-lens anymore, but a dedicated region in the far correcting lens that is carved to achieve an increased surface curvature (Fig. 1.1B). The main disadvantage remains: a visible edge between the two lens areas causes a discontinuity in vision which can be distracting for the wearer and is considered by many as unesthetic.

In 1907, Owen Awes patented the concept of building one lens that gradually changes its correcting power [12]. Those so-called progressive addition lenses (PALs) still follow the idea of far correction in the upper and near correction in the lower part of the lens. In between, as illustrated in Fig. 1.1C, the lens has a gradual increase of surface curvature towards the bottom of the lens, where the light has to be refracted more for focusing close objects [13, 14]. The progression in power removes the disturbing edge known from bifocals and allows better vision at intermediate distances when looking through the middle area of the lens. Consequently, presbyopes usually prefer PALs in a direct comparison [15]. In Germany, PALs have largely replaced bifocals as the standard multifocal spectacle lens [16].

1.1.2. Minkwitz theorem

In 1963, Minkwitz proved that a change in the surface curvature of a lens, which is necessary for the progressive increase in optical power, leads to an increase of astigmatic aberrations in the lateral areas of the lens [17]. This mathematical property limits the optical performance of a progressive lens, independent of all possible advances in optical designs and manufacturing techniques. An increase in optical power will always lead to aberrations, which are responsible for blurry regions in the periphery of the lens. A graphical illustration of the *Minkwitz theorem* is shown in Fig. 1.2.

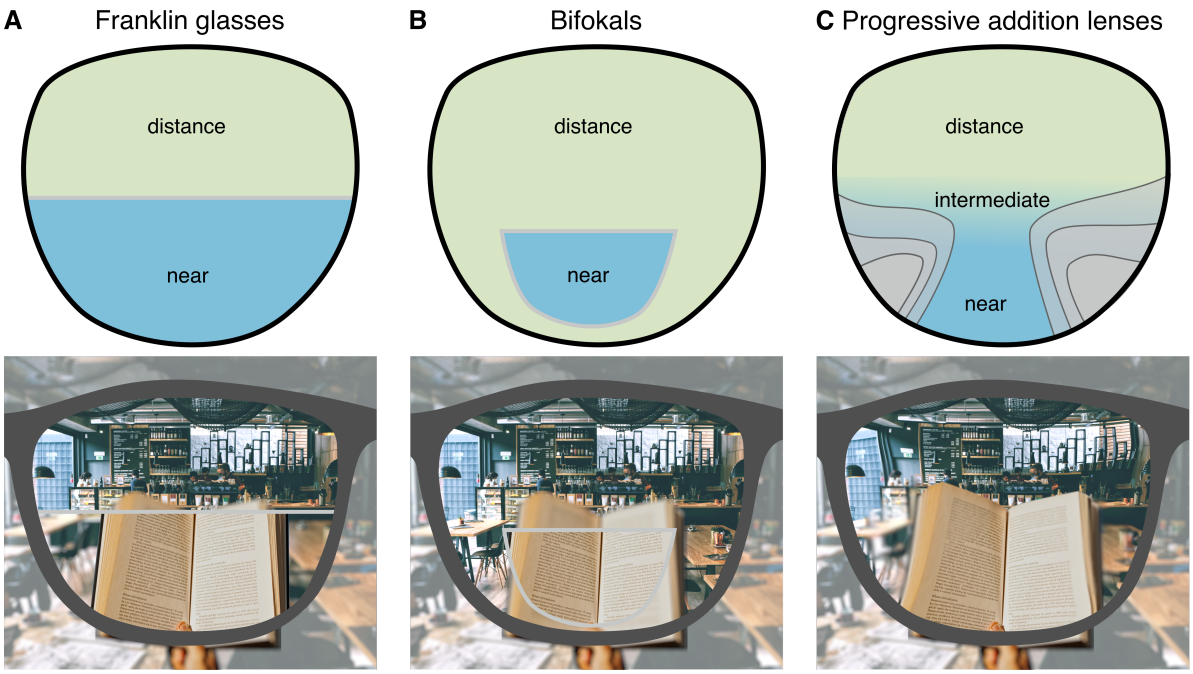

Figure 1.1.: Progress of the design of multifocal spectacle lenses

A The Franklin glasses are an early example of bifocals, where two different lenses with different curvature are cut in half and put together in one frame.

B For bifocals still often worn today, near vision is possible through a small area of increased curvature, that is carved directly into the lens for far correction. Around the near area, there is a visible edge that distracts the wearer and causes an aesthetic flaw.

C Progressive addition lenses have a gradual change in curvature which allows correction also for intermediate distances without a hard transition between areas for different viewing. The disadvantage of progressive lenses is unavoidable optical aberrations, causing blur in the periphery (illustrated as gray areas) and geometric distortions.

Advances in the manufacturing process, like freeform technology [18], allow for improved designs of the lens' surface profile, which are advertised for different use cases or preferences [19, 20, 21]. This does not overturn the fact that optical aberrations can only be redistributed in the lens, and can never be fully removed. It is mainly the aberration-free size of the far or near area, and the length or width of the progression area, which changes between designs and manufacturers [22, 19]. Presbyopes can choose designs that prioritize either far, intermediate, or near viewing. Research has shown that presbyopes exhibit different behaviors in their coordination of head and eye movements, which lead to the design of more individualized or specialized lenses

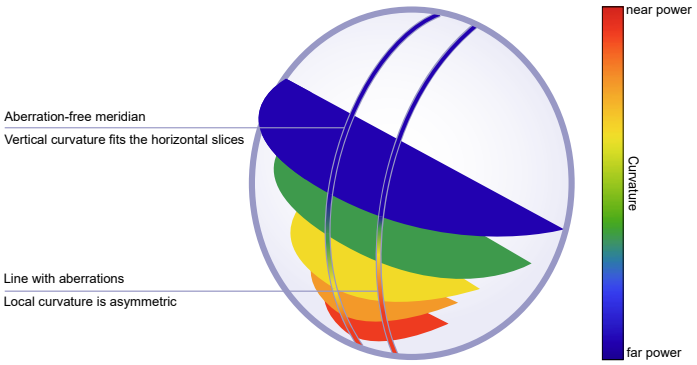

Figure 1.2.: Graphical illustration of the Minkwitz theorem
In this illustration of an idealized progressive addition lens, the horizontal slices of varying color show how the curvature of the lens would need to change from the upper to the lower part. For correcting near vision, more refractive power is necessary, requiring a higher surface curvature in the lower part of the lens. For points along the central vertical surface line shown in the figure, the local curvature can be symmetric, i.e. the same in the horizontal and vertical directions. However, when moving away from this line, the local curvature has to be asymmetric to connect the slices (illustrated by the second vertical line), which is the cause of optical aberrations. This property was formally proven by Minkwitz, who described the lateral astigmatism depending on the change of power.

for reducing blur in areas relevant to the specific use case [23, 21].

Apart from blurry vision, the optical aberrations of PALs additionally cause geometric distortions: an uneven magnification and deformation of the perceived image. Compared to the perceptual influence of blur, much less is known about the impact of distortions on visual comfort.

1.1.3. Geometric distortions and the swim effect

The complex optical properties of PALs cause a complex distortion pattern that stretches and curves parts of the wearer's visual field. Other optical devices, including single-vision lenses for correcting only far vision, can cause distortions as well [24]. However, for PALs, the progressive change of surface curvature causes a much higher degree of distortions and other aberrations that cause discomfort for many wearers. The general shape of distortions is determined by the optical power for far and near correction. Distortions for two different example lenses with different optical powers are shown in Fig. 1.3. Different design parameters, such as the placement of far and near areas or

the strength of power progression, can influence the spatial variations in the distortion pattern [25, 24]. The unnatural perception caused by distortions is considered one of the drawbacks of PALs. To improve future PALs for reduced distortions we need to understand the perceptual effects caused by them and how they relate to the optical design of the lenses.

The negative impact of PAL distortions is usually referred to as the *swim effect*, a vaguely described perceptual effect that causes an unnatural perception of the environment [13], even causing nausea for some PAL wearers [26]. Especially dynamic situations, either head or eye movements or a combination of both, seem to lead to unnatural percepts that cause discomfort and instability. A considerable number of presbyopes have problems with tripping while wearing PALs [27, 28]. Especially for the older population, falling has a high threat of injury and mortality [29]. Decreased stability during walking caused by the swim effect increases the likeliness of falling [30]. Some wearers cannot adapt to the distorted perception and reject PALs entirely [31]. Results from questionnaire-based studies of PAL wearer satisfaction can be taken as indications of possible effects: wearers perceive “distorted images during motion” or “feelings of sway” [32]. Another study reported “experience of distorted movement of objects while driving” [33]. Apart from those reports, a scientifically accurate description of the effect is missing, making it hard to predict or quantify the influence on perception when developing a new spectacle lens. First, an objective description of the perceptual impact of distortions is necessary.

Optical aberrations, including geometric distortions, can be simulated during the optical design process using ray tracing methods [34]. The influence of many aberrations (e.g. astigmatic and spherical aberrations) is reduced by varying the lens’ surface in an optimization procedure targeting a reduced weighted sum of local aberrations [35]. Optics designers can define the relative importance of clear vision in different parts of the lens by adjusting the local weights of aberrations, leading to PAL designs for different preferences and behaviors. For distortion, however, the lack of our understanding of the perceptual influence prevents the definition of an objective function for minimization. The global shape of distortions rather than local magnification or deformation might be important for the perception of motion and structure of the environment. Understanding and quantifying the perceptual effects would allow the lens designers to extend the design optimization process for finding lenses that are less prone to cause the swim effect.

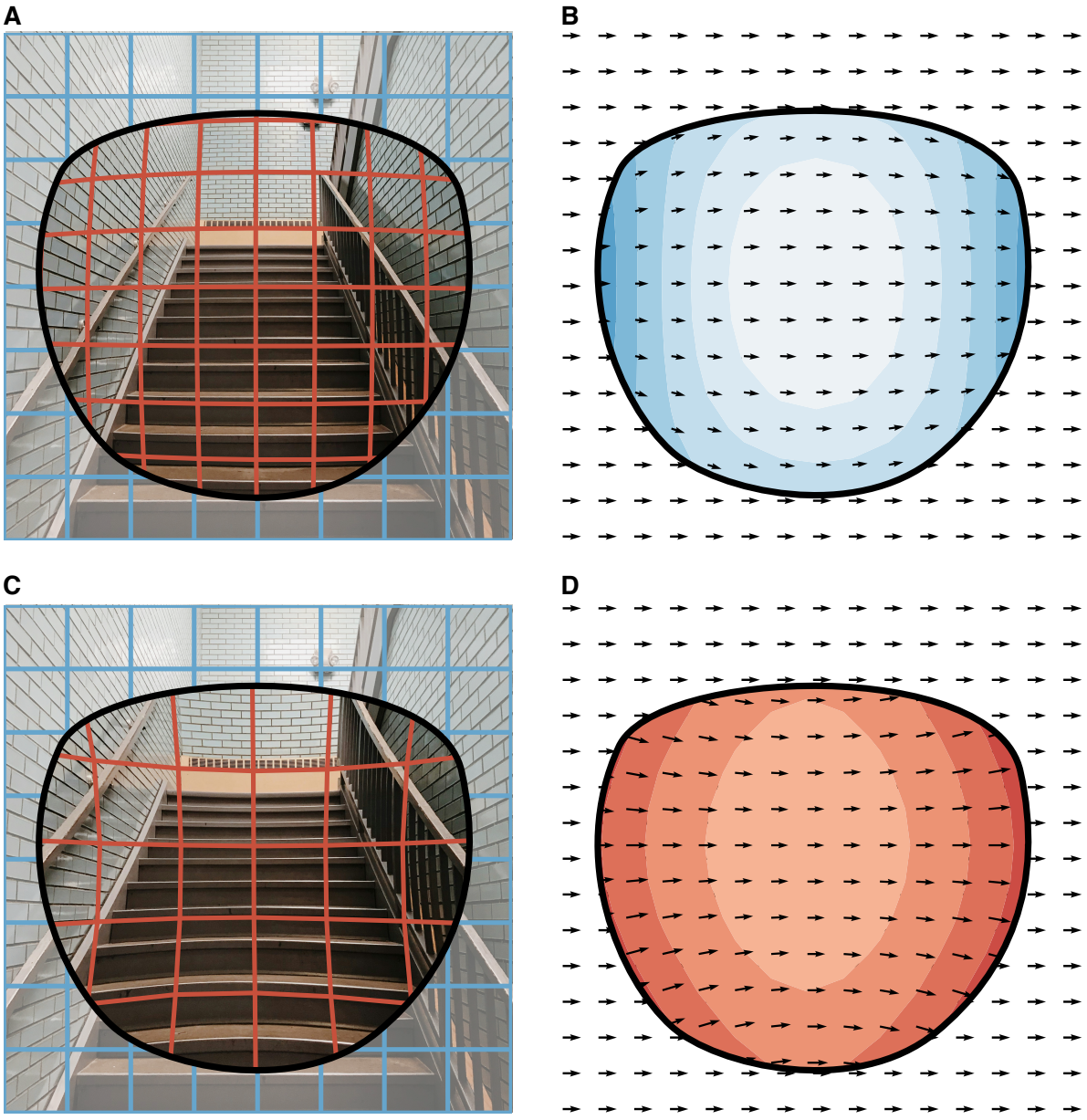

Figure 1.3.: Overview of PAL distortions

The general shape of PAL distortions is determined by the far correction power. For negative power (**A**) the image is minimized with a decrease of image size towards the periphery (barrel distortion). Positive power (**C**) leads to radially more increasing magnification (pincushion distortion). The increase in optical power breaks the symmetry of the lens. Distortions show an increase in magnification towards the lower part. Apart from changes in static features (e.g. curved lines as shown in **A** and **C**) distortions also influence motion perception. A horizontal head movement used as an illustration here causes mainly horizontal optic flow. Distortions influence the speed and direction of perceived motion, leading to curved trajectories and uneven speed distribution. The shape of curved lines as well as curved trajectories strongly depends on the power of the lens. For the negative lens, optic flow speed is slower (**B**), and for the positive lens the speed is higher (**D**)

1.2. Perceptual effects of geometric distortions

Geometric distortions change multiple visual features simultaneously. Shape, distance, size, as well as motion perception is influenced. Magnification influences perceived size and distance [36]. Skew distortions, a stretching of the image along a diagonal, influences the orientation of objects, surface slant, and motion direction [37, 38, 39]. Distortions in optical devices are usually not one spatially invariant projective transformation of the visual image, but a more complex spatially varying and gaze direction-dependent transformation, i.e. a change of magnification and skew throughout the visual field. This gradual change in the image transformation can then be perceived as bent lines and curved surfaces [40, 41]. For the perception of motion, trajectories appear curved [42]. Especially during self-motion, when the whole environment moves relative to the observer, these curved trajectories may interfere with the visual system's ability to accurately extract motion parameters and environmental structure, potentially leading to the perception of instability of the surroundings.

Combined, many perceptual influences of distortions are known. Nevertheless, there is a big step from describing individual perceptual effects measured in controlled environments to understanding the actual perception in a natural environment under natural behavior. How different effects contribute to an unnatural percept and, importantly, how perception depends on the type and amount of distortions, is not well studied.

1.2.1. Adaptation to distortions

It is important to highlight that the majority of PAL wearers adapt to the new visual perception within a few days. This means that the experience of discomfort and swim effect symptoms decreases over time [43, 26]. The human visual system is able to adjust its processing as a response to changes in the environment. Neural plasticity allows changes in the processing of sensory input [44, 45, 46]. Alterations in visual statistics lead to adaptation to optimize visual processing. This process occurs continuously and is known for many aspects of perception. For instance, changes in light levels cause a change of luminance sensitivity [47, 48], exposure to a specific color influences the perception of subsequently presented colors [49, 50], and observing a motion pattern in one direction causes the perception of opposite movement when removing the motion stimulus (motion aftereffect) [51]. When observing a curved line for an extended period, a subsequently presented straight line appears to be curved in

the opposite direction [52].

In the context of optical distortions, as multiple visual features are influenced, different forms of adaptation can occur that might be relevant for compensating for the perceptual changes introduced by PAL distortions.

Adaptation to spectacle lenses has been studied from various viewpoints already. The most prominent visual change for normal glasses is magnification, which influences motion [53] and depth perception [54]. Movements of the eyes, head, and body have to adapt to the changed relations between the perceived position and the actual position, for example during a grasping motion [55, 56]. Eye movements adapt very fast to a change of magnification [57]. Also directly on the visual level, adaptation has been shown for magnification and minimization [58, 59]. This means that both visuomotor and visual adaptation processes reduce the influence of magnification over time. Also for prismatic distortions, a uniform displacement of the whole retinal image, adaptation is known to occur in a brief timeframe [60, 61].

For PALs, adaptation is more complicated than for other spectacle lenses. Distortions are stronger and the magnification varies throughout the lens. Eye movements constantly modulate the perceived distortions. It has been hypothesized that so-called *spatiotopic* adaptation processes are involved, for which adaptation aftereffects are not bound to specific retinal locations, but occur relative to the environment or the head (craniocentric) [62]. This type of adaptation is known to occur for form and positional motion aftereffects [63, 64, 65]. For PAL distortions, spatiotopic adaptation would allow for a compensation of distortion changes with gaze, but such gaze-dependent distortion adaptation has not been shown yet. On the other hand, behavioral changes also can reduce the influence of spatially varying distortions [66], indicating that changes in the coordination of head and eye movements mitigate the influence of PAL distortions.

Combined, we know that PAL wearers usually adapt to their glasses [26, 67], but the exact mechanism and why some have more difficulties than others remains unknown. Optical distortions have an important effect on spectacle acceptance [68]. For many presbyopes, it takes multiple attempts to find a lens design that fulfills their needs and some wearers never adapt to the distortions and reject PALs [15, 31, 68]. As a consequence, it would be helpful to improve the PAL design considering the discomforting effects of distortions. However, we lack an exact understanding of the distortion effects, especially how perceptual effects depend on different lens parameters. This thesis aims to study the perceptual impact of distortions, including the role of adaptation, and to evaluate methods that could quantify these effects for a potential

application in lens design.

1.2.2. Modelling depth and motion perception

A promising approach to quantifying distortion-related perceptual effects is to model spatial perception, including motion and depth, using simulated distortions. A validated model could then predict the perceptual impact during the lens design process.

The human visual system can decode the depth and structure of the environment from the retinal disparity between the images of the two eyes [69, 70]. Optical distortions spatially transform the images, modifying the information of depth that the visual system can decode from the retinal disparity distribution. Some aspects of the unnatural perception of the environment we know from descriptions of the swim effect could be caused by the influence of distortions on depth perception. Considering the recurring change of distortions with eye movements, changes in depth information might cause the perception of an unstable environment. For modeling depth perception with distortions, we can calculate retinal disparity for defined world points by projecting 3D points for two horizontally separated simulated eyes [71]. With distortions, a spatial transformation is applied to the individual image points. Subsequently, stereo vision algorithms can be used to analyze the information of scene depth that can be retrieved from the two eyes' images [72]. This method has previously been used to model how other imaging systems influence depth perception [73]. For application to spectacle lenses, however, this approach needs to be extended to account for the gaze-dependency of distortions. This extension can then be used to quantify the impact of different lens designs and gaze behaviors on depth perception.

A possible approach to quantify the influence of distortions on motion perception could be based on the analysis of optic flow. Optic flow is the motion pattern of the retinal image caused by motion relative to the environment. This vector field contains information about the amplitude and direction of motion relative to the surroundings and about the appearance of the scene [74]. The human visual system is able to extract information from optic flow for the control of self-movement [75, 76, 77], the perception of the environmental structure and objects [78], the prevention of collision [79], and the estimation of traveled distance [80]

For a pure translational motion, optic flow consists of a radial pattern expanding from a single point in the direction of the translation, the focus of expansion (FoE). However, during natural behavior, we fixate points in the environment to check for obstacles and find adequate locations for foot placement [81, 82, 83, 84, 85], or to

adjust our gaze towards a new destination when changes on the planned path occur [86]. To stabilize the gaze on a moving fixation target, eye rotations compensate the target movement via smooth pursuit [87] or reflexive eye movements [88, 89, 90, 85]. Due to the rotation of the eye, the resulting flow structure on the retina is no longer a radial pattern but resembles a spiral with the center near the fovea [91, 92, 76]. Such patterns, while lacking retinal motion at the visual field's center, contain a large variety of motion directions at low speed in parafoveal area. The peripheral visual field, in contrast, features much higher speeds in more radially distributed directions [93]. The visual system can recover heading from such retinal flow [91, 76, 94]. PAL distortions, however, introduce alterations to the pattern that might modify the information the visual system could extract from optic flow.

So far, no one tried to predict or quantify the effect of optical distortions on optic flow perception. Some studies tried to measure the influence of only magnification on perception during self-motion by wearing magnifying glasses [53, 95]. No other distortion components have been considered. Additionally, this approach makes it challenging to study the dependence on the amount of distortions. Existing methods from computer vision for extraction of motion components, and the structure of the environment from optic flow, could be applied to predict the influence of distortions on the perception, which would result in an objective quantification distortion perception.

To model the processing of optic flow, the two-dimensional vector field can be simulated for a specific motion in a 3D environment by projecting the 3D motion relative to the observer to a 2D image plane. Different models have been used in computer vision for extracting the self-motion parameters from this vector field [96]. One model by Heeger and Jepson [97], referred to as the subspace algorithm, can compute the motion parameters in a mathematically optimum way. This is achieved by expressing the optic flow vector field as a product of two matrices, where one only contains translation information and the other the unknown rotation and depth components. The translation can be recovered first with a least squares estimate that is based on calculating residuals between the simulated optic flow and some candidate translations. The high-dimensional computational problem is reduced in complexity by first estimating the translation in a low-dimensional subspace. Subsequently, rotation and depth are estimated based on the translation flow field.

Lappe and Rauschecker suggested that this mechanism can model also human heading perception, by using the algorithm to compute a heading likelihood distribution over a simulated neuron population [98]. The method has been used successfully to test the influence of scene structure, flow vector density, and heading eccentricity on

perception in the presence of noise [96, 99] or independently moving objects [100].

The second study presented in this thesis focuses on the application of the subspace algorithm for modeling the influence of distortions on self-motion perception. We analyze the motion information in distorted optic flow for different gaze directions, giving an estimate of how perception changes for PAL wearers. Distorted optic flow fields can be simulated by transforming the position as well as the velocity of flow field vectors based on the spatial transformation given by a specific distortion. Details of the implementation are presented in Appendix B.

The application of the subspace algorithm focuses on recovering motion parameters and does not directly quantify how *unnatural* optic flow might appear regarding consistency or stability of the environment. As our analysis in chapter 3.2 will show, there are inconsistencies in the optic flow field: different parts of the visual field fit better to different physical motion parameters. This might be perceived by the visual system as an unstable, non-rigid environment. For improving lens design, it is necessary to quantify how the perception of an unnatural or unstable environment, possibly resulting from a combination of multiple perceptual effects, depends on the physical distortion parameters.

1.3. Measuring distortion appearance with machine learning algorithms

We established that optical distortions influence multiple visual features, which can cause different perceptual effects likely depending on the situation and environment. Modeling aspects of visual perception can try to explain and quantify certain visual effects of distortions. However, natural behavior and visual environments introduce many different situations in which the individual effects are combined and can depend on different optical lens parameters. How the effects in a natural environment lead to a combined sensation, and importantly, how this sensation depends on the shape and strength of lens distortions, is not clear. Additional complexity arises from the high dimensionality of distortions. The shape of PAL distortions is not only scaled by a single parameter, but the complex lens design can influence multiple independent components of the spatial transformation. Since we expect the influence of distortions on different aspects or features, also our perception might distinguish between different aspects, manifesting in different dimensions of a representation of the perceptual space. Studying complex perceptual phenomena that might include a multi-

dimensional perceptual space has recently made progress by using machine learning approaches.

There are different approaches trying to incorporate machine learning methods to predict the quality of optical imaging systems [101, 102] or directly suggest design starting points or variations [103, 104]. It seems promising to apply similar approaches also for spectacle lens design, but all the approaches so far do not try to predict human visual perception.

On the other hand, in psychophysics machine learning methods help with the efficient modeling of human visual perception. PAL distortions are a compelling area for this approach, since many different perceptual effects combined cause a perception of distortions that scales in an unknown way with the lens parameters. To map complex (multidimensional) physical stimuli to a perceptual space, a (possibly multidimensional) psychophysical *scaling function* is used [105, 106, 107]. As a mathematical function, a scaling function for PAL distortions could describe the dependence of perceptual effects on physical lens parameters, which would directly help in designing lenses with less perceived distortions, i.e. a distortion pattern that is closer to undistorted in the measured perceptual space.

Previous studies tried to find a relationship between different distortions and the resulting perceptual effects [108, 109]. The number of different distortions tested in those studies was always limited, making it impossible to derive a perceptual scaling function. More importantly, those studies used scoring methods in which participants provided a direct subjective rating for each distortion. Using this method can result in variable outcomes and is susceptible to response biases, such as central tendency and range biases [110, 111]. Other, indirect methods for deriving psychophysical scaling functions have been more successful in many areas of perceptual research. The *method of triads* is an approach that presents a triplet of stimuli to the participant for comparison [112, 113]. Answering the perceived similarity provides ordinal data of the relative distance of the stimuli in a perceptual space. Different approaches exist for obtaining a scaling function from ordinal data. Especially for higher dimensions, ordinal embedding methods from machine learning lead to better results than previous methods [113, 114]. Applying the method to distortions, covering a large range of possible PALs, requires many individual stimuli, leading to a large space of stimulus combinations. Ordinal embedding methods have been very successful in fitting an embedding with only a fraction of the complete space of stimulus combinations. Additionally, the method can be used to test for different dimensionality of perception [115]. The last study of this thesis tested how this scaling method can be applied to

the perception of distortions. Previous studies that tried to relate subjective perception depending on PAL design were not performed in a natural environment with free behavior. Either the stimulus showed distortions only as a grid while allowing motion [108], or natural stimuli in the form of real-world scenes were used [116], but no (self-)motion or stereo vision was included. Applying psychophysical scaling methods to rate distortions for natural behavior requires a complex experimental setup with a naturalistic environment, natural self-motion, and the presentation of a multidimensional distortion space. Next, I introduce the possibilities of simulating PAL distortions to meet the described requirements of a psychophysical experiment.

1.4. Simulation of optical distortions

Studying the perceptual influence of PALs is complicated by many factors. Each presbyope requires individual correction, with individual dioptric power for far and near vision. Frame and face shape will influence the fitting parameters, defining the placement of reference points inside the lens [13]. This results in an individual lens with an individual distortion pattern. Apart from distortions, other optical aberrations (mainly astigmatism and spherical error) lead to blurry parts in the lens and influence the perception and the visual comfort of the wearer. When comparing visual comfort for different PAL designs in a survey, the perception of the wearers is influenced by all aberrations, making it hard to distinguish the influence of distortions.

Furthermore, gaze and motion behavior will influence how distortions impact visual perception. Individual coordination of head, eye, and body movements determines which part of the lens the gaze is directed through and which motion pattern is perceived. Behavior can differ between different tasks or environments. Those individual differences complicate the evaluation of perception depending on the individual PAL design. A controlled experimental environment is necessary for creating reproducible distortion stimuli.

Apart from these participant-related factors, there are experimental limitations and disadvantages when measuring perception with optical lenses: psychophysical procedures for studying the dependence of perception require a change of stimulus parameter, which for optical distortions would imply changing the lenses during the experiment. This is a requirement that is hard to implement, especially with a large number of distortions. More importantly, spectacle lenses are always bound to a specific person. It's not possible to present the same distortion stimulus to all participants without

introducing individual differences in other aberrations.

To overcome the described problems, the approach I followed in the research for this thesis was to simulate optical distortions based on precalculated aberrations of real PALs.

1.4.1. Ray tracing calculations of optical distortions

Ray tracing is the simulation of the path of light rays as they interact with an optical medium [117]. For ophthalmic lenses, the ray path is calculated for passing through the spectacle lens and the eye [34]. When the ray intersects with the lens surface, the change of path direction is calculated based on the local orientation of the surface and the refraction index of the lens material, following the formula known as Snell's law [118]. The final ray direction determines under which position an object point is perceived. The deviations of this perceived direction from the actual object location are the optical distortions of the lens. The influence of gaze direction on perceived distortions can be calculated with different eye orientations by considering the position of the center of rotation of the eye relative to the spectacle lens. Other aberrations of the lens can be calculated using a bundle of rays originating from the same point, simulating not only the displacement of an object point but also the spread of rays, describing the blur of an image point.

The distortion data used for this thesis are based on ray tracing data of PAL designs provided by the manufacturer Carl Zeiss Vision. The simulations described in the next section are based on this data. I performed a comprehensive analysis of the distortions of different PALS, which is presented in Appendix C.

1.4.2. Virtual distortion simulation

A substantial part of vision research is performed with screen-based experiments, which has led to a better understanding of visual processing of distortions (e.g., [37, 62, 108]). However, a screen-based presentation of distortion stimuli lacks the complexity of a natural visual environment. Especially natural motion behavior has to be considered when studying the perception of PAL distortions. Symptoms of dizziness and nausea, which are known for the swim effect, can be caused by a sensory conflict between the visual system and the motor action or vestibular information [119]. Self-motion leads to characteristic motion patterns, which under the influence of distortions might cause a conflict with vestibular information or motor action. Therefore,

it is important to allow free and natural behavior during experiments in a naturalistic environment. Only when including those aspects instead of presenting pre-defined motion stimuli, the perception during the experiment can indicate the perception of distortions in everyday life.

Furthermore, stereo vision needs to be considered for studying distortion perception. Spatially varying magnification influences the binocular disparity throughout the visual field, which affects the perception of depth and surface curvature [120, 121]. Additionally, distortion can differ between both eyes, requiring a simulation with independent distortions for both eyes. Even if both eyes need the same corrective power, distortions differ slightly between both eyes. The near area is shifted nasally in the lens, which means that the distortions for both eyes are horizontally mirrored. For strong corrective power differences between the eyes ($>1\,\mathrm{dpt}$), magnification differs between both eyes. This condition is called aniseikonia, and symptoms of headaches, dizziness, or eye strain are well known [122, 123]. By adjusting the thickness of one lens, magnification can be approximately equalized for both eyes and symptoms can be reduced. However, lens design could be improved further by optimizing not only magnification but also other distortion components to reduce influence on binocular vision. This requires to study the perceptual influences of spatially varying distortions while considering possible differences between the eyes.

Technological and computational advances in recent years made it possible for virtual reality (VR) to meet all those requirements. Participants can explore a realistic 3D environment, changing the position and perspective of the scene based on their movements [124]. Each eye is presented with an independently rendered image, allowing realistic stereo perception. The individual eye position of the wearer is considered for the rendering [125]. Tracking systems with short delay allow natural motion in the virtual environment [126]. Computational power allows a live simulation of distortions and the presentation of individual distortions to each eye. The same defined distortion stimuli can be presented to all participants, overcoming the problem of psychophysical experiments with individual spectacle lenses.

Additionally, VR allows the recording of behavioral measures, especially head and eye movements using headset tracking and eye tracking [127]. Perception can be studied in relationship to behavior, which is relevant when trying to understand how differences in head-eye coordination or motion behavior might influence individual discomfort or severity distortion perception. Other advantages of VR include a larger field of view compared to typical screen setups. For an optical simulation, this allows the presentation of distortions to a realistic extent covering the area of typical spectacle

lenses.

In summary, VR combines multiple relevant advantages that are promising for studying the swim effect with PALs. Natural behavior and stimuli in VR minimize the lab-to-reality gap, which increases ecological validity [128, 129]. By recreating lens distortions in realistic virtual environments in which participants can move freely, the experimental results can be generalized better to the real-world context in everyday life. VR simulations offer the necessary naturalistic viewing conditions that allow the use of objective psychophysical procedures to quantify and better understand the perceptual effects related to the physical description of distortions.

For simulating optical distortions, we use a bijective mapping function as a mathematical description of how each point of the undistorted image is displaced by PAL distortions. This approach is similar to the description of camera lens distortion correction [130, 131] or the correction of VR distortions [132]. Based on distortion data at discrete points, retrieved from measurements or ray-tracing simulations, the transformation function can be approximated by fitting or interpolation to achieve a continuous representation of distortions. For the work in this thesis, the distortion function builds the basis for modeling perceived distortions, simulating distorted motion, and implementing a simulation with live rendering of distorted image frames for virtual reality. Optics simulations in VR could become an important aspect of the development of vision correction and other optical devices in the future. A method to predict perceptual effects purely based on distortion data would enable improvements to spectacle lenses by optimizing distortions during the design process.

2. Objectives

To summarize the state of research on PAL distortions at the start of this thesis: aberrations, including geometric distortions, can be calculated during the optical design process. It is well known that distortions induce various perceptual effects. However, a complete understanding of the swim effect and its relation to optical design is still lacking.

Improving PAL distortions during the design process requires investigating methods to quantify their perceptual impact. The objective of this thesis is to explore different approaches for understanding and modeling distortion perception. The focus is on dynamic, motion-related situations, with the goal of objectively quantifying the perceptual effects underlying the swim effect. This research aims to contribute to improved optical designs that offer better visual comfort and easier adaptation for wearers.

In the first study, adaptation to spatially varying distortions is tested. In contrast to simple linear geometric transformations of an adaptation stimulus, already investigated before, PAL distortions are spatially varying. The shape and strength of distortions vary throughout the lens. In this study, I assessed if the visual system can adapt individually at different retinal locations. When artificially distorting an adaptation stimulus of dynamic natural content, motion perception adapts to changes in the statistics of motion direction and speed of the stimulus. Adaptation aftereffects can be measured with a motion direction identification task. We can test the presence of parallel adaptation to spatially varying distortions by presenting two oppositely distorted stimuli simultaneously at different retinal locations.

From the motion statistics of a stimulus, i.e. the distribution of direction and speed, the visual system can extract important information. Especially during self-motion, the motion pattern in the retinal image (optic flow) is an important visual feature for navigating and estimating the structure and relative motion of the surroundings. For PAL wearers, distortions induce alterations to this motion pattern, which might describe the perceptual effects experienced during the swim effect. Simulating the influence of distortions and applying existing algorithms to analyze the changes in information content could be used as an objective quantification for perceptual distortion effects.

The goal of the second study was to develop an optic flow-based model estimation of self-motion perception. To validate the model, self-motion perception with distortions was tested in a psychophysical experiment by simulating PAL distortions in VR.

Apart from changes in the perceived direction or speed of self-motion from optic flow, we expect that an *unnatural* or unstable perception is an important contribution to the discomfort of PAL wearers. Individual descriptions of the swim effect, as well as previously examined perceptual influences of distortions, suggest that the combination of multiple effects of motion and depth perception leads to the unnatural perception reported by many PAL wearers. Potential sensory conflicts, e.g. between perceived and self-executed movement, may cause discomfort. It is unclear how the unnatural impression (the amount of *perceived distortions*) scales with the physical distortion parameters. In the third study, we investigated the quantification of distortion perception as a psychophysical scaling function. Using ordinal embedding for a triplet paradigm with simulated distortions in a naturalistic VR environment, we derived a quantification for *perceived distortions* depending on the lens parameters. The experiment was designed to include natural 3D content with dynamic vision and natural self-motion. Assessment of behavior during the experiment can be used to relate individual perception to specific behavior.

Combined, the three studies follow the approach of simulating optical distortions to study perceptual effects with psychophysical procedures. Based on the results, I will discuss the relevance for lens design and identify the necessary next steps for applying the tested methods.

3. Results and Discussion

3.1. Parallel adaptation to spatially varying distortions

This section summarizes the results published in

> Sauer, Y., Wahl, S., Rifai, K. (2020). Parallel adaptation to spatially distinct distortions. Frontiers in Psychology, 11, 544867.

Motivation

The human visual system copes with changes in the visual perception by adaptation. The processing of visual information changes in response to alterations in the statistics of visual input.

Considering that swim effect symptoms decrease for most PAL wearers over time [43, 26], existing research suggests that our visual system is able to cope with the influences of spectacle lens distortions through adaptation [133]. Complexity arises from the spatially varying nature of optical distortions. Many optical devices have radial distortions in which magnification increases towards the periphery. PALs have an asymmetry between the upper and lower visual field, especially with strong skew distortions in the lower periphery, causing motion in those areas to be altered in different ways. Previous research has shown that adaptation aftereffects are transferred to non-adapted retinal locations, i.e. locations where no adaptation stimulus was shown [37]. To reduce the influence of distortions on motion perception, the visual system would need to show different aftereffects, with opposing directions at different locations. The first study aimed to test this possibility by presenting simultaneously two adaptation stimuli, distorted in opposite directions.

Optically induced distortions simultaneously modify the statistics of multiple features, with alterations to the orientation and size of objects (static features) and motion direction and speed (motion features). Adaptation processes are well studied for

both changes of static features as well as dynamic features [37]. Interactions also exist between static and motion features, which means that a distorted static image can cause motion aftereffects [134]. Vice versa, changes in the statistics of pure motion stimuli can cause changes in the perceived orientation of static images [135]. In this study, a video of the natural environment was chosen for the stimuli, presenting changes in static as well as motion features. Adaptation aftereffects were tested with a motion direction identification task at both retinal locations.

Methods and results

To study the parallel adaptation to spatially distinct distortions, two oppositely distorted stimuli were presented on a screen while participants fixated in the center. For the adaptation stimulus, natural image sequences from an open-source movie were skew-distorted in opposite directions (Fig. 3.1A). For the same distortion stimulus, both motion and form aftereffects are known to occur [37, 136]. This study tested motion aftereffects in a motion direction identification task. A group of random dots moved coherently for $0.3\,\mathrm{s}$ diagonally upwards or downwards, randomly to the left or right (Fig. 3.1B). The angle relative to the horizontal was randomly sampled from a predefined list. Participants answered if their perceived motion direction was diagonally upwards or downwards.

The experiment comprised three phases. In the pre-adaptation phase, baseline perception was assessed. In repeated trials, the random dot test was performed consecutively at both stimulus locations, as illustrated in Fig. 3.1C. After 64 trials, the experiment continued with the adaptation phase, in which the two oppositely skew-distorted image sequences were shown simultaneously on the screen. In the last phase, adaptation aftereffects were tested, following the same procedure as the first phase. To maintain aftereffects throughout the test phase, at the beginning of each test trial, the two adaptation stimuli were presented again as so-called “top-up” adaptation for $4\,\mathrm{s}$. In the baseline phase, undistorted stimuli were used for this presentation.

Participants used a chin and forehead rest to maintain a stable position. Eye tracking was used to control for correct fixation on the target to guarantee stimulation only of the defined retinal locations.

For analysis, the participants’ answers for each experiment phase and location were fitted with a psychometric function to determine the point of subjective equality (PSE), i.e. the point where 50% of answers are in either direction. This stimulus angle can be taken as the direction perceived as horizontal. The shift of this angle between the first

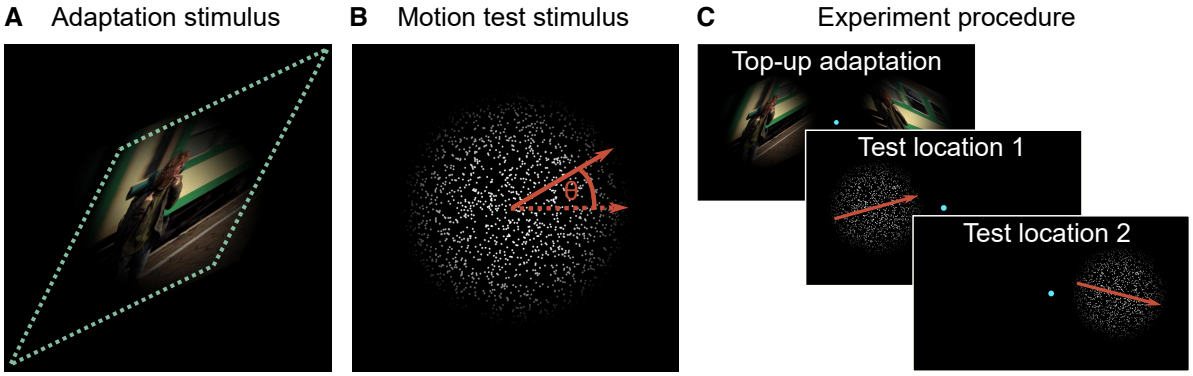

Figure 3.1.: Procedure of the adaptation experiment

A The adaptation stimulus was a skew-distorted video with natural content. Two stimuli, distorted in opposite directions, were presented simultaneously at two locations in the visual field.

B Motion direction perception was tested with a cloud of coherently moving random dots. Motion was to the left or right, with a randomly sampled angle θ relative to the horizontal.

C The experiment trials for testing baseline and post-adaptation perception included a short phase of "top-up" adaptation, followed by the consecutive motion direction test at both locations. The test order for both locations as well as stimulus angle θ were randomized between trials. For fixation, a target was presented during the entire experiment in the center of the screen.

and last phase shows the influence of adaptation. Fits for one example participant and all shifts ΔPSE are shown in Fig. 3.2. The results show a significant shift ΔPSE at both locations ($p < 0.01$), which is oppositely oriented between both locations. The change of motion direction perception was opposing the skew direction of the corresponding adaptation stimulus. This implies that participants perceived less distorted motion at both locations. The visual system can at least partially compensate for spatially varying distortions by altering the perceived motion direction depending on the retinal location.

Discussion

This experiment tested the parallel presence of motion aftereffects at two different locations in the visual field stimulated with two oppositely distorted stimuli. The results show opposing shifts of PSE at the two locations, corresponding to a change of perception *away* from the distortion direction. Perception at both locations can be

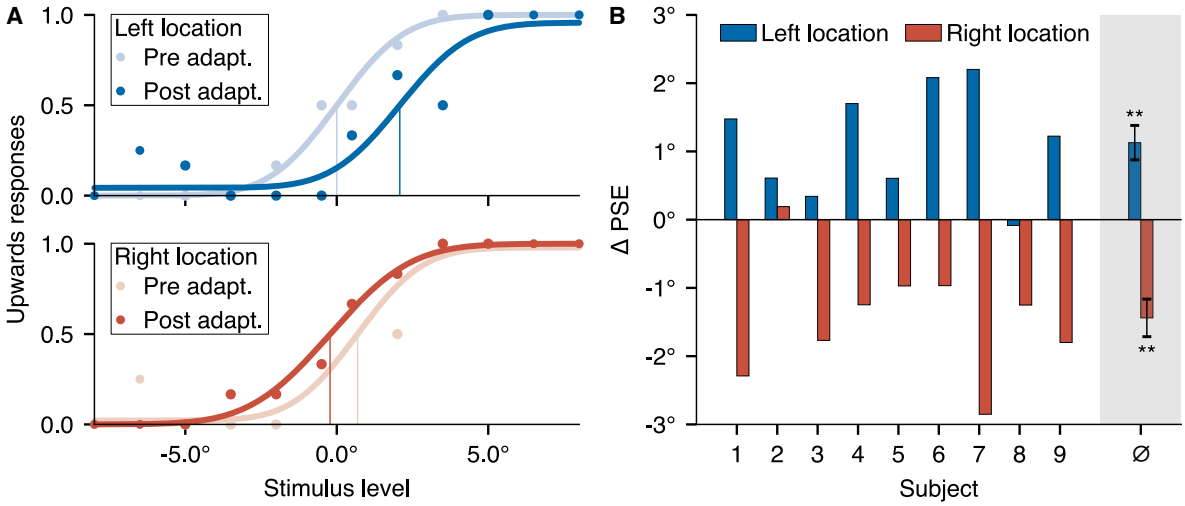

Figure 3.2.: Results of the adaptation experiment

A Example data for one participant fitted with psychometric functions for both stimulus locations before and after adaptation. The $50\,\%$ point of the fit is different between baseline and post-adaptation measurements. This shift of PSE is in opposite directions at the two stimulus locations.

B For all participants combined, there is a significant amount of motion aftereffect at both stimulus locations, measured by the shift ΔPSE. On average, the perceived motion direction shifted away from the distortion direction.

described as less distorted. This proves that the human visual system is able to adapt to multiple different distortions simultaneously. The participants' perception changed locally in the visual field depending on the distortion present at the test locations. Therefore, distortion adaptation can not only mitigate the influence of a homogeneous distortion of the whole visual field but also mitigate spatially varying distortions.

Adaptation aftereffects result from response changes of neurons tuned to attributes changed by the adaptation stimulus [46]. Adaptation to features processed in lower levels, like tilt [137] or contrast [138], shows purely retinotopic aftereffects, meaning the changes in perception are only present at the locations exposed to the adapting stimulus but not transferred to non-adapted locations. Neurons in higher cortical areas have larger receptive field sizes [139, 140], therefore aftereffects are at least partially transferred to non-adapted retinal locations, as has been shown for adaptation to complex facial features [141]. For this face aftereffect, it has also been shown that the effect size decreases during the simultaneous presentation of conflicting stimuli [142]. For distortion adaptation with natural stimuli, higher cortical levels with large receptive field sizes are also involved, since it has been shown that distortion adapta-

tion aftereffects are transferred to non-adapted retinal locations [37]. The presence of multiple opposing aftereffects in our experiment again suggests the involvement of lower cortical areas, where different neuron populations are able to adapt differently for different retinal locations.

For the relevance of adaptation to spectacle lenses, future research should consider that adaptation to spatially varying distortions could also be part of a 3D surface curvature adaptation. It has been shown that the perceived curvature of a frontal plane can change due to adaptation [143, 144]. This curvature distortion leads to local skew distortions. Therefore, the adaptation to the local skew distortions in the context of progressive lenses could be driven by a 3D adaptation process, not necessarily by independent localized adaptation effects.

To summarize, this study shows that neural adaptation mechanisms exist that can reduce the influence of complex spatially varying distortions on perception. Still, some presbyopes never fully adapt to their PALs and sometimes reject them. The following studies of this thesis concentrated on understanding better the perceptual influence of distortions without adaptation and how those effects could be quantified for an application in distortion optimization.

3.2. Self-motion illusions from distorted optic flow

This section summarizes the research published in the article

> Sauer, Y., Scherff, M., Lappe, M., Rifai, K., Stein, N., Wahl, S. (2022). Self-motion illusions from distorted optic flow in multifocal glasses. Iscience, 25(1).

and additional results presented as a conference poster

> Sauer, Y., Scherff, M., Stein, N., Habtegiorgis, S. W., Lappe, M., Wahl, S. (2022). Inconsistent self-motion perception between hemifields from optic flow distorted by progressive addition lenses. VSS, St. Pete Beach (Florida, USA).

Motivation

Descriptions of the swim effect focus on the perception of unnatural or unstable motion, especially during self-motion. The two-dimensional retinal motion pattern we perceive during self-motion is called optic flow. The translational and rotational movements of the body, head, and eyes in combination with the natural scene statistics determine the flow field, which follows a typical characteristic. When moving forward while fixating a point, for example, the perceived motion is an expanding spiral pattern around the fixation target [91, 92, 76].

Optical distortions alter the speed and direction of the flow field vectors and consequently, the information that the visual system can extract from optic flow. We wondered how the motion-related problems described by PAL wearers might be related to the distorted optic flow perceived during motion. The goal of this study was to simulate distorted optic flow as a PAL wearer would perceive it during natural self-motion situations. This allows for studying the effect distortions have on optic flow perception. By using an algorithm for motion direction extraction, we analyze the changes in motion information based on calculated distorted optic flow.

When PAL-wearers move their eyes, distortions are not fixed in the visual field but change with gaze direction. During central view through the far vision area of the lens, distortions are visible mainly in the visual field's periphery. Alternatively, gaze direction through the lower left or right area of the lens leads to substantial distortions in the visual field center.

During walking, many gaze changes occur. Depending on the complexity of the terrain and the speed of walking, fixation is usually switched between different points a few meters ahead to control for foot placement and scan for obstacles [81, 82, 83, 84,

85]. Various combinations of head and eye movements are possible for the fixation. One possible way is to keep the head orientation straight in the walking direction and direct the eye downward to fixate on the ground. Alternatively, one might tilt the head downward while keeping the orientation of the eye straight with respect to the head. While these two behaviors result in the same structure of optic flow for eyes without glasses, they lead to different distortions for PAL wearers. When the eye is directed downwards but the head remains level, the gaze is through the peripheral, more distorted part of the lens. In contrast, when the head is oriented downwards, the gaze is directed through the less distorted central area of the PAL and the distortions occur mainly in the visual periphery. If distortions influence self-motion perception, then this misperception regarding one's own movement should be influenced by the gaze direction relative to the lens.

Our study aimed to investigate the influence of PAL distortions on heading perception, and additionally determine differences in perception between the central and peripheral views in a typical self-motion scenario. First, to assess the general influence of distortions on optic flow, we simulated distorted optic flow based on ray-traced PAL distortion data. Next, we used an established model of heading perception in humans to estimate the expected effects of PAL distortions on heading. Following this, we tested heading estimation in human participants in a psychophysical experiment with simulated PAL distortions in VR. We concentrated on motion parameters that provided the strongest predicted misperception in the model simulations. The implementation of the distortion simulation in VR builds a basis for multiple experiments and is discussed in more detail in Appendix A.

Methods and results

Simulation of distorted optic flow

We simulated the optic flow vector field for an observer moving across a ground plane while fixating on a point on the floor. We considered two distortion conditions corresponding to central view and peripheral view through the PAL. Optic flow fields were calculated for the motion scenario with and without distortions. A pinhole camera model is used for projecting the relative motion of the environment on an image plane for calculating the (undistorted) optic flow field. To transform the flow field based on ray-tracing simulated PAL distortion data, we interpolate a transformation function that maps undistorted to distorted points. Distorted optic flow is based on the deriva-

tive of the transformation function. More details about the simulation of distorted optic flow are described in Appendix B.

Fig. 3.3A shows an example of the distorted optic flow (red arrows) of a translational motion compared to the undistorted (green arrows) retinal flow field. In this specific simulation, the direction of self-motion (heading) was to the left. The overall pattern appears very similar in both cases and exhibits the typical spiral flow field structure for the fixation of a target on the ground. Fig. 3.3B shows how the peripheral view distortion changes direction (angle) and speed (ratio) across the visual field and reveals that there are large areas of systematic differences between the distorted and the undistorted flow. The parafoveal area exhibits directional changes of the flow, clockwise on one side and anti-clockwise on the other side of the fovea, as well as increases and decreases of speed in the upper and lower parafoveal field. Due to the typically low flow speeds in this area, even small changes may already impact the spiral structure emerging from the center and impact heading perception. Fig. 3.3C shows the differences in direction and speed in the central view condition. They exhibit a different retinal distribution than in the peripheral view condition and are overall smaller. This analysis shows that the distortions impose a systematic and continuous pattern of changes to the optic flow field. These differences in flow, though small in value, might lead to misestimations or increased variability in heading estimates. Due to the complexity of the flow field, however, it is not directly clear which alterations of self-motion perception may be expected. We therefore used computational modeling to better understand the potential implications of distorted optic flow.

Model simulations for heading estimation

To estimate the influence of distorted optic flow on self-motion perception, we used the subspace algorithm for heading estimation [97] that computes a 2D distribution of likelihood for potential heading directions in retinal coordinates. The likelihood for each candidate heading direction quantifies *how well* the specific optic flow field is explained by the candidate direction. This algorithm has been used before in models for the heading perception of humans [98, 76, 145]. For undistorted optic flow, the likelihood distribution has a clear and defined peak at the true heading direction. Distorted optic flow seems to blur the distribution. Different sub-parts of the visual field also show different distributions of likelihood. To model the integration of the visual system, our simulation selects patches of optic flow, similar to receptive fields of neurons in the visual motion pathway [146]. Individual likelihood distributions are summed

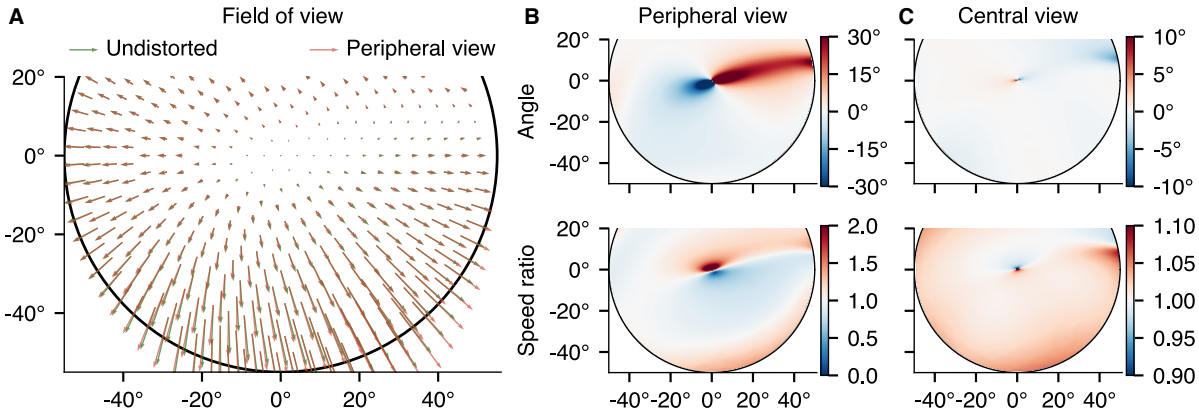

Figure 3.3.: Influence of distortions on optic flow

A Example flow field used in the simulation for a translation parallel to the ground to the left of the fixation point. Green arrows show the undistorted flow, red arrows show the distorted flow in the peripheral view condition.

B Influence of peripheral view distortions on angle and speed of flow vectors. The top panel shows the angle between undistorted and distorted flow vectors calculated across the visual field. The bottom panel shows the ratio of the speed of the distorted vector to the speed of the undistorted vector. Values greater than 1 indicate an increase in the speed of the distorted optic flow at the specific location.

C Directional and speed changes with central view distortions. In the central area, undistorted optic flow is almost vanishing. Therefore, the interpretability of the angle and speed ratio close to the center is limited.

up for a combined distribution, in which the most likely heading candidate is taken as model estimation. More details of the simulation are described in Appendix B. The resulting likelihood distribution of our model simulation suggests an uncertainty in the vertical component of heading, with a stronger deviation from the actual heading direction for the peripheral view condition.

Psychophysical experiment

To test the model prediction in a psychophysical experiment, we recreated the simulated motion scenario in VR. The experiment is based on my simulation of optical distortions described in more detail in Appendix A. The virtual image was distorted to simulate PAL distortions for either central view or peripheral view. In a third condition, we measured baseline perception with an undistorted stimulus. The self-motion scenario simulated movement across a ground plane while fixating a point on the floor.

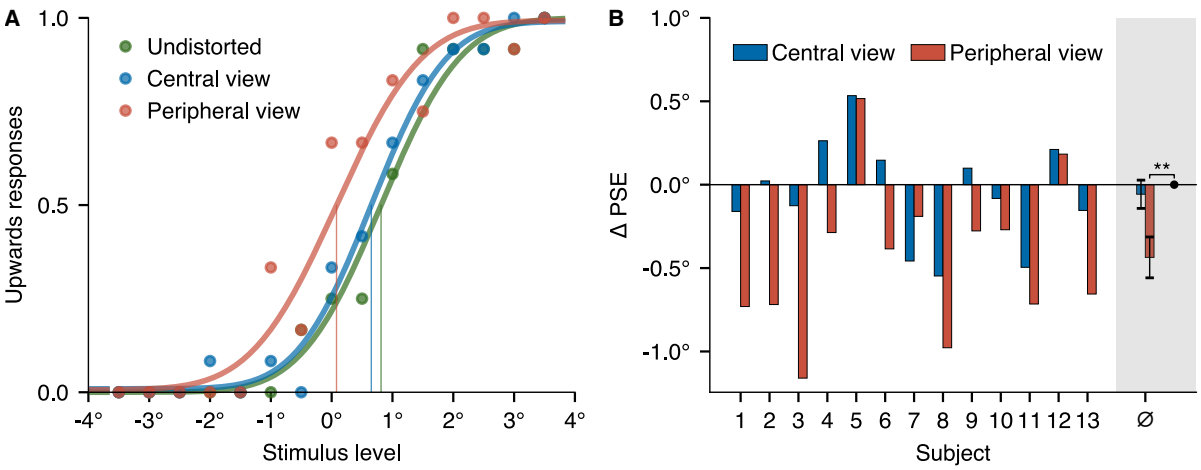

Figure 3.4.: Results of the heading experiment in VR experiment

A Percentage of upward responses and psychometric fits for one example subject. The green data points were obtained in the undistorted trials. The blue and orange data points show the answers in the two distortion conditions for the simulated central view and simulated peripheral view, respectively. All three data sets were fitted with a psychometric function. The $50\,\%$ point of the fit function is taken as the point of subjective equality (PSE) (vertical lines).

B Difference of the PSEs between the distortion conditions and the undistorted condition for all tested subjects. The rightmost bars are the mean value of ΔPSE with standard deviation as error bars.

Based on the model estimation, we concentrated on the vertical component in the experiment. The virtual self-motion was either parallel to the ground or contained a small upward or downward component. Participants reported their perceived direction of self-motion by indicating their perception of either *sinking in* or *lifting off* in each trial. The three distortion conditions were measured in one session in randomized trial order.

For each participant and each distortion condition, the vertical translation angle perceived as a motion parallel to the floor, i.e. the point of subjective equality (PSE), was determined by fitting a psychometric function to the participants' responses depending on the vertical translation angle. Then, the difference in PSE between the distorted condition and the undistorted condition was calculated. This relative shift ΔPSE provided a measure for the influence of simulated distortions in the two view conditions.

Fig. 3.4A shows the answers and psychometric fits for all three conditions for one example subject. There is a clear shift of the psychometric function in the case of

simulated gaze through the periphery of the PAL compared to the undistorted condition. This subject perceived the translational movements more upward than in the undistorted condition. In the central view condition, the PSE is similar to the undistorted condition. Fig. 3.4B shows the change of PSE in the two distortion conditions relative to the undistorted condition across all participants. In the peripheral view condition, there is a significant deviation of the PSE from the undistorted condition (t-test, $p < 0.01$). On average, the angle perceived as a straight movement was $0.43°$ smaller than in the undistorted condition, i.e. the ΔPSE was negative. Thus, in the peripheral gaze condition, participants reported a perception of self-motion that appeared as if they were slightly lifting up from the ground, when in fact the motion was parallel to the ground. For the simulated gaze through the center of the PAL, there is no significant difference between the distorted and undistorted cases.

Follow-up simulations

The results of the VR experiment showed that PAL distortions of the optic flow indeed produced a misperception of self-motion along the vertical dimension. To test if our model simulations can quantify the perception of subjects, we recreated the same experiment with the simulated observer model. Distorted optic flow fields were calculated for all sampled vertical stimulus angles of the experiment. To recreate the psychophysical procedure, model heading estimates were converted from a direction into upward and downward answers, depending on the sign of the vertical component. Then, for each distortion condition, the vertical heading angle perceived as a motion parallel to the floor was determined by fitting a psychometric function to the answers using the same fitting procedure as for the experimental analysis. As the model in the undistorted condition always produced a PSE of 0, i.e. it recovered the correct heading, the shift in ΔPSE corresponds directly to the extracted PSE for the distortion conditions.

For the model simulations, the maximum field of view (FoV) was set to be circular with a radius of $55°$. This matched the specifications of the VR headset we used for the experiment. However, the effective FoV when wearing an HMD is often smaller because parts of the screen are not visible due to individual adjustments in fitting the HMD on the head [147]. Therefore, we also performed the simulation procedure with slightly reduced sizes of the FoV. The heading estimation changes when reducing the FoV sizes. For FoVs smaller than $45°$, the PSE in the peripheral view condition even becomes positive. On the one hand, this FoV dependency can explain individual

differences between subjects. On the other hand, it shows that the PAL distorted optic flow is inconsistent in its heading information. The central optic flow alone results in a positive estimation of PSE, but the combined optic flow results in a negative estimation of PSE.

To summarize, the optic flow simulations can give a qualitative estimation of the influence of distortions on heading perception. The possibility for exact quantitative modeling of perceived heading seems limited, as in case of inconsistent optic flow the simulations are sensitive to FoV size and subjects showed individual variations in their perceived shift. Those variations in the model estimation, as well as individual perception, strengthen the hypothesis that distorted optic flow leads to inconsistent or ambiguous information that might be perceived as unnatural motion or an unstable environment.

The following section summarizes our additional study that tested this hypothesis and was presented as a conference poster [148].

Inconsistent perception from distorted optic flow

We performed a follow-up experiment that tested the inconsistency in distorted optic flow. Based on pre-simulations, in which heading direction was estimated individually for different halves of the visual field, we expected opposite heading information between the upper and lower visual field. We tested two different lenses with positive and negative distance correction (see Fig. 1.3) leading to radially increasing magnification or minification, respectively. The simulations suggested opposite changes in heading direction between the two lenses. For experimental validation, we followed the same approach as the previous study with additional conditions for optic flow presentation in only one hemifield. The participants' answers were fitted again, independently for each lens and each visual field condition. The results show a significant difference in perceived heading direction between the upper and lower half of the visual field for both lenses. For the positive lens, heading is perceived more upwards in the upper part of the visual field compared to the lower. For the negative lens, the effect is in the opposite direction, heading is perceived more downward in the upper visual field. The different distortions lead to changes in the optic flow pattern that cause inconsistent heading information between different parts of the visual field. The optical power, determining the general shape of distortions, is an important factor to consider.

Discussion

Simulations and psychophysical experiments showed an influence of optical distortions on self-motion perception from optic flow. Previous research has shown that manipulation of the flow field, for example by adding noise [96, 149], increases heading estimation error. Even though the influence of PAL distortions on optic flow seems subtle, the distortions cause estimation errors as well. The errors are more systematic in the form of bias to a certain direction. Our modeling approach of summing local heading estimates with a weighting motivated by cortical magnification can qualitatively predict the bias in perceived heading. Distortions cause a continuous change in the speed and direction of flow field vectors. During self-motion, the typical flow field structure is a spiral, with more radially oriented vectors in the periphery and rotational flow in the central area. Therefore, the induced change of heading information always depends on the combination of local flow and local distortions. The peripheral gaze, bringing more distortions in the center of the visual field, causes stronger changes in the central spiral pattern leading to higher heading misestimation. PAL wearers who look more through the central area while walking might perceive less heading misestimation. This would lead to increased head movements for PAL wearers compared to other people, a change in behavior that was already found in a natural scenario [150, 151, 152].

Heading illusions as shown in this study would put visual perception in conflict with other self-motion perceptions and might be one aspect of the swim effect, possibly causing discomfort or nausea. An illusory, gaze-dependent perception of motion during self-motion is an often reported side effect for PAL wearers [153, 26], although the exact mechanism is not well described in the literature. In everyday life, we constantly change gaze direction, which modulates for PAL wearers the perceived distortions. This can produce motion perception characterized by recurring changes in perceived motion direction. In complicated walking scenarios, e.g. climbing stairs, misperception of heading changing during every eye movement can lead to complications with foot placement and tripping [27], especially considering decreased capabilities of elderly people for heading control from optic flow [154]. Evaluating distorted optic flow for quantifying motion illusions is a first step for an objective characterization of the swim effect. The optic flow modeling approach could be one part of a quantification method for the improvement of lens designs.

The experimental results showed some individual differences in the effect size between participants, with two showing a different sign in the vertical heading direction,

which does not match the model simulations. Based on simulations with varying FoV sizes, the experimental variations could be explained by differences in effective FoV in the HMD. In another study, we could prove that perceived FoV in VR depends on individual factors, like physiological face properties and headset tightness [147]. This indicates that also for real PALs, where the FoV covered by distortions is determined by the spectacle frame size, perception for the same lens might change depending on frame size. Additionally, the frame creates a discontinuity between distorted optic flow inside and undistorted optic flow outside of the lens. This discontinuity might contribute to discomfort. In the next study, we considered this by selecting a VR headset that can present a FoV larger than a typical spectacle frame.

Regarding the everyday problems of PAL wearers, not only heading illusions but also other aspects of the optic flow field have to be considered. Distorted vision results in unnatural flow fields, which becomes clear from the heading likelihood maps: the distribution of likely headings is wide with no clear best-fitting direction. This is also indicated by flatter slopes in the fitted psychophysical functions. It is not clear to what extent the widened distribution of heading directions contributes to the discomfort of PAL wearers. In the follow-up experiment, which tested the heading perception for isolated parts of the distorted optic flow, we showed that different parts of the visual field give different heading information. The optic flow pattern is inconsistent in itself, which might be perceived as unnatural or cause additional illusory perception of rotation or instability.

The results of the follow-up experiment and modeling suggest a strong dependency of perceptual effects on the correction power of the PAL. Differences in the shape and strength of distortions between positive and negative power lenses lead to different effects in the optic flow field (see also Fig. 1.3 for comparison). Positive lenses cause a magnification of the image with radially increasing distortions (pincushion distortions). Negative lenses minify the image with radial distortions more similar to barrel distortions. The speed and angle changes in the optic flow vector field caused opposite perceptual effects in our experiment. For a quantification of distortion perception, it's important to consider the differences in the shape of PAL distortions and to study how perceptual effects scale with lens parameters. The next study investigated this further.

3.3. Psychophysical scaling for distortions in a natural environment

This section is a summary of the work described in the publication

> Sauer, Y., Künstle, D. E., Wichmann, F., Wahl, S. (2024). An objective measurement approach to quantify the perceived distortions of spectacle lenses. Scientific Reports, 14(1), 3967.

Motivation

We have seen that distortions induce alterations in perceived motion direction as well as inconsistency of optic flow during self-motion. The application of the heading estimation model is a first step towards quantifying the swim effect. However, the previous study had certain limitations.

We simulated a defined motion scenario, which did not correspond to the actual self-motion of the participants. To guarantee the presentation of the same defined optic flow to all participants, position and orientation tracking of the VR headset was turned off. This is well justified by the objective to measure the perception based on optic flow alone. However, since the participants did not perform the simulated movement by themselves, there is a sensory mismatch between visual information and vestibular or motor action information [119, 155]. We expect that distortions alone cause a sensory mismatch and that this conflict is a relevant part of distortion-related discomfort and the swim effect. To study this influence, in the next study we allowed free behavior to participants. The perceived motion was only caused by the participants themselves.

The previous study only simulated translational movements (e.g. walking while keeping the head stable). When simulating the distorted optic flow of head movements while fixating on a static point in the scene, perceived distortions change continuously, leading to unnaturally curved trajectories of points. Those simulations indicate the necessity to include head movements in the analysis of the swim effect.

We also have shown that perception of motion differs between different lenses. Positive and negative power lenses cause different distortions of the perceived image, causing opposite alterations in the optic flow field. It is not clear how perceptual effects scale with the shape and strength of distortions (mainly determined by the refractive power of the lens). Relating the lens parameters to perceived distortions would build a foundation for understanding the relationship between the perceptual

effects and the design parameters.

In this study, we tested the application of a psychophysical scale (a mathematical relation of the level of sensation of a corresponding physical stimulus) to quantify the relative change of perceived distortions with changing lens power. Again, we used the VR simulation for PAL distortions. Participants could move freely in a more natural indoor environment, inducing distorted motion perception under natural self-motion. In each trial, participants had to judge the perceived similarity of triplets of different distortions, with varying far and near correction. This ordinal data can be used to fit the participants' perceptual distortion scale with ordinal embedding methods [113]. The advantage of using a comparison-based approach with embedding methods is that they provide an objective estimate of the scaling function. Scoring methods, used in previous studies about lens distortions [108], can lead to variable results and are susceptible to response bias (e.g. central tendency and range biases [110]). An indirect measurement method, like the triplet paradigm, is applied in many areas of perceptual research [156, 157, 158]. Applying this method in a VR distortion simulation is a first test of how those methods can be used for complex perceptual scenarios in a natural environment (compared to typical lab experiments).

The free behavior of participants in this experiment, and the relatively open task, should include multiple perceptual distortion effects. This also causes the problem that participants might use different strategies or concentrate on different effects, leading to differences in perceptual scaling. To explore this possibility, VR offers easy tracking of head movements and gaze. After the experiment, we can compare behavior and individual scaling.

Methods and results

The psychophysical experiment used again our VR simulation of optical distortions, presented to the participants in a virtual indoor environment. Based on the findings in the previous study indicating a possible influence of FoV on distortion perception, we decided to use a high FoV VR headset that would cover the complete size of a typical spectacle frame. Based on typical frame dimensions, we calculated the size of a mask that was used to simulate the edges of the frame. Only the image inside this defined region was distorted.

The experiment used a triplet paradigm, presenting three distortions in each trial (corresponding to three different lenses). The distortions were chosen randomly from a set of ten PALs: five different values for the far correction (spherical power *Sph*)

between $-5\,\mathrm{dpt}$ and $5\,\mathrm{dpt}$, each with two different values for the near correction (addition power *Add*) at $1\,\mathrm{dpt}$ and $3\,\mathrm{dpt}$ were tested. One additional possible stimulus was undistorted. After each trial, participants answered if the first or last distortion stimulus (referred to as choice 1 and choice 2) was more similar to the one presented in the middle (anchor). The answers give ordinal information about the perceived similarity of distortions, which can be used to estimate a perceptual scaling function.

Participants could move and look around freely. To induce the swim effect, the study volunteers were encouraged to move their head. This was done by tracking head movements during the initial training phase and only continuing the trials when participants moved their head.

Psychophysical scaling function models perception of PAL distortions

The participants' perceived distortion was estimated from their trial responses (choice 1 or 2 is more similar to the anchor) using *Soft Ordinal Embedding* (SOE) [159]. This method assigns coordinates to each stimulus so that their distances agree with the participant's similarity judgments. Each participant was evaluated individually resulting in an individual scale.

Although physical descriptions of PAL distortions require many parameters, the perception of lenses can deviate from this parametrization. In our experiment, we use PALs of different *Sph* and *Add*, which influence the physical distortions differently: *Sph* influences more the overall shape and strength of distortions, while *Add* introduces more asymmetry in the distortion pattern. Multidimensional perception of these multidimensional distortions seems plausible. To test for the dimensionality of perception, we chose the lowest dimensional scale that still is a good predictor of unseen triplet responses. This predictive accuracy is approximated with a cross-validation procedure [115].

All participants' scales are one-dimensional (Figure 3.5) and show a comparable influence of *Sph* interacting with *Add*. Additional dimensions do not increase the predictive accuracy. This may be regarded as surprising, given the two varied lens parameters *Sph* and *Add* and their non-linear spatial effect on distortions. A single dimension can quantify the perception of complex PAL distortions in our experiment.

The results do not describe a measure of absolute value or individual sensitivity, but how the perception scales for the participant. Therefore, arbitrary shifts and scales of the perceptual functions are possible. To compare individual participants, the individual scales were aligned using general Procrustes analysis [160]. This method

minimizes the Euclidean distance between scales by iterative similarity transformations (translation, scaling, and flipping in our case) towards the mean scale. After alignment, we shifted all scales such that the origin—on average—corresponds to the undistorted lens (*Sph* 0 and *Add* 0). Accordingly, the average scaling value of the distorted lens *Sph* 5 *Add* 3 has a distance of 1 to the origin.

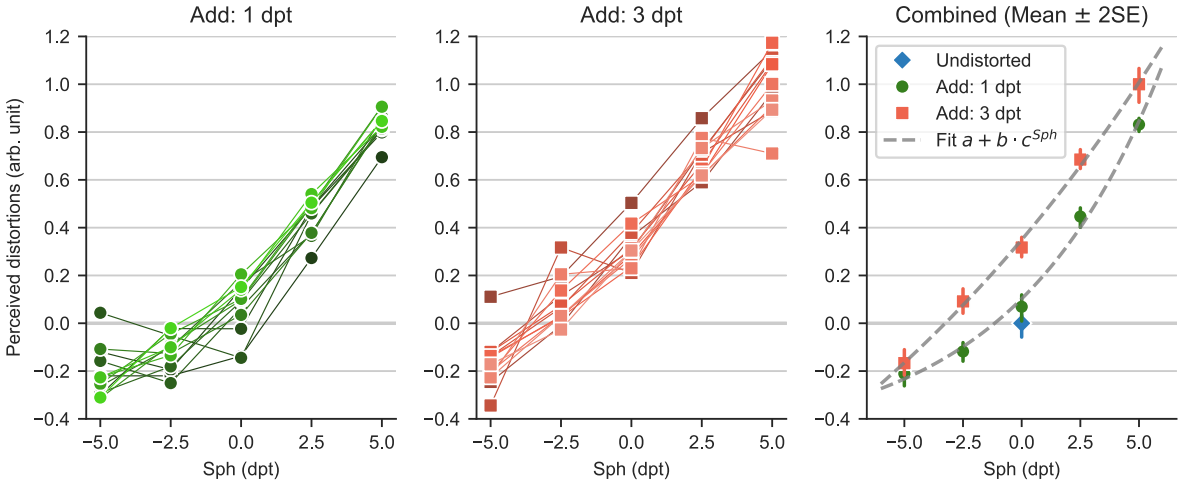

Figure 3.5.: Psychophysical scaling functions of "perceived distortion"

The lines in the left and middle plots show individual participants "perceived distortion" depending on the *Sph* and *Add* power of the simulated PALs. The right plot shows the mean and standard error of the scaling functions along an exponential function fit.

The amount of perceived distortion increases monotonically with both *Sph* and *Add*. For negative *Sph* values, an increase in *Add* leads to less perceived distortions (closer to undistorted), implying a compensation of perceived distortions; for positive *Sph*, an increase in *Add* only increases perceived distortions further. All in all, if *Sph* is strong compared to *Add*, the shape of distortions is primarily influenced by the sign of *Sph*, resulting in either pincushion or barrel distortions. This is also reflected in perception, as shown by the change in the sign of the perceived distortions (with undistorted defined as reference point 0).

The relation between perceived distortions and *Sph* can be modeled with an exponential function $a + b \cdot c^{\mathrm{Sph}}$ for each value of *Add*, shown in Fig. 3.5 (right), illustrating a higher rate of increase for positive *Sph* compared to negative *Sph*. Fits between *Add* 1 and *Add* 3 mainly differ in the offset a and slope b, but barely in the base c. Close to *Sph* 0, the exponential fits show a similar rate of increase for *Sph* and *Add*. With higher correction values for *Sph*, the relative influence of *Add* decreases, indicating that for

high-power lenses, *Sph* dominates distortions. The individual deviations from this exponential model do not have to be due to perceptual differences or measurement accuracy alone but can also be explained by behavior. If the distortion is perceived locally, it makes a difference where the participant looks through the lens and how they move.

Behavior analysis with head and gaze tracking

From tracking data of headset position and gaze direction, the individual behavior during the experiment was analyzed. The tracked headset orientation during the experiment was transformed into yaw, pitch, and roll angles (Tait-Bryan angles with order y-x-z) as illustrated in Fig. 3.6A. The movement velocity was computed independently for each rotation component. We calculated the mean velocity for each participant over each trial to illustrate changes in motion behavior over time.

Considering the reports about the swim effect, we expected that especially dynamic behavior might lead to a heightened perception of distortions and thus help participants in discriminating the stimuli. We introduced participants to this idea by explaining the possibility of distortions becoming apparent more clearly during self-motion. Furthermore, during the training phase of the experiment, head movement was actively enforced by our experimental design. However, results of the head tracking show that participants used two different strategies: one group performed continuous head movements, usually a nodding movement (pitch oscillation like in Fig. 3.6B and C), some also yaw movements, while the other group did not move their head or stopped after a few trials.

Since participants usually followed the same movement type throughout the experiment, we calculated the mean velocity over the whole experiment, as shown in Fig. 3.6D. Based on this mean head movement velocity, we grouped participants into static and dynamic observers. The static observers had to rely only on static distortion features in the scene for their comparison judgment. During the training phase, head movements were enforced. Consequently, dropping this strategy during the main experiment either indicates that the movement does not convey relevant cues for the observers or that the non-moving observers were less motivated to perform well. To test this, we compared the consistency of dynamic and static observers regarding embedding accuracy and catch-trial performance. There is a significantly better embedding accuracy ($p < 0.05$) as well as performance in the catch trials ($p < 0.01$) for the static observers using the Mann-Whitney U rank test. Consequently, it is unlikely that static

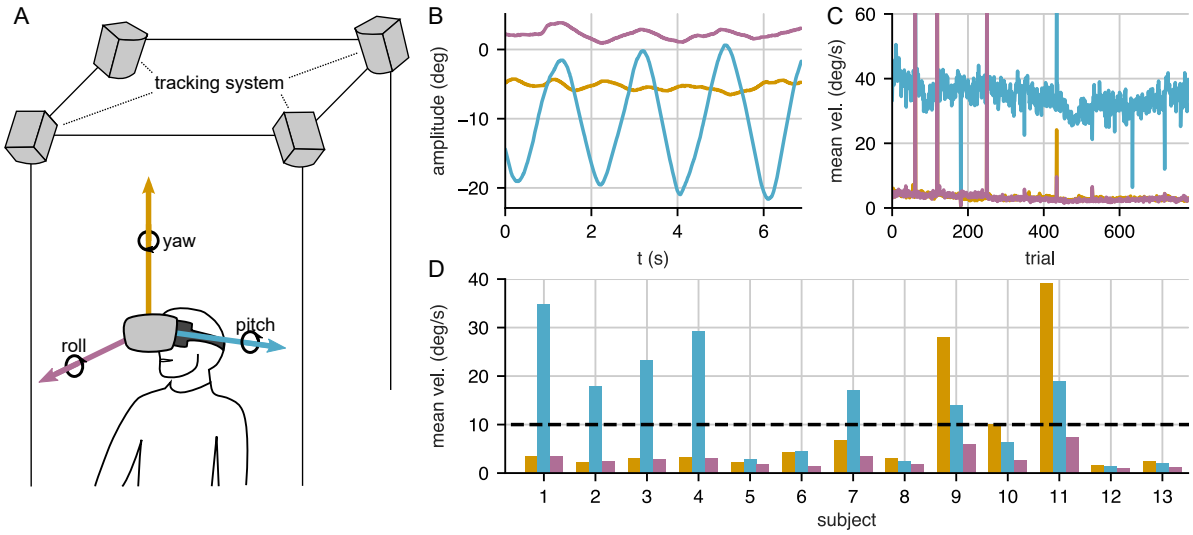

Figure 3.6.: Head movement behavior

A Headset tracking data is recalculated in yaw, pitch, and roll angles of the participants' head orientation.

B Example data for one trial. This participant performed a continuous pitch movement (head nodding), while the roll and yaw angles stayed relatively stable.

C The mean rotational velocities for each head rotation component were calculated across individual trials. The data shown is from one example participant who consistently followed the same head movement pattern.

D The overview of mean angular velocities for all participants shows different head movement strategies: some observers did not move their head, while others performed mainly a nodding (pitch) or mainly a horizontal movement (yaw).

observers were less motivated. Instead, for those participants, dynamic features contributed less to the perception of distortions. This result contrasts with the expectation that especially dynamic behavior, associated with the swim effect, would give a clear cue for distinguishing distortions and more reliable results from dynamic observers.

We compared gaze behavior between participants by the area covered in the visual field. First, a heatmap of individual gaze distribution was calculated from gaze samples over the whole experiment. The distribution of gaze in the FoV for the individual participants is shown in Fig. 3.7. The gaze was mainly oriented along the center vertical axis, with variations in the latitude between individual observers. The solid angle of the 5% percentile, meaning the area in the heatmap which includes 95% of the distribution's mass, can be used for comparing the gaze area covered by different participants. Some participants showed a high spread in gaze direction, while others stayed in a more defined area of the FoV. This finding suggests that some participants

continuously fixated on the same part of PAL distortions, while others looked more at different parts of the distortion pattern. Next, we tested if the described differences in behavior also influence the scaling of perceived distortions.

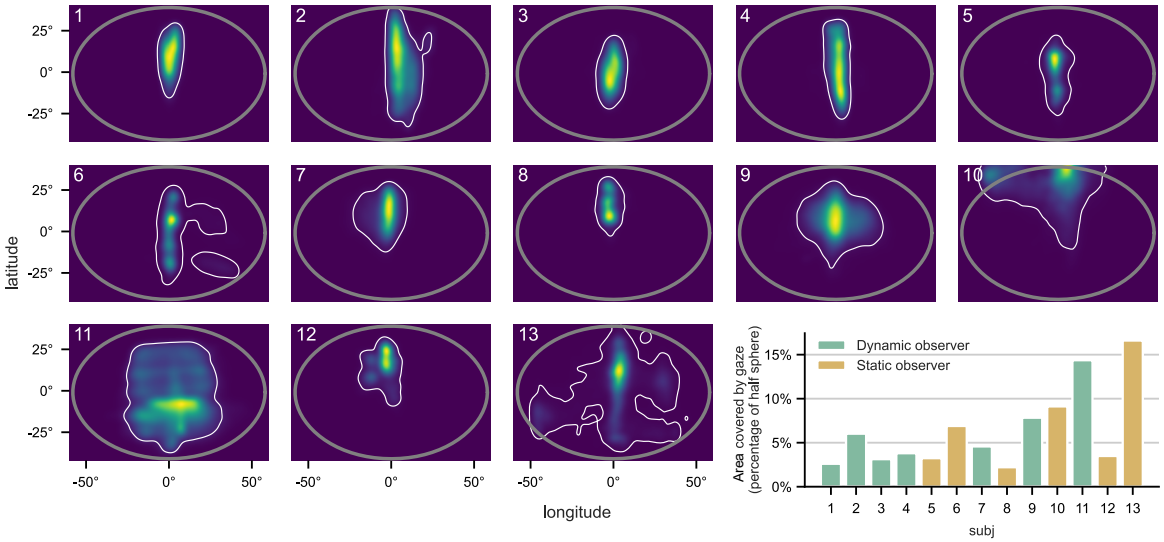

Figure 3.7.: Gaze behavior

Individual gaze distribution of all observers with Gaussian kernel smoothing. Binocular gaze samples of the whole experiment were combined to calculate the gaze distribution in the observers' FoV. The grey ellipse represents the virtual frame size, which was visible as a black border during the experiment. The white contour encompasses 95% of the gaze distribution mass. The area enclosed by this contour for individual participants is shown in the bar diagram as a percentage of the half-sphere area.

Testing the relationship between perception and behavior

Our behavior during the perception of distortions can influence which visual features we perceive. For example, head movements introduce perceived distorted motion, while in other scenarios without movement, only static features are visible. If the various aspects of distortion perception (static and dynamic features) scale differently with the PAL distortion components, then this should be revealed by differences in the scaling function between participants of different behavior. Especially the difference between static and dynamic observers should show how the swim effect, associated with dynamic situations, contributed to distortion perception. Additionally, different gaze strategies might cause differences in perceived distortion and thus in the recov-

ered perceptual scales. The results of the eye tracking revealed differences in the spread of gaze. A wider area of gaze implies that participants see a higher variability in distortions.

To test the possible influence of behavior on the scaling function, a linear model was used with *Sph*, *Add*, head movement behavior group, as well as the visual area covered by gaze. The model shows a significant increase of perceived distortion, both with *Sph* and *Add* ($p < 0.001$), but no significant influence of behavior differences, which indicates that perceptual effects of both static and dynamic features scale similarly with the amount of PAL distortions.

For application in lens design, this is a useful result. It implies that the general scaling of distortion perception is similar for all observers, independent of their specific and often idiosyncratic head and eye movements. Different behavior does not lead to differently perceived distortions, which in turn allows a general quantification of perceived distortions for a specific PAL.

Prediction of perception of PAL distortions

To improve lens design based on our perception quantification method, it is important to test how well we can predict perceived distortions for unmeasured observers. Individual perception quantification would require individual lens design changes. Only if we can predict the perception of unmeasured participants, perception models can be used for general improvements of lens design.

We assessed the predictive ability of three differently complex regression models in a leave-one-subject-out procedure: the models are trained on all but one subject's scaling functions and subsequently tested on the omitted subject. The assessed models include the exponential fit from Fig. 3.5 along with baseline and ceiling performance models to provide a reference. The baseline model was a linear regression, and the ceiling model was a random forest regressor [161], known for excellent out-of-the-box performance in non-linear problems. We found that the perception of most participants follows the same regularities, well captured by an exponential model. For most participants, the exponential and random forest models substantially increase prediction over the linear model, again underlining the non-linear influence of *Sph* and *Add*. The exponential model and random forest regressor are similar in their prediction performance.

Discussion

We performed a VR study to determine a psychophysical scale of perceived distortions. In the explorative study, observers could move their heads and eyes freely to induce the perception of unnatural motion associated with the swim effect. For the first time, a considerable amount of different lenses were tested, with varying *Sph* power (far correction) and *Add* power (near correction).

The scaling functions retrieved by fitting the ordinal data of the triplet paradigm show a similar trend for all observers: perceived distortions increase with spherical power. For positive *Sph*, increasing the *Add* power results in stronger distortions. In contrast, the positive *Add* power in combination with negative *Sph* power reduces the perceived distortions (closer to undistorted), suggesting an advantage for short-sighted PAL wearers. For very high or very low *Sph*, the relative influence of *Add* on perceived distortions seems less relevant; close to *Sph* 0, *Add* and *Sph* seem to have a similar influence on perceived distortions. This relationship is very well modeled by a simple exponential function.

Behavior measurements of head and eye movements show that observers followed different strategies in the experiment. Some participants moved their heads continuously (nodding or shaking motion) while others kept their heads stable, despite being instructed in the training of the experiment to perform head movements. This indicates that some observers might be less sensitive to perceive distortions from optic flow. This also agrees with the experience of PAL wearers: some individuals are more sensitive to the swim effect than others [26]. A speculative explanation would be that participants who relied on head movements perceived the influence of distortions on optic flow more clearly and might suffer more from the swim effect.

However, no influence of behavior was found on the psychophysical scaling function. We conclude that the global distortion pattern, not only the local distortions at specific points in the visual field, influences the perception of distortions with static and dynamic features. For the specific virtual scene and the specific lenses, distortions perceived from static or dynamic features scale similarly. Additionally, the scales generalize well to new observers, confirming that our psychophysical scale can be used as an objective quantification method for PAL distortions. The remaining differences between individual scaling functions (for example, differences in the relative influence of *Add* power) could result from individual differences in perception or behavior and should be investigated in controlled follow-up experiments.

This study introduced a new method for measuring a psychophysical scale of optical

distortions. Results show a high agreement between participants, allowing predictions of PAL distortion perception in general. The results confirm that it is possible to apply experimental paradigms like the triplet method with natural experimental conditions of free behavior and naturalistic scene content. This shows the potential of using psychophysical methods for understanding complex perceptual phenomena, like the swim effect, that include a combination of different perceptual effects and environmental influences.

The retrieved psychophysical scaling could help to improve future optical designs of PALs. Choosing a design with a lower amount of perceived distortions can contribute to reducing distortion-related discomfort for PAL wearers and increase satisfaction. To quantify different designs for their perceived distortion, it is required to repeat our experiment to measure perception not only depending on the correction power (*Sph* and *Add*) but directly on parameters describing the possible differences in PAL designs for a given correction. With a model based on the results of this suggested experiment, an arbitrary PAL design could be quantified for perceived distortions purely based on ray-traced distortion data without testing it in an additional experiment. I will outline the necessary further research in the next chapter when discussing the outcomes of all studies combined.

4. Outlook and conclusion

4.1. General discussion

I investigated the influence of geometric distortions on visual perception in three different research projects. PAL distortions cause a complex transformation of the retinal image, that influences multiple visual features. Especially during dynamic situations, when moving relative to the environment, PAL wearers seem to experience an unnatural and often discomforting perception. Therefore, one focus of all studies was the interplay between motion features and distortions. The first study investigated motion effects after skew distortion adaptation. In the second study, the influence of distortions on heading perception during self-motion was analyzed. For the last study, we concentrated more on head movements, to test the perceptual scaling of perceived distortions in a natural environment with free behavior. At the same time, multiple perceptual effects and possible interactions were considered by including naturalistic 3D content and free motion behavior. For the research performed with the VR simulation, depth perception was also included as an additional aspect possibly relevant for the swim effect. All studies combined give important insights into the different perceptual effects caused by optical distortions and how they might relate to the typical problems experienced by PAL wearers. The presented methods build the basis for developing a lens design approach for optimizing PALs for less distortion-related perceptual effects. I will now discuss the important outcomes of the thesis and suggest further steps for the ongoing goal of reducing the swim effect.

What is the swim effect?

In chapter 1, I introduced the swim effect as a vaguely described effect of unnatural, often discomforting, perception caused by optical distortions of spectacle lenses. So far, the exact mechanisms of the effect have not been clear. The research presented in this thesis helps explain how different perceptual effects could contribute to the swim effect. Simulations, theoretical analysis of distortions, and experimental results

show that multiple perceptual effects can be attributed to an unnatural perception. When interpreting the results of the different studies combined, we realize that apart from obvious changes in the size or shape of the stimulus, distortions have a strong influence on motion perception. We showed that distortions cause illusions in heading perception, which can create a sensory conflict and contribute to dizziness. The follow-up simulations and experiment [148, 162] additionally indicate influences for rotational components of the motion and the perception of curved or uneven surfaces from optic flow.

Especially during head movements, when our eyes perform compensatory rotational movements, the coordination between head and eye movement is changed by distortions [163, 164]. This is supported also by other research showing that even magnification alone can cause discomfort during head movements [95]. Nonetheless, not all participants seem to be sensitive to the motion-related (dynamic) effects. The influence on distance perception and surface curvature from binocular disparity [40, 41] has to also be considered as a contributing factor for unnatural perception.

How those effects combine to the swim effect depends on the stimulus features in the specific situation but also on individual sensitivity. For some of our experiment participants, motion-related effects were a clear feature of distortions. For others, the static effects (depth perception or change in the shape of objects) seemed to be more relevant than dynamic effects. A necessary follow-up experiment should test different conditions to isolate certain effects: stereo vision, static effects, and motion perception during different dynamic situations.

In an experiment already planned during the time of writing, we implemented a paradigm that removes the static features of the scaling experiment by presenting random dot stereograms, similar to the stimuli used for studying stereopsis [69]. Without movement, the monocular stimulus is indistinguishable between different distortions. Only movement and binocular disparity can give information about distortions. By projecting the random dot stereograms onto a 3D scene, the distribution of depth and optic flow still follows a natural stimulus. As a next step, VR offers the possibility to isolate the motion and stereo vision effects. When removing binocular disparity by presenting the same image to both eyes, we can study only the motion effects. The other way around, by restricting head movements, we can study only depth perception. As a result, scaling functions for individual conditions help in understanding the contribution of individual effects to the combined distortion perception during more natural behavior.

This approach can reveal if the different effects scale differently with the distortion

parameters. This would imply that lens designs could be optimized for different aspects of the distortions, which could be recommended to different types of wearers. The presented results did not show differences in the perceptual scaling for different categories of observers. This is also due to the fact that all distortion components are correlated in the selected lenses, which I will discuss below. Therefore, it is important to measure perception with different distortion components individually to better test for the influence of behavior.

Apart from individual perceptual sensitivity, also behavioral differences can determine the experience with PAL distortions: the results of the optic flow study show perceptual changes dependent on gaze direction, which suggests that a careful gaze strategy, reducing the changes in perceived distortion pattern, can reduce misestimations. It is possible that the changes in the behavior of PAL wearers in their coordination of head and eye movements also contribute to reducing the initial distortion-related problems. Both neural adaptation in the visual processing, as well as behavioral changes, can mitigate the swim effect.

4.2. Outlook

4.2.1. Distortion components

For manufacturers of optical devices, the question of how to apply the methods suggested in this thesis has to concentrate on the degrees of freedom given by the lens design. For the research presented in this thesis, I used distortions for PALs of varying correction power since those parameters mainly determine the distortion pattern. This is an important first step to study perception across the whole range of possible PALs. However, to be able to predict possible design influences, perception has to be quantified based on independent distortion components instead of optical parameters. For a model that predicts *perceived distortions* for a general lens, we need a mathematical decomposition that is well suited for covering possible design differences, while at the same time reducing the number of distortion parameters to a size that can be covered experimentally. In Appendix C I give a preliminary description of a possible decomposition. Using the developed paradigms in combination with defined distortion parameters, lens manufacturers could quantify the perceptual influence of the given degrees of freedom. The different components might cause different effects (e.g. magnification alone does not cause curvature illusions), but experiments should

still consider combinations of the components to cover the interaction between effects and to quantify how the combination of effects in a natural environment with natural behavior leads to a percept of distortions.

The described optic flow simulations can be tested with different distortion components and should be extended to simulations of depth perception from binocular disparity. Direct quantification of altered information of structure, motion, and stability of the environment from optic flow and binocular disparity depending on distortion components can reveal which components cause which perceptual effects and how they combine during natural behavior.

A perceptual scaling function can reveal the relative influence of the components and possible interactions. The different components in combination determine the potential of a specific lens for causing the swim effect. The approach chosen in the last study is promising for measuring this scaling function for independent components. A generalized observer model, using machine learning methods based on such an experiment with a higher number of participants, could be used as a quantification method during the development of new optical designs. From the results of the last study, we can already confirm that magnification (mainly influenced by *Sph*) and radial distortion (strongly influenced by *Add*) individually cannot explain the scaling function. Multiple components and multiple effects contribute to the combined sensation. The shape of the scaling function suggests interaction between the components.

4.2.2. Influence of adaptation

A limitation to consider before relating the results of our perceptual studies directly to the experience of PAL wearers is the possible influence of distortion adaptation. Most PAL wearers adapt to their spectacle lenses over a couple of weeks, even if they initially experience a strong influence of the swim effect [43, 26, 67]. Our experiments were designed to represent the perception of a novel PAL wearer. Especially for presbyopes who have difficulties with adapting to distortions, improved lens design could reduce the symptoms of the swim effect. Others can still benefit from reduced initial discomfort before they have fully adapted.

Nonetheless, it is important to consider how adaptation would influence the results of the individual experiments. Especially for the suggested approach, studying perception depending on different components of distortions, it might be fruitful to test if adaptation also differs between distortion components. Existing research suggests that adaptation to prismatic displacement and pure magnification takes place in a rel-

atively short time frame (a few hours) [164, 57]. In this case, the adaptation of motor actions, i.e. how body and eye movements are performed depending on the visually perceived position, can compensate for the perceptual changes. More complex distortions require adaptation of form or motion features as shown in the study presented in chapter 3.1. Radial distortions introduce a spatial variation of distortions that changes with eye movements, complicating visual adaptation. Combined, different adaptation processes with different time frames can be involved in adaptation to optical distortions. Studying adaptation to different distortion components can help in evaluating the relative difficulty of adapting to various optical designs.

4.2.3. Other optical aberrations

Apart from geometric distortions, PALs have other optical aberrations which negatively impact vision. Spherical, astigmatic, and higher-order aberrations lead to blurry vision for some parts of the lens. The relative importance of distortions and blur on wearer satisfaction remains unclear. To achieve a comprehensive perceptual approach to lens design optimization, we need to consider blur, distortions, and their possible interactions. The experimental approaches introduced in this thesis can be extended by including other aberrations in our VR simulation [147]. The influence of blur is expected to change the behavior to gaze through the clear areas of the lens [151, 152]. This is evident through increased "head-mover" behavior in PAL wearers [66]. At the same time, the head and eye coordination will influence the perception of distortions and motion. Therefore, for an evaluation of the swim effect, it is necessary to consider the behavior of PAL wearers under the influence of blur.

As I will discuss in the next section, there are technical limitations for simulating realistic blur in VR. Consequently, it is important to study the behavior of presbyopes in different far- and near-viewing scenarios wearing actual PALs using eye- and head-tracking technology. Based on the tracking data, different static and dynamic distortion effects can be modeled for the natural behavior of PAL wearers and compared with the previous experimental results.

4.2.4. Use of VR in vision science

This thesis demonstrates the potential of using VR in vision science and psychophysics. The possibility to present stimuli with natural self-motion and binocular vision with a large FoV is a major improvement for psychophysical experiments studying natu-

ral vision. VR provides a controlled and reproducible experimental environment that simultaneously elicits more natural behavior than traditional psychophysical experiments [165, 166, 167]. Despite constant technical improvements, some limiting factors prevent VR simulations from recreating a fully naturalistic environment for vision science.

The virtual image is rendered for a fixed eye position. Gaze changes rotate the eye, for which a precise simulation would require updating the origin of the rendered camera [125]. Furthermore, the FoV of VR headsets is limited, usually to a size smaller than typical spectacle frames [147]. These factors can contribute to an unnatural perception [168, 169], additionally to influences of the simulated PAL distortions.

Another concern regarding VR is the vergence-accommodation conflict [170]: considering that the optical image distance is fixed (fixed focal length of the optics) and accommodation is coupled to vergence eye movements [171], the eyes often do not focus correctly. The additional defocus can blur the image whenever there is a mismatch between vergence distance and image distance. Furthermore, there is no natural depth of field blur in VR [172]. All objects are presented at the same focus distance, limiting natural blur perception. Therefore, simulating blur in virtual reality to study the influence of other optical aberrations requires more advances in the development of natural focusing conditions in VR [173].

Moreover, VR headsets rely on optics that introduce additional optical aberrations [174, 175, 41] which might influence the aspects of visual perception we want to study. Lenses in VR headsets have radial distortions by themselves, which can be corrected by presenting an oppositely distorted image on the screen [176]. However, this digital correction fully compensates for the distortions only for a defined eye position and orientation. Deviations from this ideal eye and gaze position can lead to a small amount of perceived distortions [177]. This influence has to be considered when interpreting results about distortion perception in VR. Other confounding factors are simulator sickness caused by tracking delay [178] or the vergence-accommodation conflict, causing eye strain and blurry images [179]. Modern VR headsets improved the projection and tracking quality, which reduced the problem of simulator sickness [180]. Nonetheless, it has to be considered that not all study participants might be able to perform a VR experiment.

There is still potential for improvement in the distortion simulation itself. To study the change of distortions with eye movements, eye tracking with low latency for gaze-contingent distortion rendering is necessary. Currently, latency is too high to update the simulated distortions fast enough after a saccade [181], but technical improve-

ments could also solve this problem. Alternatively, experiments could include a fixation target. Then the gaze direction is always known implicitly and gaze-contingent distortion simulation is possible without delay. This allows only restricted experimental paradigms but still might help study certain situations, like the change of perceived positions during pursuit eye movements or after a saccade with defined gaze targets.

To increase the level of realism, the current developments in video-see-through AR devices can be a helpful tool. Instead of distorting a virtual 3D environment, we could apply the distortion simulation directly to the camera images to present a distorted view of the natural environment. Studying the perception with this approach allows more natural interaction and behavior. Video signal latency can again pose a limitation [182], affecting perception in addition to the simulated distortions. If latency can be kept below the perceptual threshold, researchers should focus on developing studies that allow participants to behave freely in their actual environment. This would allow us to study complicated scenarios like walking stairs, a scenario that is typically problematic for PAL wearers, but very difficult to recreate in a virtual environment.

4.2.5. Application for other optical devices

The methods and results presented in this thesis can be applied not only to spectacle lenses but also to other optical devices. For example, for binoculars there is a perceptual effect that suggests that for a high magnification, a certain amount of radial distortions is perceived as more natural [183, 184]: during panning of the binoculars, the moving image is perceived as undistorted only if additional radial distortions are included in the optical design. This phenomenon shows that the approach of aiming for a *distortion-free* lens design is not justified. Manufacturers are aware of this so-called *globe effect* and try to reduce it by aiming for a distortion profile that subjectively reduces the effect. However, an objective evaluation of the best distortion profile does not exist. The techniques suggested in this thesis could be applied to binoculars' distortions, to give an objective recommendation of radial distortion profile for specific magnification. It can be worthwhile to evaluate differences in individual perceptions of individual designs.

For digital devices with wearable optics (AR/VR), distortions can be corrected by oppositely distorting the rendered image. However, as described before, changes in eye position can diminish the distortion correction. Therefore, VR and AR devices can also profit from an optimized lens design with (gaze-dependent) distortions shaped for less perceptual impact.

4.3. Conclusion

In this thesis, I presented different approaches for simulating, measuring, and quantifying the influence of optical distortions on perception. The individual studies helped form a better understanding of the perceptual effects of optical distortions and underscore applications of virtual simulation for lens design. I have shown that the swim effect can not be described by one perceptual effect, but rather is formed by different phenomena, potentially depending on different distortion components. As a next step, relating physical simulations of the different effects (similar to our optic flow-based approach) with the perceptual sensation (as measured by our psychophysical scaling approach) would be fruitful for both understanding which effects play an important role in perception and how lens design can be improved.

The results show the potential of combining simulation techniques, enabled by technical advancements, with psychophysical procedures and modeling for a better understanding and prediction of distortion-related perceptual effects. I suggest considering this approach as a new perspective on optical design.

A key concept of this approach is the use of virtual reality technology for the simulation of optical aberrations, which allows the application of psychophysical paradigms necessary for an objective quantification of perceptual effects. Researchers and engineers working on the improvement of optical systems can profit from this new approach.

References

[1] A. Glasser and P. L. Kaufman. “The mechanism of accommodation in primates”. *Ophthalmology* 106.5 (1999), pp. 863–872.

[2] W. N. Charman. “The eye in focus: accommodation and presbyopia”. *Clinical and experimental optometry* 91.3 (2008), pp. 207–225.

[3] A. Duane. “Studies in monocular and binocular accommodation with their clinical applications”. *American Journal of Ophthalmology* 5.11 (1922), pp. 865–877.

[4] D. A. Atchison. “Accommodation and presbyopia”. *Ophthalmic and Physiological Optics* 15.4 (1995), pp. 255–272.

[5] T. R. Fricke et al. “Global prevalence of presbyopia and vision impairment from uncorrected presbyopia: systematic review, meta-analysis, and modelling”. *Ophthalmology* 125.10 (2018), pp. 1492–1499.

[6] T. Young. “II. The Bakerian Lecture. On the mechanism of the eye”. *Philosophical Transactions of the Royal Society of London* 91 (1801), pp. 23–88.

[7] H. v. Helmholtz. “Über die Akkommodation des Auges”. *Archiv für Ophthalmologie* 1.2 (1855), pp. 1–74.

[8] S. A. Strenk, L. M. Strenk, and J. F. Koretz. “The mechanism of presbyopia”. *Progress in retinal and eye research* 24.3 (2005), pp. 379–393.

[9] J. Tabernero, E. Chirre, L. Hervella, P. Prieto, and P. Artal. “The accommodative ciliary muscle function is preserved in older humans”. *Scientific Reports* 6.1 (2016), p. 25551.

[10] N. J. Wade. *A natural history of vision*. MIT press, 2000.

[11] J. R. Levene. “Benjamin Franklin, F.R.S., Sir Joshua Reynolds, F.R.S., P.R.A., Benjamin West, P.R.A. and the Invention of Bifocals”. *Notes and Records of the Royal Society of London* 27.1 (1972), pp. 141–163.

[12] J. E. Sheedy, M. Buri, I. Bailey, J. Azus, and I. M. Borish. “Optics of progressive addition lenses”. *Am. J. Optom. Physiol. Opt* 64 (1987).

[13] D. J. Meister and S. W. Fisher. “Progress in the spectacle correction of presbyopia. Part 1: Design and development of progressive lenses”. *Clinical and experimental optometry* 91.3 (2008), pp. 240–250.

[14] D. R. Pope. “Progressive addition lenses: history, design, wearer satisfaction and trends”. In: *Vision science and its applications*. Optica Publishing Group. 2000, NW9.

[15] H. J. Boroyan et al. “Lined multifocal wearers prefer progressive addition lenses.” *Journal of the American Optometric Association* 66.5 (1995), pp. 296–300.

[16] J Wetzel. *Branchenbericht 2022*. Düsseldorf: Zentralverband der Augenoptiker und Optometristen (ZVA), 2022.

[17] G Minkwitz. “Über den Flächenastigmatismus bei gewissen symmetrischen Asphären”. *Optica Acta: International Journal of Optics* 10.3 (1963), pp. 223–227.

[18] J. Alonso, J. A. Gómez-Pedrero, and J. A. Quiroga. *Modern ophthalmic optics*. Cambridge University Press, 2019.

[19] D. A. Atchison. “Optical performance of progressive power lenses”. *Clinical and Experimental optometry* 70.5 (1987), pp. 149–155.

[20] J. E. Sheedy, C. Campbell, E. King-Smith, and J. R. HAYES. “Progressive powered lenses: the Minkwitz theorem”. *Optometry and Vision science* 82.10 (2005), pp. 916–922.

[21] W. Jaschinski, M. König, T. M. Mekontso, A. Ohlendorf, and M. Welscher. “Comparison of progressive addition lenses for general purpose and for computer vision: an office field study”. *Clinical and Experimental Optometry* 98.3 (2015), pp. 234–243.

[22] E. A. Villegas and P. Artal. “Comparison of aberrations in different types of progressive power lenses”. *Ophthalmic and Physiological Optics* 24.5 (2004), pp. 419–426.

[23] J. Forkel, J. L. Reiniger, A. Muschielok, A. Welk, A. Seidemann, and P. Baumbach. “Personalized progressive addition lenses: correlation between performance and design”. *Optometry and Vision Science* 94.2 (2017), pp. 208–218.

[24] S. Barbero and J. Portilla. “Geometrical interpretation of dioptric blurring and magnification in ophthalmic lenses”. *Optics Express* 23.10 (2015), pp. 13185–13199.

[25] D. J. Meister and S. W. Fisher. “Progress in the spectacle correction of presbyopia. Part 2: Modern progressive lens technologies”. *Clinical and experimental optometry* 91.3 (2008), pp. 251–264.

[26] T. L. Alvarez et al. “Adaptation to progressive lenses by presbyopes”. In: *2009 4th International IEEE/EMBS Conference on Neural Engineering*. IEEE. 2009, pp. 143–146.

[27] L. Johnson, J. G. Buckley, A. J. Scally, and D. B. Elliott. “Multifocal spectacles increase variability in toe clearance and risk of tripping in the elderly”. *Investigative ophthalmology & visual science* 48.4 (2007), pp. 1466–1471.

[28] S. R. Lord, J. Dayhew, B. A. Sc, and A. Howland. “Multifocal glasses impair edge-contrast sensitivity and depth perception and increase the risk of falls in older people”. *Journal of the American Geriatrics Society* 50.11 (2002), pp. 1760–1766.

[29] S. L. James et al. “The global burden of falls: global, regional and national estimates of morbidity and mortality from the Global Burden of Disease Study 2017”. *Injury prevention* 26.Suppl 2 (2020), pp. i3–i11.

[30] D. H. Chang. “Multifocal spectacle and monovision treatment of presbyopia and falls in the elderly”. *Journal of Refractive Surgery* 37.S1 (2021), S12–S16.

[31] P. Hrynchak. “Prescribing spectacles: reasons for failure of spectacle lens acceptance”. *Ophthalmic and Physiological Optics* 26.1 (2006), pp. 111–115.

[32] J. Gresset et al. “Validation of a questionnaire on distorsion perception among progressive addition lenses wearers”. In: *Vision Science and its Applications*. Optica Publishing Group. 2000, p. MD2.

[33] B. S. Chu, J. M. Wood, and M. J. Collins. “Effect of presbyopic vision corrections on perceptions of driving difficulty”. *Eye & contact lens* 35.3 (2009), pp. 133–143.

[34] P. Rojo, S. Royo, J. Ramírez, and I. Madariaga. “Numerical implementation of generalized Coddington equations for ophthalmic lens design”. *Journal of Modern Optics* 61.3 (2014), pp. 204–214.

[35] J. Loos, G. Greiner, and H.-P. Seidel. “A variational approach to progressive lens design”. *Computer-Aided Design* 30.8 (1998), pp. 595–602.

[36] H. Wallach, K. J. Frey, and K. A. Bode. “The nature of adaptation in distance perception based on oculomotor cues”. *Perception & Psychophysics* 11.1 (1972), pp. 110–116.

[37] S. W. Habtegiorgis, K. Rifai, M. Lappe, and S. Wahl. “Adaptation to skew distortions of natural scenes and retinal specificity of its aftereffects”. *Frontiers in psychology* 8 (2017), p. 1158.

[38] J. A. Saunders and B. T. Backus. “Perception of surface slant from oriented textures”. *Journal of Vision* 6.9 (2006), pp. 3–3.

[39] J. Farber and R. R. Rosinski. “Geometric transformations of pictured space”. *Perception* 7.3 (1978), pp. 269–282.

[40] F. H. Durgin and Z. Li. “Controlled interaction: Strategies for using virtual reality to study perception”. *Behavior Research Methods* 42.2 (2010), pp. 414–420.

[41] J. Tong, R. S. Allison, and L. M. Wilcox. “The impact of radial distortions in vr headsets on perceived surface slant”. *Electronic Imaging* 32 (2019), pp. 1–11.

[42] J. Zhang, M. L. Braunstein, and G. J. Andersen. “Effects of changes in size, speed, and distance on the perception of curved 3-D trajectories”. *Attention, Perception, & Psychophysics* 75 (2013), pp. 68–82.

[43] K Krause. “Acceptance of progressive lenses”. *Klinische Monatsblätter für Augenheilkunde* 209.2-3 (1996), pp. 94–99.

[44] C. W. Clifford et al. “Visual adaptation: Neural, psychological and computational aspects”. *Vision research* 47.25 (2007), pp. 3125–3131.

[45] A. Kohn. “Visual adaptation: physiology, mechanisms, and functional benefits”. *Journal of neurophysiology* 97.5 (2007), pp. 3155–3164.

[46] M. A. Webster. “Visual adaptation”. *Annual review of vision science* 1 (2015), pp. 547–567.

[47] H. D. Baker. “The instantaneous threshold and early dark adaptation”. *JOSA* 43.9 (1953), pp. 798–803.

[48] S. Hecht, C. Haig, and A. M. Chase. “The influence of light adaptation on subsequent dark adaptation of the eye”. *The Journal of general physiology* 20.6 (1937), pp. 831–850.

[49] M. Alpern et al. “Color adaptation: Sensitivity, contrast, after-images”. *Visual psychophysics* (1972), pp. 568–581.

[50] O. Rinner and K. R. Gegenfurtner. “Time course of chromatic adaptation for color appearance and discrimination”. *Vision research* 40.14 (2000), pp. 1813–1826.

[51] S. Anstis, F. A. Verstraten, and G. Mather. “The motion aftereffect”. *Trends in cognitive sciences* 2.3 (1998), pp. 111–117.

[52] J. J. Gibson. “Adaptation, after-effect and contrast in the perception of curved lines.” *Journal of experimental psychology* 16.1 (1933), p. 1.

[53] J. Campos, P. Freitas, E. Turner, M. Wong, and H.-J. Sun. “The effects of optical magnification/minimization on distance estimation by stationary and walking observers”. *Journal of Vision* 7.9 (2007), pp. 1028–1028.

[54] J. Mayhew and H. Longuet-Higgins. “A computational model of binocular depth perception”. *Nature* 297.5865 (1982), pp. 376–378.

[55] G. M. Gauthier and D. A. Robinson. “Adaptation of the human vestibuloocular reflex to magnifying lenses”. *Brain research* 92.2 (1975), pp. 331–335.

[56] K.-M. Tuan and R. Jones. “Adaptation to the prismatic effects of refractive lenses”. *Vision research* 37.13 (1997), pp. 1851–1857.

[57] H Collewijn, A. Martins, and R. Steinman. “Compensatory eye movements during active and passive head movements: fast adaptation to changes in visual magnification.” *The Journal of physiology* 340.1 (1983), pp. 259–286.

[58] J. Scheuhammer and B. Timney. “Adaptation to optically reduced size”. *Perception* 11.2 (1982), pp. 139–152.

[59] J. Droulez and V. Cornilleau. “Adaptive changes in perceptual responses and visuomanual coordination during exposure to visual metrical distortion”. *Vision Research* 26.11 (1986), pp. 1783–1792.

[60] H. Wallach and E. W. Flaherty. “Rapid adaptation to a prismatic distortion”. *Perception & Psychophysics* 19.3 (1976), pp. 261–266.

[61] H. L. Pick Jr and J. C. Hay. “Adaptation to prismatic distortion”. *Psychonomic Science* 1.1-12 (1964), pp. 199–200.

[62] S. W. Habtegiorgis, K. Rifai, and S. Wahl. “Transsaccadic transfer of distortion adaptation in a natural environment”. *Journal of vision* 18.1 (2018), pp. 13–13.

[63] D. Melcher. “Spatiotopic transfer of visual-form adaptation across saccadic eye movements”. *Current biology* 15.19 (2005), pp. 1745–1748.

[64] M. Turi and D. Burr. “Spatiotopic perceptual maps in humans: evidence from motion adaptation”. *Proceedings of the Royal Society B: Biological Sciences* 279.1740 (2012), pp. 3091–3097.

[65] E. Zimmermann, R. Weidner, R. O. Abdollahi, and G. R. Fink. “Spatiotopic adaptation in visual areas”. *Journal of Neuroscience* 36.37 (2016), pp. 9526–9534.

[66] N. Hutchings, E. L. Irving, N. Jung, L. M. Dowling, and K. A. Wells. “Eye and head movement alterations in naïve progressive addition lens wearers”. *Ophthalmic and Physiological Optics* 27.2 (2007), pp. 142–153.

[67] T. L. Alvarez, E. H. Kim, and B. Granger-Donetti. “Adaptation to progressive additive lenses: potential factors to consider”. *Scientific Reports* 7.1 (2017), p. 2529.

[68] J. Bist, D. Kaphle, S. Marasini, and H. Kandel. “Spectacle non-tolerance in clinical practice–a systematic review with meta-analysis”. *Ophthalmic and Physiological Optics* 41.3 (2021), pp. 610–622.

[69] B. Julesz. “Foundations of cyclopean perception.” (1971).

[70] N. Qian. “Binocular disparity and the perception of depth”. *Neuron* 18.3 (1997), pp. 359–368.

[71] D. Marr, T. Poggio, E. C. Hildreth, and W. E. L. Grimson. *A computational theory of human stereo vision*. Springer, 1991.

[72] S. M. Seitz, B. Curless, J. Diebel, D. Scharstein, and R. Szeliski. “A comparison and evaluation of multi-view stereo reconstruction algorithms”. In: *2006 IEEE computer society conference on computer vision and pattern recognition (CVPR’06)*. Vol. 1. IEEE. 2006, pp. 519–528.

[73] J. Wang, S. Wang, K. Ma, and Z. Wang. “Perceptual depth quality in distorted stereoscopic images”. *IEEE Transactions on Image Processing* 26.3 (2016), pp. 1202–1215.

[74] J. J. Gibson. *The perception of the visual world*. Boston: Houghton Mifflin, 1950.

[75] W. H. Warren and D. J. Hannon. “Direction of self-motion is perceived from optical flow”. *Nature* 336.6195 (1988), pp. 162–163.

[76] M. Lappe, F. Bremmer, and A. Van den Berg. “Perception of self-motion from visual flow”. *Trends in cognitive sciences* 3.9 (1999), pp. 329–336.

[77] W. H. Warren, B. A. Kay, W. D. Zosh, A. P. Duchon, and S. Sahuc. “Optic flow is used to control human walking”. *Nature neuroscience* 4.2 (2001), pp. 213–216.

[78] G. J. Andersen. “Perception of three-dimensional structure from optic flow without locally smooth velocity.” *Journal of Experimental Psychology: Human Perception and Performance* 15.2 (1989), p. 363.

[79] B. Sidaway, M. Fairweather, H. Sekiya, and J. Mcnitt-Gray. “Time-to-collision estimation in a simulated driving task”. *Human factors* 38.1 (1996), pp. 101–113.

[80] M. Lappe, M. Jenkin, and L. R. Harris. “Travel distance estimation from visual motion by leaky path integration”. *Exp. Brain Res.* 180 (2007), pp. 35–48.

[81] M. A. Hollands, D. E. Marple-Horvat, S. Henkes, and A. K. Rowan. “Human Eye Movements during Visually Guided Stepping”. *Journal of Motor Behavior* 27.2 (1995), pp. 155–163.

[82] A. E. Patla and J. N. Vickers. “Where and when do we look as we approach and step over an obstacle in the travel path?:” *NeuroReport* 8.17 (1997), pp. 3661–3665.

[83] D. Calow and M. Lappe. “Efficient encoding of natural optic flow”. *Network Comput. Neural Syst.* 19.3 (2008), pp. 183–212.

[84] B. M. ‘t Hart and W. Einhauser. “Mind the step: complementary effects of an implicit task on eye and head movements in real-life gaze allocation”. *Exp. Brain Res.* 223.2 (2012), pp. 233–249.

[85] J. S. Matthis, J. L. Yates, and M. M. Hayhoe. “Gaze and the control of foot placement when walking in natural terrain”. *Current Biology* 28.8 (2018), pp. 1224–1233.

[86] M. A. Hollands, A. E. Patla, and J. N. Vickers. ““Look where you’re going!”: gaze behaviour associated with maintaining and changing the direction of locomotion”. *Experimental Brain Research* 143.2 (2002), pp. 221–230.

[87] T Niemann, M Lappe, A Büscher, and K.-P. Hoffmann. “Ocular responses to radial optic flow and single accelerated targets in humans”. *Vision research* 39.7 (1999), pp. 1359–1371.

[88] F. A. Miles and C. Busettini. “Ocular compensation for self-motion”. *Ann. N.Y. Acad. Sci.* 656 (1992), pp. 220–232.

[89] M. Lappe, M. Pekel, and K. P. Hoffmann. “Optokinetic eye movements elicited by radial optic flow in the macaque monkey”. *J. Neurophysiol.* 79.3 (1998), pp. 1461–1480.

[90] D. E. Angelaki and B. J. M. Hess. “Self-motion-induced eye movements: effects an visual acuity and navigation”. *Nat. Rev. Neurosci.* 6 (2005), pp. 966–976.

[91] W. H. Warren and D. J. Hannon. “Eye movements and optical flow”. *J. Opt. Soc. Am. A* 7.1 (1990), pp. 160–169.

[92] M. Lappe and J. P. Rauschecker. “Motion anisotropies and heading detection”. *Biological Cybernetics* 72.3 (1995), pp. 261–277.

[93] D. Calow and M. Lappe. “Local statistics of retinal optic flow for self-motion through natural sceneries”. *Network: Computation in Neural Systems* 18.4 (2007), pp. 343–374.

[94] F. Bremmer, M. Kubischik, M. Pekel, K.-P. Hoffmann, and M. Lappe. “Visual selectivity for heading in monkey area MST”. *Experimental brain research* 200.1 (2010), p. 51.

[95] I. R. McLean, I. M. Erkelens, E. F. Sherbak, L. T. Mikkelsen, R. Sharma, and E. A. Cooper. “The contribution of image minification to discomfort experienced in wearable optics”. *Journal of Vision* 23.8 (2023), pp. 10–10.

[96] A. van den Berg. “Robustness of perception of heading from optic flow”. *Vision Research* 32.7 (1992), pp. 1285–1296.

[97] D. J. Heeger and A. D. Jepson. “Subspace methods for recovering rigid motion I: Algorithm and implementation”. *International Journal of Computer Vision* 7.2 (1992), pp. 95–117.

[98] M. Lappe and J. P. Rauschecker. “A neural network for the processing of optic flow from ego-motion in man and higher mammals”. *Neural Comp.* 5.3 (1993), pp. 374–391.

[99] A. J. Foulkes, S. K. Rushton, and P. A. Warren. “Heading recovery from optic flow: comparing performance of humans and computational models”. *Frontiers in Behavioral Neuroscience* 7 (2013), p. 53.

[100] F. Raudies and H. Neumann. “Modeling heading and path perception from optic flow in the case of independently moving objects”. *Frontiers in behavioral neuroscience* 7 (2013), p. 23.

[101] G. Côté, Y. Zhang, C. Menke, J.-F. Lalonde, and S. Thibault. “Inferring the solution space of microscope objective lenses using deep learning”. *Optics Express* 30.5 (2022), pp. 6531–6545.

[102] M. Luo, B. Bhandari, H. Li, S. Aberdeen, and S.-S. Lee. “Efficient lens design enabled by a multilayer perceptron-based machine learning scheme”. *Optik* 273 (2023), p. 170494.

[103] T. Yang, D. Cheng, and Y. Wang. “Designing freeform imaging systems based on reinforcement learning”. *Optics Express* 28.20 (2020), pp. 30309–30323.

[104] G. Côté, J.-F. Lalonde, and S. Thibault. “Deep learning-enabled framework for automatic lens design starting point generation”. *Optics express* 29.3 (2021), pp. 3841–3854.

[105] G. T. Fechner. *Elemente der Psychophysik*. Vol. 2. Breitkopf u. Härtel, 1860.

[106] G. A. Gescheider. “Psychophysical scaling”. *Annual review of psychology* 39.1 (1988), pp. 169–200.

[107] J. B. Kruskal. “Multidimensional scaling by optimizing goodness of fit to a nonmetric hypothesis”. *Psychometrika* 29.1 (1964), pp. 1–27.

[108] G. Marin, E. Terrenoire, and M. Hernandez. “Compared Distortion Effects between Real and Virtual Ophthalmic Lenses with a Simulator”. In: *Proceedings of the 2008 ACM Symposium on Virtual Reality Software and Technology*. VRST ’08. Bordeaux, France: Association for Computing Machinery, 2008, 271–272. ISBN: 9781595939517.

[109] M. García García, Y. Sauer, T. Watson, and S. Wahl. “Virtual reality (VR) as a testing bench for consumer optical solutions: a machine learning approach (GBR) to visual comfort under simulated progressive addition lenses (PALs) distortions”. *Virtual Reality* 28.1 (2024), pp. 1–13.

[110] S. S. Stevens. “Issues in psychophysical measurement.” *Psychological review* 78.5 (1971), p. 426.

[111] R. N. Shepard. “Psychological relations and psychophysical scales: On the status of “direct” psychophysical measurement”. *Journal of Mathematical Psychology* 24.1 (1981), pp. 21–57.

[112] W. S. Torgerson. “Theory and methods of scaling.” (1958).

[113] S. Haghiri, F. A. Wichmann, and U. von Luxburg. “Estimation of Perceptual Scales Using Ordinal Embedding”. *Journal of Vision* 20.9 (2020), p. 14.

[114] L. C. Vankadara, M. Lohaus, S. Haghiri, F. U. Wahab, and U. Von Luxburg. “Insights into ordinal embedding algorithms: A systematic evaluation”. *Journal of Machine Learning Research* 24.191 (2023), pp. 1–83.

[115] D.-E. Künstle, U. von Luxburg, and F. A. Wichmann. “Estimating the Perceived Dimensionality of Psychophysical Stimuli Using a Triplet Accuracy and Hypothesis Testing Procedure”. *Journal of Vision* 22.14 (2022), p. 3331.

[116] S. Barbero and J. Portilla. “Simulating real-world scenes viewed through ophthalmic lenses”. *J. Opt. Soc. Am. A* 34.8 (2017), pp. 1301–1308.

[117] A. S. Glassner. *An introduction to ray tracing*. Morgan Kaufmann, 1989.

[118] M. Born and E. Wolf. *Principles of optics: electromagnetic theory of propagation, interference and diffraction of light*. Oxford: Pergamon, 1964.

[119] C. M. Oman. “Motion sickness: a synthesis and evaluation of the sensory conflict theory”. *Canadian journal of physiology and pharmacology* 68.2 (1990), pp. 294–303.

[120] J. P. Wann, S. Rushton, and M. Mon-Williams. “Natural problems for stereoscopic depth perception in virtual environments”. *Vision research* 35.19 (1995), pp. 2731–2736.

[121] B. Rogers and R. Cagenello. “Disparity curvature and the perception of three-dimensional surfaces”. *Nature* 339.6220 (1989), pp. 135–137.

[122] B. N. Vlaskamp, H. R. Filippini, and M. S. Banks. “Image-size differences worsen stereopsis independent of eye position”. *Journal of Vision* 9.2 (2009), pp. 17–17.

[123] S. McNeill and W. R. Bobier. “The correction of static and dynamic aniseikonia with spectacles and contact lenses”. *Clinical and Experimental Optometry* 100.6 (2017), pp. 732–734.

[124] C. Anthes, R. J. García-Hernández, M. Wiedemann, and D. Kranzlmüller. “State of the art of virtual reality technology”. In: *2016 IEEE aerospace conference*. IEEE. 2016, pp. 1–19.

[125] R. Konrad, A. Angelopoulos, and G. Wetzstein. “Gaze-contingent ocular parallax rendering for virtual reality”. *ACM Transactions on Graphics (TOG)* 39.2 (2020), pp. 1–12.

[126] D. C. Niehorster, L. Li, and M. Lappe. “The accuracy and precision of position and orientation tracking in the HTC Vive Virtual Reality system for scientific research”. *i-Perception* 8.3 (2017), p. 2041669517708205.

[127] V. Clay, P. König, and S. Koenig. “Eye tracking in virtual reality”. *Journal of eye movement research* 12.1 (2019).

[128] E. Brunswik. “Representative design and probabilistic theory in a functional psychology.” *Psychological Review* 62.3 (1955), pp. 193–217.

[129] T. D. Parsons. “Virtual reality for enhanced ecological validity and experimental control in the clinical, affective and social neurosciences”. *Frontiers in human neuroscience* 9 (2015), p. 660.

[130] S. Shah and J. Aggarwal. “Intrinsic parameter calibration procedure for a (high-distortion) fish-eye lens camera with distortion model and accuracy estimation”. *Pattern Recognition* 29.11 (1996), pp. 1775–1788.

[131] Z. Zhang. “A flexible new technique for camera calibration”. *IEEE Transactions on pattern analysis and machine intelligence* 22.11 (2000), pp. 1330–1334.

[132] J. P. Rolland and T. Hopkins. *A method of computational correction for optical distortion in head-mounted displays*. University of North Carolina at Chapel Hill. Department of Computer Science, 1993.

[133] S. W. Habtegiorgis, K. Rifai, M. Lappe, and S. Wahl. “Experience-dependent long-term facilitation of skew adaptation”. *Journal of vision* 18.9 (2018), pp. 7–7.

[134] S. Habtegiorgis, C. Erlenwein, K. Rifai, and S. Wahl. “Interaction between form and motion processihabng contributes to habituation to distortions of the natural visual world”. *Journal of Vision* 18.10 (2018), pp. 626–626.

[135] K. Rifai, S. W. Habtegiorgis, C. Erlenwein, and S. Wahl. “Motion-form interaction: Motion and form aftereffects induced by distorted static natural scenes”. *Journal of vision* 20.13 (2020), pp. 10–10.

[136] S. W. Habtegiorgis, C. Jarvers, K. Rifai, H. Neumann, and S. Wahl. “The role of bottom-up and top-down cortical interactions in adaptation to natural scene statistics”. *Frontiers in neural circuits* 13 (2019), p. 9.

[137] S. Mathôt and J. Theeuwes. “A reinvestigation of the reference frame of the tilt-adaptation aftereffect”. *Scientific reports* 3.1 (2013), pp. 1–7.

[138] J. L. Gardner, P. Sun, R. A. Waggoner, K. Ueno, K. Tanaka, and K. Cheng. “Contrast adaptation and representation in human early visual cortex”. *Neuron* 47.4 (2005), pp. 607–620.

[139] D. C. Van Essen and C. H. Anderson. “Information processing strategies and pathways in the primate visual system”. *An introduction to neural and electronic networks* 2 (1995), pp. 45–76.

[140] S. Suzuki, C Clifford, and G Rhodes. “High-level pattern coding revealed by brief shape aftereffects”. In: *Fitting the mind to the world: Adaptation and after-effects in high-level vision*. Vol. 2. Oxford University Press Oxford, England, 2005, pp. 135–172.

[141] M. Zimmer and G. Kovacs. “Position specificity of adaptation-related face aftereffects”. *Philosophical Transactions of the Royal Society B: Biological Sciences* 366.1564 (2011), pp. 586–595.

[142] S.-R. Afraz and P. Cavanagh. “Retinotopy of the face aftereffect”. *Vision research* 48.1 (2008), pp. 42–54.

[143] F. Domini, W. Adams, and M. S. Banks. “3D after-effects are due to shape and not disparity adaptation”. *Vision research* 41.21 (2001), pp. 2733–2739.

[144] H. Wallach and W. Barton. “Adaptation to optically produced curvature of frontal planes”. *Perception & Psychophysics* 18.1 (1975), pp. 21–25.

[145] L. Li, L. Ni, M. Lappe, D. C. Niehorster, and Q. Sun. “No special treatment of independent object motion for heading perception”. *Journal of Vision* 18 (4).19 (2018), pp. 1–16.

[146] M. Lappe, F. Bremmer, M. Pekel, A. Thiele, and K.-P. Hoffmann. “Optic Flow Processing in Monkey STS: A Theoretical and Experimental Approach”. *The Journal of Neuroscience* 16.19 (1996), pp. 6265–6285.

[147] Y. Sauer, A. Sipatchin, S. Wahl, and M. García García. “Assessment of consumer VR-headsets’ objective and subjective field of view (FoV) and its feasibility for visual field testing”. *Virtual Reality* 26.3 (2022), pp. 1089–1101.

[148] Y. Sauer, M. Scherff, N. Stein, S. W. Habtegiorgis, M. Lappe, and S. Wahl. “Inconsistent self-motion perception between hemifields from optic flow distorted by progressive addition lenses”. *Journal of Vision* 22.14 (2022), pp. 4177–4177.

[149] A. J. Foulkes, S. K. Rushton, and P. A. Warren. “Flow parsing and heading perception show similar dependence on quality and quantity of optic flow”. *Front. Behav. Neurosci.* 7 (2013), p. 49.

[150] M Guillon. “Pilot evaluation of head and eye tracker system to study visual behavior with PAL amd single vision lenses”. *J. Am. Academy Optometry* 76 (1999), p. 181.

[151] K. Rifai and S. Wahl. “Specific eye–head coordination enhances vision in progressive lens wearers”. *Journal of Vision* 16.11 (2016), pp. 5–5.

[152] S. L. Smith, C. Maldonado-Codina, P. B. Morgan, and M. L. Read. “Gaze and behavioural metrics in the refractive correction of presbyopia”. *Ophthalmic and Physiological Optics* (2024).

[153] Y. Han, K. J. Ciuffreda, A. Selenow, and S. R. Ali. “Dynamic interactions of eye and head movements when reading with single-vision and progressive lenses in a simulated computer-based environment”. *Invest Ophthalmol Vis Sci* 44.4 (2003), pp. 1534–1545.

[154] J. R. Berard, J. Fung, B. J. McFadyen, and A. Lamontagne. “Aging affects the ability to use optic flow in the control of heading during locomotion”. *Experimental brain research* 194 (2009), pp. 183–190.

[155] A. Bubka, F. Bonato, and S. Palmisano. “Expanding and contracting optic-flow patterns and vection”. *Perception* 37.5 (2008), pp. 704–711.

[156] G. Aguilar, F. A. Wichmann, and M. Maertens. “Comparing sensitivity estimates from MLDS and forced-choice methods in a slant-from-texture experiment”. *Journal of Vision* 17.1 (2017), pp. 37–37.

[157] K. Emrith, M. Chantler, P. Green, L. Maloney, and A. Clarke. “Measuring perceived differences in surface texture due to changes in higher order statistics”. *JOSA A* 27.5 (2010), pp. 1232–1244.

[158] C. Charrier, L. T. Maloney, H. Cherifi, and K. Knoblauch. “Maximum Likelihood Difference Scaling of Image Quality in Compression-Degraded Images”. *Journal of the Optical Society of America A* 24.11 (2007), p. 3418.

[159] Y. Terada and U. Luxburg. “Local Ordinal Embedding”. In: *International Conference on Machine Learning*. 2014, pp. 847–855.

[160] J. C. Gower. “Generalized procrustes analysis”. *Psychometrika* 40 (1975), pp. 33–51.

[161] L. Breiman. “Random forests”. *Machine learning* 45 (2001), pp. 5–32.

[162] M. Scherff, Y. Sauer, M. Lappe, K. Rifai, N. Stein, and S. Wahl. “The effects of distorted optic flow in multifocal glasses on self-motion perception”. *Journal of Vision* 22.14 (2022), pp. 3911–3911.

[163] S. C. Cannon, R. J. Leigh, D. S. Zee, and L. A. Abel. “The effect of the rotational magnification of corrective spectacles on the quantitative evaluation of the VOR”. *Acta oto-laryngologica* 100.1-2 (1985), pp. 81–88.

[164] J. Demer, J. Goldberg, H. A. Jenkins, and F. I. Porter. “Vestibulo-ocular reflex during magnified vision: adaptation to reduce visual-vestibular conflict.” *Aviation, Space, and Environmental Medicine* 58.9 Pt 2 (1987), A175–9.

[165] P. B. Hibbard. “Virtual reality for ision science”. In: *Virtual Reality in Behavioral Neuroscience: New Insights and Methods*. Springer, 2023, pp. 131–159.

[166] P. Scarfe and A. Glennerster. “Using high-fidelity virtual reality to study perception in freely moving observers”. *Journal of vision* 15.9 (2015), pp. 3–3.

[167] K. Thurley. “Naturalistic neuroscience and virtual reality”. *Frontiers in Systems Neuroscience* 16 (2022), p. 896251.

[168] P. Pretto, M. Ogier, H. H. Bülthoff, and J.-P. Bresciani. “Influence of the size of the field of view on motion perception”. *Computers & Graphics* 33.2 (2009), pp. 139–146.

[169] S. Masnadi, K. P. Pfeil, J.-V. T. Sera-Josef, and J. J. LaViola. “Field of view effect on distance perception in virtual reality”. In: *2021 IEEE Conference on Virtual Reality and 3D User Interfaces (VR)*. IEEE. 2021, pp. 542–543.

[170] D. M. Hoffman, A. R. Girshick, K. Akeley, and M. S. Banks. “Vergence–accommodation conflicts hinder visual performance and cause visual fatigue”. *Journal of vision* 8.3 (2008), pp. 33–33.

[171] M. W. Morgan. “Accommodation and vergence”. *Optometry and Vision Science* 45.7 (1968), pp. 417–454.

[172] M. Kakimoto, T. Tatsukawa, Y. Mukai, and T. Nishita. “Interactive simulation of the human eye depth of field and its correction by spectacle lenses”. In: *Computer Graphics Forum*. Vol. 26. 3. Wiley Online Library. 2007, pp. 627–636.

[173] G. Kramida. “Resolving the vergence-accommodation conflict in head-mounted displays”. *IEEE transactions on visualization and computer graphics* 22.7 (2015), pp. 1912–1931.

[174] R. Beams, A. S. Kim, and A. Badano. “Transverse chromatic aberration in virtual reality head-mounted displays”. *Optics express* 27.18 (2019), pp. 24877–24884.

[175] C. Zhao, R. Beams, and A. Badano. “Radially variant contrast measurement in virtual reality headsets using circular concentric ring patterns”. *Journal of the Society for Information Display* 31.5 (2023), pp. 387–397.

[176] W. Robinett and R. Holloway. “The visual display transformation for virtual reality”. *Presence: Teleoperators & Virtual Environments* 4.1 (1995), pp. 1–23.

[177] J. Martschinke, J. Martschinke, M. Stamminger, and F. Bauer. “Gaze-dependent distortion correction for thick lenses in hmds”. In: *2019 IEEE Conference on Virtual Reality and 3D User Interfaces (VR)*. IEEE. 2019, pp. 1848–1851.

[178] R. S. Kennedy, N. E. Lane, K. S. Berbaum, and M. G. Lilienthal. “Simulator sickness questionnaire: An enhanced method for quantifying simulator sickness”. *The international journal of aviation psychology* 3.3 (1993), pp. 203–220.

[179] L. Fan et al. “Eye movement characteristics and visual fatigue assessment of virtual reality games with different interaction modes”. *Frontiers in Neuroscience* 17 (2023), p. 1173127.

[180] N. Dużmańska, P. Strojny, and A. Strojny. “Can simulator sickness be avoided? A review on temporal aspects of simulator sickness”. *Frontiers in psychology* 9 (2018), p. 2132.

[181] N. Stein et al. “A comparison of eye tracking latencies among several commercial head-mounted displays”. *i-Perception* 12.1 (2021).

[182] T. Sielhorst, W. Sa, A. Khamene, F. Sauer, and N. Navab. “Measurement of absolute latency for video see through augmented reality”. In: *2007 6th IEEE and ACM International Symposium on Mixed and Augmented Reality*. IEEE. 2007, pp. 215–220.

[183] A Sonnefeld. “Über die Verzeichnung bei optischen Instrumenten, die in Verbindung mit dem rollenden Auge gebraucht werden”. *Deutsche Optische Wochenschrift* 13 (1949), pp. 97–99.

[184] H. Merlitz. “Distortion of binoculars revisited: Does the sweet spot exist?” *JOSA A* 27.1 (2010), pp. 50–57.

[185] P. S. Heckbert. “Survey of texture mapping”. *IEEE computer graphics and applications* 6.11 (1986), pp. 56–67.

[186] P. Rojo, S. Royo, J. Ramírez, and I. Madariaga. “Numerical implementation of generalized Coddington equations for ophthalmic lens design”. *Journal of Modern Optics* 61.3 (2014), pp. 204–214.

[187] I. Amidror. “Scattered data interpolation methods for electronic imaging systems: a survey”. *Journal of electronic imaging* 11.2 (2002), pp. 157–176.

[188] N. Stein, K. Rifai, S. Wahl, and M. Lappe. “Simulating Lens Distortion in Virtual Reality”. In: *Proceedings of the 13th International Conference on Disability, Virtual Reality & Associated Technologies*. 2021.

[189] H. C. Longuet-Higgins and K. Prazdny. “The interpretation of a moving retinal image”. *Proceedings of the Royal Society of London. Series B, Biological Sciences* 208.1173 (1980), pp. 385–397.

[190] T. Albright and R. Desimone. “Local precision of visuotopic organization in the middle temporal area (MT) of the macaque”. *Experimental Brain Research* 65.3 (1987).

[191] K Prazdny. “Egomotion and relative depth map from optical flow”. *Biological cybernetics* 36.2 (1980), pp. 87–102.

[192] R. Hartley and S. B. Kang. “Parameter-free radial distortion correction with center of distortion estimation”. *IEEE Transactions on Pattern Analysis and Machine Intelligence* 29.8 (2007), pp. 1309–1321.

Appendices

A. Shader-based simulation of optical distortions

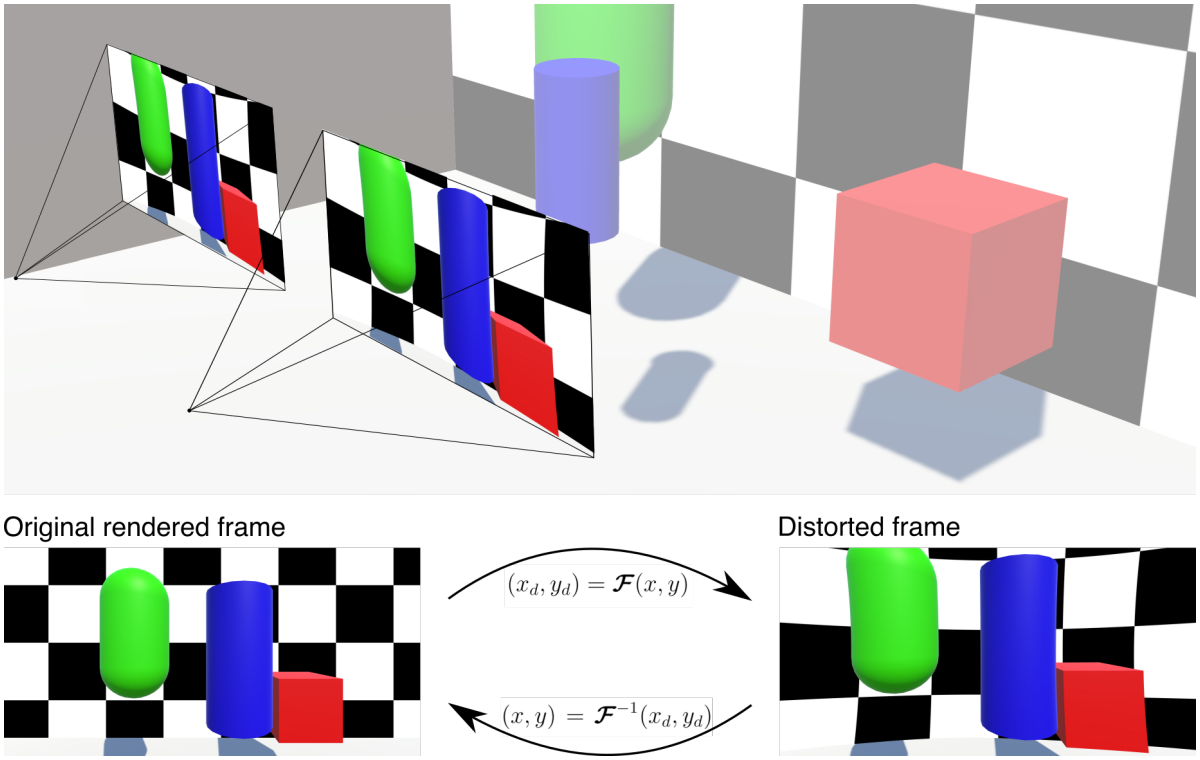

Figure A1.: Illustration of the VR distortion simulation
The rendering procedure for VR creates two independent textures for the left and right eye, illustrated here as two individual image planes in the 3D scene. Each rendered frame is transformed to represent a distorted image. The image transformation to distort the rendered texture is implemented as inverse mapping. For each location (x_d, y_d) in the output texture, the corresponding input position (x, y) can be mapped with the inverse distortion function $\mathcal{F}^{-1}$.

The psychophysical studies presented in this thesis used our newly developed VR simulation of optical distortions. The simulation is based on transforming the VR-rendered image, as a final post-processing step, based on precomputed distortion data.

In general, arbitrary distortion transformations are possible, allowing not only the simulation of real lens designs but also the presentation of artificial distortions for more control over the experimental stimulus.

As illustrated in Fig. A1, the image transformation (image warping) is applied independently to the left and right eye, which is necessary to account for possible differences in the distortion pattern between the two spectacle lenses. Each transformation individually follows the same procedure, described in the following.

We use a mathematical description of the distortions to model and simulate the transformation of visual input. For a point (x, y) in the visual field, the perceived distorted position when wearing PALs (x_d, y_d) can be described as a geometric transformation function (bijective mapping):

$$(x_d, y_d) = \boldsymbol{\mathcal{F}}(x, y) \tag{1}$$

Based on a measurement or simulation (ray tracing) of the optical displacement at discrete points, the transformation function can be approximated by subsequent fitting or interpolation for a continuous representation of distortions. For the work in this thesis, the distortion function builds the basis for modeling perceived distortions, simulating distorted optic flow, as well as implementing the VR simulation of optical distortions.

The distortion simulation was implemented in the game engine Unity (Unity Technologies, CA, USA) as a post-processing shader (a program part manipulating the rendered image), which acts as a final transformation of the rendered image. In the shader, for a point (x_d, y_d) in the output texture, we need the corresponding position (x, y) in the (undistorted) rendered image. This inverse mapping procedure is a fast way of applying image transformations [185], allowing to distort each frame of the simulation during runtime without compromising on resolution or frame rate. For this approach, it is necessary to determine the inverse distortion function $\boldsymbol{\mathcal{F}}^{-1}$ which maps the output (distorted) position (x_d, y_d) to the input (undistorted) position $(x, y) = \boldsymbol{\mathcal{F}}^{-1}(x_d, y_d)$. Based on this idea, the distortion simulation procedure can be divided into three steps:

- Precalculation of the inverse mapping function $\boldsymbol{\mathcal{F}}^{-1}$
- Adjusting the transformation for rendering parameters and saving as texture
- During runtime, loading the transformation function and performing inverse mapping in the post-processing shader

Precalculation of inverse mapping The transformation function $\boldsymbol{\mathcal{F}}$ as well as its inverse $\boldsymbol{\mathcal{F}}^{-1}$ can be interpolated from defined pairs of undistorted points (x, y) and distorted position (x_d, y_d). For a grid of points (x, y), the corresponding distorted points (x_d, y_d) are calculated by ray tracing (as described in [186]). Arbitrary points in between can then be interpolated. This means both components of $\boldsymbol{\mathcal{F}}$ or $\boldsymbol{\mathcal{F}}^{-1}$ are interpolated independently. As a result of the ray tracing, the point pairs do not lay on a perfect grid. I used Delaunay triangulation for the interpolation of scattered sample points [187].

Adjusting for rendering parameters Each VR headset has defined rendering parameters that determine the projection properties, including the rendered FoV. During runtime, in the post-processing shader, the render texture is accessed with relative coordinates (u, v) (in the range 0 to 1). Each relative location in the texture corresponds to point (x, y) in the visual field. By extracting the FoV extent of the rendered texture from the projection matrix in Unity, we can precalculate the mapping function $\boldsymbol{\mathcal{F}}^{-1}$ directly for relative coordinates (u, v). In general, the center of the rendered texture does not correspond to the center of the visual field for a straight gaze, for example, if the temporal FoV in VR is larger than the nasal. Therefore, we need four values l, r, b and t to describe the FoV extent of the rendered texture in the left, right, bottom, and top direction relative to the coordinate origin located in the center of the visual field. The inverse function $\boldsymbol{\mathcal{F}}^{-1}$ is transformed in advance for the specific VR headset (with specific rendering parameters l, r, b and t):

$$\begin{aligned} x &= u\,(r-l)+l \\ y &= v\,(t-b)+b \\ (u_{\text{inv}}, v_{\text{inv}}) &= \boldsymbol{\mathcal{F}}^{-1}\left(u\,(r-l)+l, v\,(t-b)+b\right) \end{aligned} \tag{2}$$

The two components of the mapping function are sampled for a high-resolution grid (u, v), and saved in independent color channels of a texture. The red value at a certain pixel in this texture describes horizontal inverse position u_{inv}, and the green value the vertical inverse position v_{inv} displacement at the corresponding location in the render texture. Saving the data as a texture has the advantage of easy loading in the shader because it is stored in the memory of the GPU and the shader automatically interpolates the mapping for arbitrary pixel locations.

Post processing shader for inverse mapping The pixel transformation is implemented as a fragment shader. For the location (u, v) the inverse transformed point is accessed from the red and green channels of the distortion texture. By performing the main calculations all beforehand, the complexity of the distortion simulation during runtime reduces to a simple texture sampling. First, the inverse distorted positions are read from the red and green color channels of the distortion texture.

```
uv_inverse = tex2D(_DistortionTex,i.uv).rg
```

Then the shader returns the main texture (undistorted input) sampled at the inverse distorted positions.

```
return tex2D(_MainTex,uv_inverse);
```

The use of eye tracking would also allow the simulation of gaze-contingent distortions. There can be small differences in the distortion pattern calculated for different gaze directions. This effect should also be considered as a possible contribution to the discomfort of PAL wearers since it describes how objects change perceived position between saccades or how the environment seems unstable during a smooth pursuit eye movement. Therefore, the implementation of a gaze-contingent distortion simulation can be a valuable tool for further research. To do so, distortion textures are precalculated for multiple gaze directions in a defined gaze location grid. During runtime, the current gaze direction is used to interpolate the current distortion pattern from precomputed distortion patterns. First, the four gaze-grid points around the current gaze location are determined. Then the inverse mapping function for the current gaze direction is calculated from those four distortion textures using bilinear interpolation. Currently the delay in eye tracking in VR in possible gaze tracking noise [188] limits the realism of this stimulation.

B. Simulation of distorted optic flow

For simulating the optic flow of a moving observer, a perspective projection is usually used, representing a simple pinhole camera model [189, 97, 92]. I will derive how this optic flow vector field is altered for a defined transformation function $\boldsymbol{\mathcal{F}}$, to represent the influence of distortions. Subsequently, distorted optic flow can be compared to the undistorted, and the influence on the information content of translation, rotation, and depth can be analyzed.

The perspective projection of a 3D point (X, Y, Z) in coordinates relative to the observer onto an image plane with coordinates (x, y) is

$$\begin{pmatrix} x \\ y \end{pmatrix} = \frac{1}{Z} \begin{pmatrix} X \\ Y \end{pmatrix} \tag{3}$$

where we chose the image plane distance $f = 1$ for simplification. The relative motion of a point (X, Y, Z) for an observer moving with translation $\boldsymbol{T} = (T_x, T_y, T_z)$ and rotation $\boldsymbol{\Omega} = (\Omega_x, \Omega_y, \Omega_z)$ is

$$\begin{pmatrix} \dot{X} \\ \dot{Y} \\ \dot{Z} \end{pmatrix} = - \left(\boldsymbol{T} + \boldsymbol{\Omega} \times \begin{pmatrix} X \\ Y \\ Z \end{pmatrix} \right) . \tag{4}$$

From eq. 3 and eq. 4 we can derive the optic flow $(\dot{x}, \dot{y})$:

$$\begin{pmatrix} \dot{x} \\ \dot{y} \end{pmatrix} = \frac{1}{Z} \begin{pmatrix} -1 & 0 & x \\ 0 & -1 & y \end{pmatrix} \boldsymbol{T} + \begin{pmatrix} xy & -(1+x^2) & y \\ 1+y^2 & -xy & -x \end{pmatrix} \boldsymbol{\Omega} \tag{5}$$

When simulating an observer fixating a point at distance d, we can account for the eye rotation that keeps the image centered at the fixation target (vestibulo-ocular reflex) by defining $\boldsymbol{\Omega}$ in a way that keeps the motion of the center point $(0, 0)$ at zero:

$$\boldsymbol{\Omega} = \frac{1}{d} \begin{pmatrix} T_y \\ -T_x \\ 0 \end{pmatrix} \tag{6}$$

With this approach, we can simulate optic flow for arbitrary motion scenarios in arbitrary environments. Usually, the three-dimensional points describing the environment (e.g. the ground plane used in 3.2) are calculated by back-projecting defined two-dimensional points in the visual field into the 3D scene. Using this method, we

can analyze the optic flow vector field at predefined points in the visual field, allowing the comparison of flow vectors between different distortions, motion scenarios, or environments.

Optical distortions do not only change the perceived position but also the velocity of points in the visual field. To simulate the influence of distortions on optic flow, we take the derivative of the distorted position with respect to time.

$$\begin{pmatrix} \dot{x}_d \\ \dot{y}_d \end{pmatrix} = \frac{d}{dt} \begin{pmatrix} \mathcal{F}_x\left(x, y\right) \\ \mathcal{F}_y\left(x, y\right) \end{pmatrix} = \begin{pmatrix} \frac{\partial \mathcal{F}_x}{\partial x} & \frac{\partial \mathcal{F}_x}{\partial y} \\ \frac{\partial \mathcal{F}_y}{\partial x} & \frac{\partial \mathcal{F}_y}{\partial y} \end{pmatrix} \begin{pmatrix} \dot{x} \\ \dot{y} \end{pmatrix}. \tag{7}$$

This is the distorted optic flow perceived at location (x_d, y_d) in the visual field. To compare undistorted and flow fields at the same retinal locations, we need to calculate the distorted optic flow originating from a different point in 3D space. By applying the inverse distortion function to a location (x, y) before projecting back into 3D space, we get the distorted optic flow perceived at location $\boldsymbol{\mathcal{F}}\left(\boldsymbol{\mathcal{F}}^{-1}(x, y)\right) = (x, y)$.

To summarize, we compare distorted and undistorted optic flow fields, by first defining locations in the visual field for which we want to evaluate optic flow. Then we calculate the corresponding points in 3D, individually for undistorted and distorted perception. Using eq. 5 we calculate undistorted optic flow fields, individually for both sets of 3D points. For the distorted optic flow, we have to additionally multiply the flow field vectors with the Jacobian of the transformation function as derived in eq. 7.

A more refined version of the simulation could account for the adjustment of eye movements for the new magnification, by modifying the rotational component Ω.

In our implementation, the transformation function $\boldsymbol{\mathcal{F}}$ and the derivatives are interpolated from ray-traced distortion grid points.

Estimation of heading and rotation

For the estimation of heading and rotation from distorted optic flow, we followed the subspace algorithm [97] as implemented in the population heading map model [92, 146]. This algorithm computes least-squares residuals over a defined set of heading candidates. The lower the residual value, the better the heading candidate describes the given flow field. The minimum in the residual surface is taken as an estimation of the heading. To calculate the residual values, we split the flow field into smaller, locally restricted patches that are evaluated separately. The estimation then takes the minimum of the sum of the individual residual surfaces to increase the robustness of

the estimation. Optic flow is calculated inside randomly placed patches. For the simulations presented in chapter 3.2, we used 50 random patches with 50 total simulation runs. The residual surfaces are calculated per patch. To account for cortical magnification we scale the size of patches with eccentricity ϵ. Based on findings in the visual system of primates [190, 93, 83] we chose to scale the patch area with

$$A = (1.04^\circ + 0.61\epsilon)^2 \tag{8}$$

After the estimation of the heading, the remaining difference between the distorted and estimated flow fields can be used to extract rotational motion components and the depth of the scene [191, 97].

C. Analysis of PAL distortions

As described in chapter 1, PAL distortions can never be fully removed, only variations in the shape are possible. The given individual far and near correction determines the overall shape of distortions. A positive spherical power, correcting vision for hyperopia, causes a magnification of the image which increases towards the periphery. This type of distortion is called pincushion distortion. Straight lines are bowed inwards.

For a negative lens (concave) the image is scaled down and gets smaller towards the periphery, causing straight lines to bend outwards (barell distortion). For many optical devices distortions are radially symmetric. For PALs, the increase of power towards the lower part introduces an asymmetry in the distortion pattern. Increasing power in the lower part of the lens leads to increasing magnification. For positive lenses this increases the overall radial distortions. In case of negative lenses though, the increase in power can partly compensate the distortion in the lower visual field. The pattern in the lower part looks closer to undistorted, but at the same time the overall image is more asymmetrically distorted.

The transformation function $\mathcal{F}$, interpolated from ray-traced distortion data, can be analyzed through different decompositions. The local derivative (Jacobian matrix), which we used before in the simulation of distorted optic flow, locally describes an affine transformation. An intuitive interpretation is given the decomposition of the Jacobian into horizontal magnification, vertical magnification, skew distortion, and rotation:

$$\begin{pmatrix} \frac{\partial \mathcal{F}_x}{\partial x} & \frac{\partial \mathcal{F}_x}{\partial y} \\ \frac{\partial \mathcal{F}_y}{\partial x} & \frac{\partial \mathcal{F}_y}{\partial y} \end{pmatrix} = \text{magn}_{\text{hor}} \begin{pmatrix} 1 & 0 \\ 0 & 0 \end{pmatrix} + \text{magn}_{\text{ver}} \begin{pmatrix} 0 & 0 \\ 0 & 1 \end{pmatrix} + \text{skew} \begin{pmatrix} 0 & 1 \\ 1 & 0 \end{pmatrix} + \text{rot} \begin{pmatrix} 0 & 1 \\ -1 & 0 \end{pmatrix} \quad (9)$$

The location-dependent values of this decomposition are shown for two example PALs in Fig. A2. The rotation component is negligible. Magnification and skew distortions are the only contributions. In general, PALs either magnify or minify the image, depending on the sign of optical power, both increasing towards the periphery. Additionally, the image is skewed in different directions in the four quadrants.

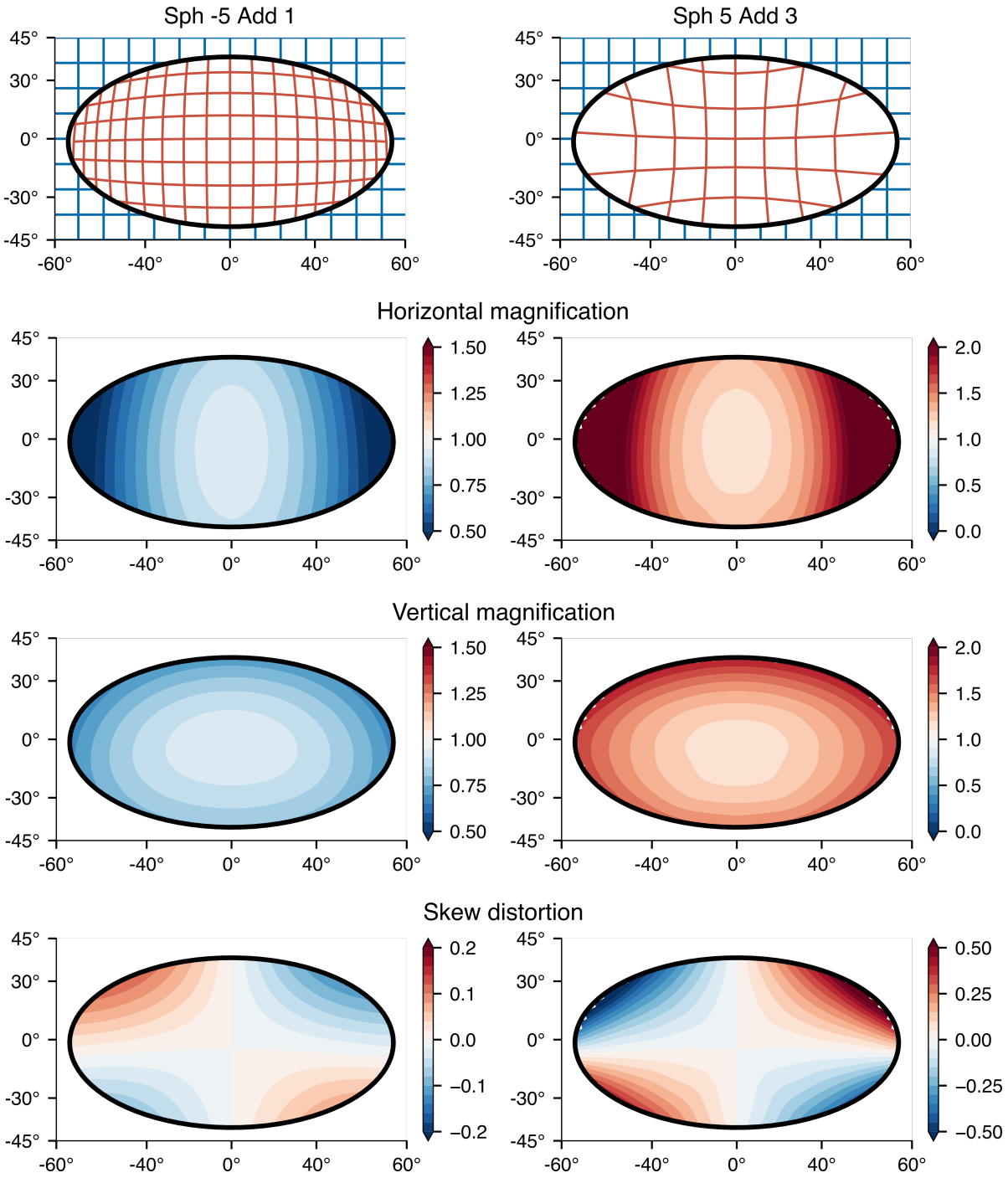

Figure A2.: Distortion components of magnification and skew distortions computed locally for two example PALs, a negative power lens (Sph -5 dpt) and a positive power lens (Sph +5 dpt). Axes labels are in visual angle, describing the position in the visual field. Distortions are computed inside of an ellipse, representing the FoV of a typical spectacle frame. For the negative lens, the image is minified (magnification < 1), for the positive lens it is magnified, with increasing minification/magnification towards the periphery. Both lenses lead to skew distortions with changing direction between the four quadrants in the visual field. The orientation of skew is opposite between the two lenses.

While a decomposition in magnification and skew help for a more intuitive understanding of PAL distortions, they describe the transformation only locally. For modeling and quantifying the perceptual effects of PAL distortions, it would be beneficial to describe the global distortion pattern using a suitable parameterization. This reduced number of parameters would help in describing the actual degrees of freedom of PAL distortions in lens design, and allow psychophysical experiments to describe perception depending on a few parameters. The goal would be to describe perception based on those parameters.

A decomposition into radial and tangential distortions is usually used for parameterizing camera distortions [130, 131]. The displacement vector $d = (x_d, y_d) - (x, y)$ is decomposed into a radial component d_{rad} and a tangential component d_{tang}:

$$d = d_{\text{rad}} \begin{pmatrix} x \\ y \end{pmatrix} \frac{1}{r} + d_{\text{tang}} \begin{pmatrix} -x \\ y \end{pmatrix} \frac{1}{r} \tag{10}$$

where $r = \sqrt{x^2 + y^2}$. This decomposition still describes the displacement locally, but the radial and tangential components can parametrized more easily.

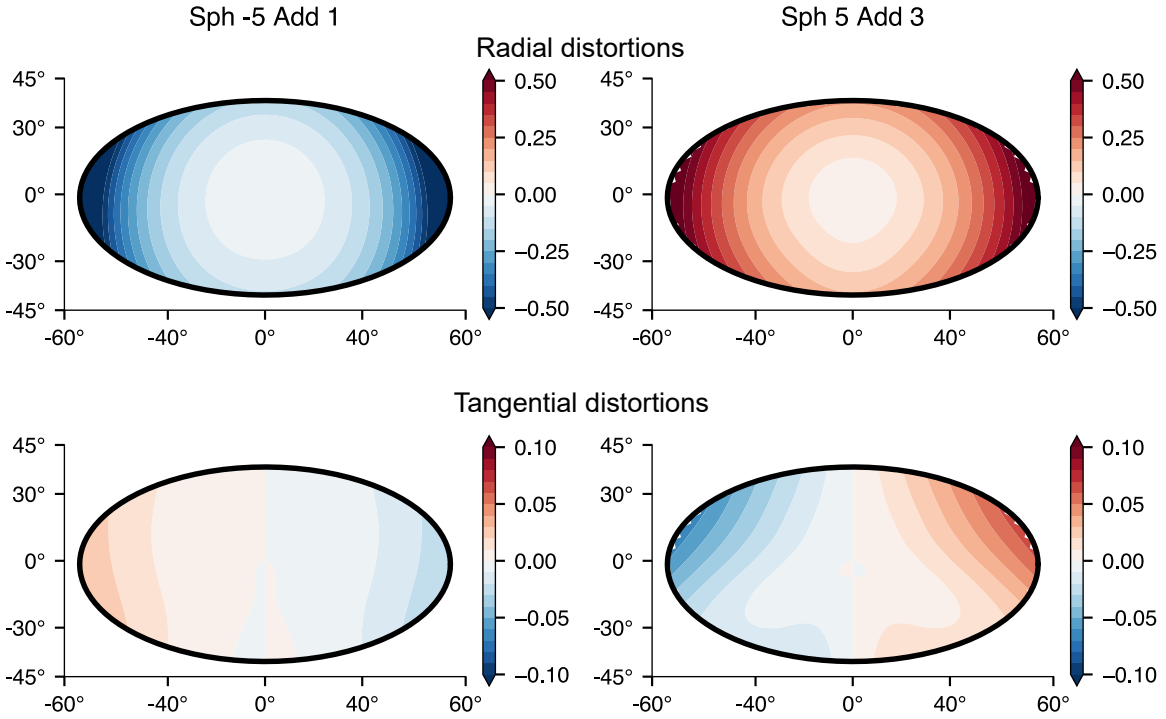

Figure A3.: PAL distortions expressed as a combination of radial and tangential displacement. Radial displacement increases radially. The systematic tangential displacement shows the vertical asymmetry in radial displacement.

Tangential distortions can often be neglected for camera lens calibration. For PAL distortions, as the decomposition in Fig. A3 shows, there is a not negligible amount of tangential distortions. Additionally, the radial distortion changes, with a vertical asymmetry in the displacement caused by the change of curvature along the vertical direction. I suggest modeling this asymmetry as a displacement of the center of radial distortions, an approach that has been suggested before to improve camera calibration for possibly misaligned optical elements [192]. An approximation for PAL distortions could be described by a combination of magnification (as a global linear scaling factor), additional radial distortions (as a polynomial of the eccentricity), and one additional parameter for the vertical displacement of the radial distortion center. This parameterization can be used to describe differences between designs and, at the same time, the number of parameters is manageable for performing psychophysical experiments that quantify the relative influence of each parameter. A quantification of the relative influence of each component of distortions could help in developing a predictive model to rate lens designs in terms of distortion perception already during the development process.

Publications

frontiers in Psychology

ORIGINAL RESEARCH
published: 20 November 2020
doi: 10.3389/fpsyg.2020.544867

Parallel Adaptation to Spatially Distinct Distortions

Yannick Sauer[1]*, *Siegfried Wahl*[1,2] and *Katharina Rifai*[1,2]

[1] Institute for Ophtalmic Research, University of Tuebingen, Tuebingen, Germany, [2] Carl Zeiss Vision International GmbH, Aalen, Germany

Optical distortions as a visual disturbance are inherent in many optical devices such as spectacles or virtual reality headsets. In such devices, distortions vary spatially across the visual field. In progressive addition lenses, for example, the left and right regions of the lens skew the peripheral parts of the wearers visual field in opposing directions. The human visual system adapts to homogeneous distortions and the respective aftereffects are transferred to non-retinotopic locations. This study investigates simultaneous adaptation to two opposing distortions at different retinotopic locations. Two oppositely skewed natural image sequences were presented to 10 subjects as adaptation stimuli at two distinct locations in the visual field. To do so, subjects were instructed to keep fixation on a target. Eye tracking was used for gaze control. Change of perceived motion direction was measured in a direction identification task. The point of subjective equality (PSE), that is, the angle at which a group of coherently moving dots was perceived as moving horizontal, was determined for both retinal locations. The shift of perceived motion direction was evaluated by comparing PSE before and after adaptation. A significant shift at both retinal locations in the direction of the skew distortion of the corresponding adaptation stimulus is demonstrated. Consequently, parallel adaptation to two opposing distortions in a retinotopic reference frame was confirmed by this study.

Keywords: visual adaptation, distortions, motion aftereffect, natural scenes, psychophysics, visual system

OPEN ACCESS

Edited by:
Jesús Malo,
University of Valencia, Spain

Reviewed by:
Guido Marco Cicchini,
National Research Council (CNR), Italy
Takahiro Kawabe,
Nippon Telegraph and Telephone, Japan

***Correspondence:**
Yannick Sauer
yannick.sauer@uni-tuebingen.de

Specialty section:
This article was submitted to Perception Science, a section of the journal Frontiers in Psychology

Received: *23 March 2020*
Accepted: *01 September 2020*
Published: *20 November 2020*

Citation:
Sauer Y, Wahl S and Rifai K (2020) Parallel Adaptation to Spatially Distinct Distortions. Front. Psychol. 11:544867. doi: 10.3389/fpsyg.2020.544867

1. INTRODUCTION

Many optical devices induce spatial distortions of the visual field as a part of their optical aberrations. An example is the progressive addition lens (PAL) (Meister and Fisher, 2008). But also other optical devices like virtual-reality-headsets (Kuhl et al., 2009) cause geometric distortions, which alter different features of visual perception, such as size, motion, form, and distance of objects (Faubert, 2002; Lord et al., 2002; Habtegiorgis et al., 2018b). This interference with visual perception can have negative impacts on day-to-day life in the form of nausea and discomfort (Johnson et al., 2007), distance misjudgment (Kuhl et al., 2009), or tripping (Timmis et al., 2010). Additional severity is given by the fact that usually optically induced distortions are not homogeneous but vary across the visual field. For example, in progressive addition lenses, distortions are oppositely oriented in the left and right periphery (Meister and Fisher, 2008) or in virtual-reality-headsets they are radially varying (Kuhl et al., 2009).

The human visual system copes with changes in the perception by visual adaptation. Visual adaptation is the change of information processing as a response to alterations in visual input statistics (Clifford et al., 2007; Webster, 2015). Adaptation processes take place over many levels

of the visual system continuously changing perception as a reaction to changes of all kinds of visual features from simple attributes such as orientation (Jin et al., 2005), contrast (Bao and Engel, 2012), or motion direction (Clifford, 2002; Knapen et al., 2009), which are processed in early levels of the visual system, to more complex attributes such as facial features (Leopold et al., 2005). Adaptation expresses in a normalization of visual information, which may be a benefit for the visual system in the form of efficiency of coding information (Clifford et al., 2007) or supporting constancy of perception (Foster, 2011).

Optical distortions change multiple visual features at the same time. Depending on the feature content of the distorted stimulus, adaptation occurs in multiple cortical areas. The visual system can adapt to changed orientation of objects, which could be caused by distortions. The perceived orientation of test stimuli changes after adaptation to tilted stimuli. This is known for adaptation with simple rotated geometric patterns (Gibson and Radner, 1937), as well as natural stimuli with a preferred orientation (Dekel and Sagi, 2015). Also motion statistics of a stimulus are altered by distortions. Adaptation can change perceived motion direction as well as speed of a test stimulus (Anstis et al., 1998). Furthermore, there are experiments proving interaction between visual perception of form and motion features (Mather et al., 2012). Adaptation to still images depicting motion can evoke motion aftereffects (Winawer et al., 2008). Vice versa motion signals can influence the perception of form (Uttal et al., 2000; Apthorp et al., 2011).

In progressive addition lenses skew distortions are the prominent type of distortion. After adaptation to skew distorted natural stimuli, the perceived level of image skew of a static pattern changes (Habtegiorgis et al., 2017) as well as perceived motion direction of a test stimulus (Habtegiorgis et al., 2019). The first study also showed that during fixation, the aftereffect is transferred to retinal locations without adaptation stimulation. Thus, adaptation to homogeneous skew distortions is, at least in parts, independent of the retinal location. This result is an indication for the involvement of higher cortical levels with larger receptive field sizes and processing mechanisms for complex form and motion features. It is not clear what kind of aftereffects will occur when different retinal locations are exposed simultaneously to adaptation stimuli with different distortions, similar to the situation of progressive lens wearers. Spatially localized aftereffects have been shown for several different adaptation processes: Low and also mid-level visual features like orientation (Blakemore and Campbell, 1969), spatial frequency (Ejima and Takahashi, 1984), perceived numerosity (Burr and Ross, 2008), or duration perception (Johnston et al., 2006) presumably have a small receptive field size, allowing localized aftereffects. With natural stimulus, content processed in higher visual areas and also the receptive field size increases leading to the transfer of aftereffects. Even for simple geometric shapes, transfer of distortion aftereffects has been shown, leading to a changed perception of elongation or curvature after brief presentation of elongated or curved shapes preceding the test stimulus (Suzuki and Cavanagh, 1998). Consequently, the presence of localized aftereffects in distortion adaptation with natural stimuli is not clear and requires investigation.

In this study, we want to examine the rivalry between global aftereffects, as they would be expected from transfer of adaptation, and local aftereffects, which would occur for local independent adaptation. To discriminate between the two cases, we designed a psychophysical experiment in which the two types of adaptation would lead to aftereffects with opposite directions. We use an adaptation stimulus for which the transfer of aftereffects has been shown and a second adaptation stimulus is added with the opposite skew direction. Local adaptation to the second stimulus should lead to a shift of perception in the direction opposite to the aftereffect from transferred adaptation. Usually distortions of optical devices are not homogeneous but vary across the visual field. To cope with the changed visual input by adaptation, the visual system needs to be able to adapt locally with a spatial variation of aftereffect directions.

In this experiment, parallel adaptation to two distorted stimuli at spatially distinct locations is studied. The homogeneously but oppositely skewed adaptation stimuli in the form of natural image sequences are shown simultaneously at two distinct locations in the visual field with the same eccentricity. For the same skew distorted natural stimulus, both motion and form aftereffects are known to occur (Habtegiorgis et al., 2017, 2019), since both motion and form features are altered by skew distortions. Additionally, because of interaction between the processes of motion and form adaptation only one type of aftereffect is used in our experiment as measurement for skew distortion adaptation. Aftereffects were measured in a motion direction identification task, at the same retinal locations as the presentation of adaptation stimuli. Results show a simultaneous shift of perceived direction in opposing directions for both retinal test locations after parallel adaptation. Each shift corresponds to the skew direction of the corresponding adaptation stimulus.

2. METHODS

Adaptation to spatially varying distortions was studied by presenting oppositely skewed natural image sequences at two distinct locations in the periphery simultaneously. Gaze was fixed centrally between the stimulus locations. Aftereffects to adaptation were measured in a motion direction identification task at the same two distinct locations.

2.1. Study Approval

The study was approved by the Ethics Committee of the Medical Faculty of the Eberhard Karls Universität Tübingen and the University Hospital.

2.2. Observers

Nine observers (six male and three female aged between 21 and 28) with normal or corrected-to-normal vision participated in the study. All but one were naive about the purpose of the study. The experiment was conducted in accordance with the Declaration of Helsinki and participants gave their informed written consent.

2.3. Set-Up

Stimuli were shown on a ViewPixx monitor (VPixx Technologies Inc., Canada) with a resolution of $1,920 \times 1,200$ pixels and a refresh rate of 120 Hz viewed at a distance of 65 cm. The monitor covered a visual angle of 41° horizontally and 24° vertically. Gaze of the subjects was controlled by an EyeLink 1000 Plus eye tracker (SR Research, Canada) at a sampling rate of 1 kHz. Viewing distance and head position was fixed by using a chin and forehead rest. The up and down keys on a keyboard were used by the subjects to respond in the test phase. The experiment was run with the Psychophysics Toolbox (Brainard, 1997) in Matlab (Mathworks, USA). Viewing was monocular.

2.4. Stimuli

2.4.1. Adaptation Stimulus

Adapting stimuli were generated by skew distorting natural image sequences from an open source movie (Baumann, 2010). The frames of size $1,200 \times 720$ pixels were skewed using MATLAB (Mathworks, USA) by mapping the pixel position (x, y) in the undistorted frame to the new positions (x_s, y_s) given by the transformation:

$$\begin{pmatrix} x_s \\ y_s \end{pmatrix} = \begin{pmatrix} x + y \tan\theta \\ y + x \tan\theta \end{pmatrix} \quad (1)$$

with the angle θ defining a shear mapping in vertical and horizontal direction with the same amount. To reduce boundary effects, the frames were cropped to a size of 650×650 pixels and masked with a Hanning window function

$$w(r) = \cos^2\left(\frac{\pi r}{N}\right) \quad (2)$$

where r is the distance to the center of the frame and $N = 650$ pixels is the width of the frame. Two kinds of stimuli, with opposite skew of $\theta = 25°$ and $\theta = -25°$, were prepared. They are shown in **Figure 1A**.

2.4.2. Test Stimulus

To test adaptation aftereffects, a random dot test was used. White dots with diameter 5 pixels on a black background were randomly positioned within a circle of diameter 14° visual angle and moved coherently at a speed of 6.6° visual angle per second. Direction of motion was diagonally upwards or downwards randomly to the left or right with an angle to the horizontal chosen randomly out of $\pm 8, \pm 6.5, \pm 5, \pm 3.5, \pm 2, \pm 0.5°$. Dots moving outside of the circle were randomly repositioned at the opposite side of the circle ($\varphi \in [90° + \theta, 270° + \theta]$). The dot stimulus was masked with the same Hanning window function as the adaptation image sequences.

2.5. Procedure

Subjects were lead into the study room, seated on a chair, and introduced to the experiment procedure. The room was darkened and subjects performed a few test trials before the actual experiment started. Three different phases of the experiment are illustrated in **Figure 1C**. In the pre-adaptation phase, the baseline perception of motion direction was assessed. In repeated trials, random dots moved on the screen and subjects answered the perceived direction of motion. The second phase was the adaptation phase. Two oppositely distorted adaptation stimuli were shown simultaneously on the screen. The perception after adaptation was measured in the post-adaptation phase in a procedure similar to the first phase.

As illustrated in **Figure 1**, two distinct stimulus locations on the screen were used for both adaptation and the test stimuli. They were on the left and right side of the screen with their centers both at a distance of 9° visual angle to the screen center. In the middle between the stimulus locations during the whole experiment, a small dot (14 pixels in diameter, 0.3° visual angle) indicated the fixation target for the subjects.

In the trials of the pre-phase, the moving dot test was performed consecutively on the left and right side with the first position chosen randomly from the two stimulus locations. The dots moved for 0.3s randomly to the left or right with an angle to the horizontal chosen randomly form the given set, after which subjects answered the perceived direction of motion by clicking up or down on a keyboard. The experiment continued only after a valid key was pressed. Then, after a 0.5-s break after the key press, the test was repeated at the opposite stimulus location. Each of these trials was followed by a short top-up adaptation of 4 s. In the pre-phase, undistorted image sequences were used and presented simultaneously at both stimulus locations. After a break of 0.5 s, the next trial started with a random dot test. In 64 trials, each stimulus angle was tested 6 times (only 4 times for large angles of ±8 and ±6.5°) in a randomized order.

The second phase induced adaptation by presenting the skewed images sequences for 5 min without interruption. Always oppositely distorted stimuli were used for the two stimulus locations, but location was randomly interchanged between subjects. Also in this phase the fixation point was shown in the center of the screen.

The third phase, the post-adaptation phase, was similar to the first phase, but distorted stimuli consistent with the adaptation phase were used as top-up adaptation.

To ensure that always the same retinal locations were stimulated, during adaptation and test the subjects' gaze was controlled and the adaptation stimuli vanished in <20 ms (under two monitor refresh cycles Saunders and Woods, 2014) when subjects blinked or their gaze deviated from the fixation point by more than 2°. The stimuli appeared back as soon as measured gaze was inside the fixation area again. In the test trials, the subjects' gaze was controlled before presentation of the stimulus and the dots were only shown when gaze was inside the fixation area. Otherwise, the current trial was aborted and repeated at the end of the phase.

3. ANALYSIS

To measure aftereffects following adaptation to skewed natural image sequences, the change of perceived motion direction

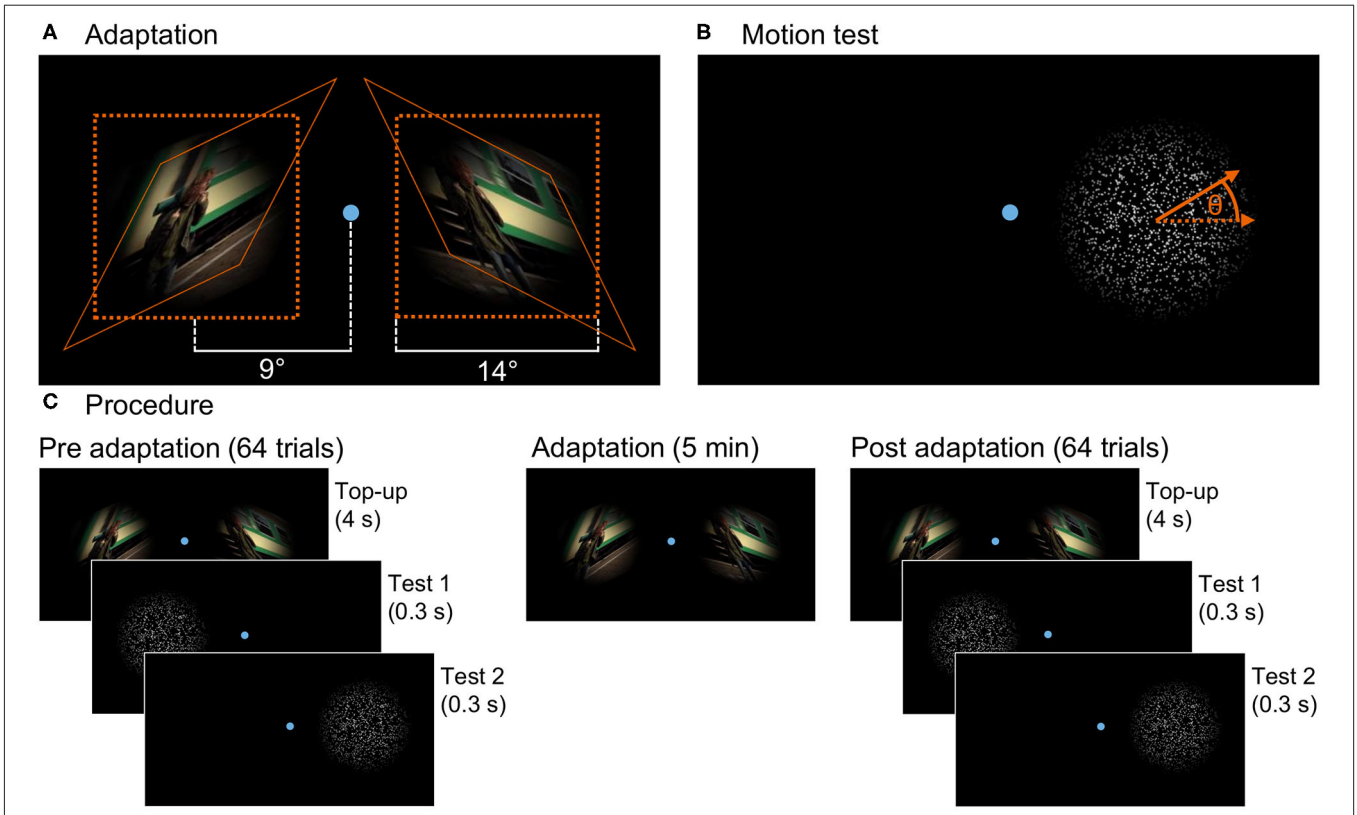

FIGURE 1 | (A) Presentation in the adaptation phase: The figure shows one frame of both skewed stimuli and their placement on the screen together with the fixation point. The natural image sequence was skewed with angle $\theta = 25^\circ$ for the left and $\theta = -25^\circ$ for the right stimulus. After skewing, the stimuli were masked with a Hanning window function. The orange lines indicate how a square of the original video gets transformed by the skew mapping. **(B)** Test stimulus: Randomly distributed dots moving coherently in one direction with the angle θ to the horizontal randomly chosen out of a limited set for each trial. Here, the test for the right stimulus location is shown. During the experiment, both stimulus locations were tested sequentially. **(C)** Three phases of the experiment: In the pre- and post-adaptation phases, the motion direction perception test is presented at both locations on the screen (in a random order) interrupted by top-up adaptation stimuli in 64 trials each. In the adaptation phase, only the adaptation stimuli are shown for a duration of 5 minutes.

was evaluated by comparing the stimulus level perceived as a horizontal movement between pre- and post-adaptation phases.

The percentage of trials answered upwards depending on the stimulus level was determined for both stimulus locations in the pre- and post-phase. Dots perceived as moving to the left diagonally downwards correspond to the same axis of motion (and therefore the same level of skew distortion) as dots moving to the right but upwards. Thus, to collapse data from trials with different horizontal motion direction for analysis, answers for trials with movement to the left were inverted. The obtained curves of percentage of upwards answers depending on stimulus level were fitted for every subject with a psychometric function (cumulative normal distribution function with free but equal asymptotes) using Psignifit (Schütt et al., 2016) in Matlab. The 50% point of the fit function is used as a measurement for the point of subjective equality (PSE), that is, the stimulus level in degree which is perceived as a horizontal motion. The shift $\Delta\text{PSE} = \text{PSE}_{\text{post}} - \text{PSE}_{\text{pre}}$ between pre- and post-adaptation phases is computed as a measurement of aftereffects.

To collapse data from subjects with positive skew on the left and negative on the right stimulus location and other subjects with negative skew on the left and positive skew on the right stimulus location, in our analysis all subjects were treated as having positive skew at the left location and negative skew at the right location by inverting ΔPSE for subjects with the negatively skewed adaptation stimulus at the left stimulus location. In this way, for the left stimulus location a positive shift ΔPSE represents a change of perceived motion direction (into the negative) opposing the skew direction of the corresponding adaptation stimulus. For the right stimulus location, ΔPSE is negative if motion perception changes opposing the adaptation stimulus.

For statistical analysis, one-sample *t*-test was used with ΔPSE for the left and right stimulus location to test the presence of a shift in perceived motion direction. A paired *t*-test was conducted with both ΔPSE to evaluate the significance of the difference between both stimulus locations.

4. RESULTS

Figure 2 shows the number of upwards answers depending on the stimulus level and the fits of the psychometric function for

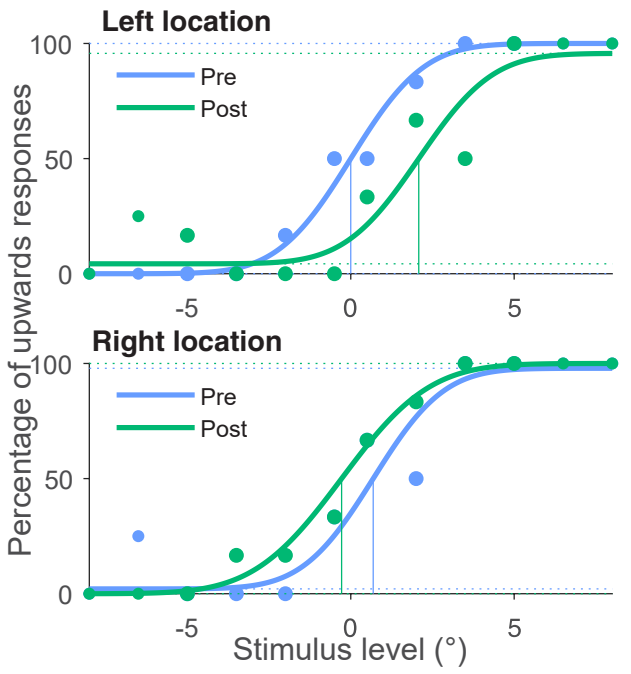

FIGURE 2 | Percentage of upwards responses and psychometric fits for one exemplary subject. The blue data points were obtained in the baseline measurement in phase one of the experiment and the green data points in the last phase after adaptation. All four curves were fitted with a psychometric function. The 50% point of the fit function is taken as the Point of Subjective Equality (PSE). The PSE for this subject shifted by 2.1° for the left stimulus location, where the adaptation stimulus was left skewed (negative skewing angle). For the right stimulus location, this subject's PSE shifted by −1.0° in accordance with the positive skewing angle.

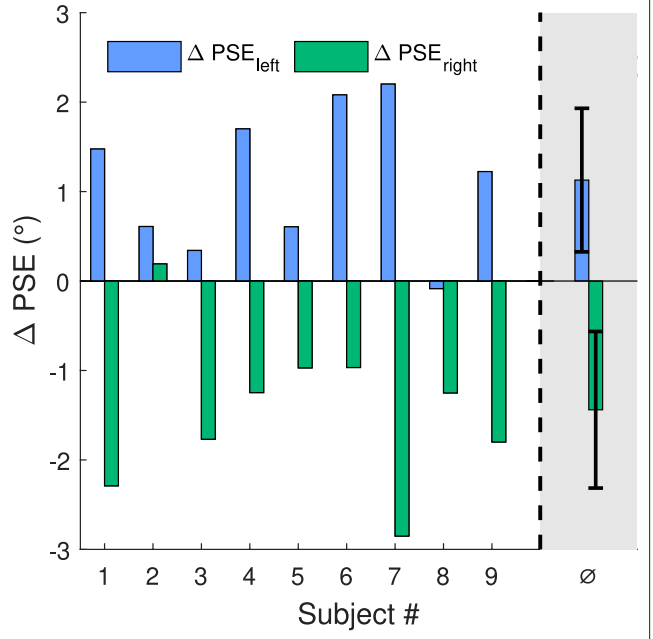

FIGURE 3 | Shifts of PSE for the 2 stimulus locations on the screen. For location one (blue bars), to agree with the right skewed adaptation stimulus, a positive shift of PSE is expected. For the second location (green bars) with the oppositely skewed adaptation stimulus, the expected shift in PSE is negative. The rightmost bars are the mean values of ΔPSE with standard deviation as error bars.

one representative example subject. At the left stimulus location, where the adaptation stimulus was skewed with an positive angle, the PSE shifted by 2.1°. At the second location at the right side of the screen, there is a negative shift $\Delta\text{PSE} = -1.0°$. This means that for the left side motion, direction is perceived by this subject more downwards and on the right side more upwards. So motion direction perception has shifted away from the adaptation stimulus at both locations.

This change of perception indicates that the subject saw both image sequences less distorted after adaptation than in the beginning of adaptation.

Figure 3 shows ΔPSE for all subjects at both stimulus locations. On the left side, all subjects but one show a positive shift PSE ($p < 0.01$ for $\Delta\text{PSE}_{\text{left}}$). On the right side, for all subjects but one the shift of PSE was negative ($p < 0.01$ for $\Delta\text{PSE}_{\text{right}}$). Thus, the shifts of perception were always in opposite directions for the left and right side ($p < 0.001$ for $\Delta\text{PSE}_{\text{left}} - \Delta\text{PSE}_{\text{right}}$). In average, the shift for the left stimulus position was 1.13° ($s = 0.8°$) and for the right position −1.4° ($s = 0.9°$). Skew direction of the adaptation stimulus was positive for the left and negative for the right stimulus location. This means the change of motion direction perception was opposing to the skew direction of the corresponding adaptation stimulus at both stimulus locations.

5. DISCUSSION

This study assessed the parallel presence of spatially separated aftereffects after adaptation to two spatially distinct opposing distortions in a psychophysical experiment. Subjects were exposed to two homogeneously but oppositely skew distorted natural image sequences shown at two distinct locations in the visual field at identical eccentricity. Aftereffects were measured at the identical locations by evaluating the shift of perceived motion direction measured in a direction identification task. The results show opposing shifts of PSE at the left and right side. At both stimulus locations, the direction of aftereffects opposes the skew direction of the corresponding adaptation stimulus. This shows that the human visual system is able to adapt to multiple, spatially separated distortions simultaneously. Perception is changed locally in the visual field depending on the distortions present at the test locations. So distortion adaptation does not only take place globally, but can vary across the visual field.

Aftereffects result from response changes of neurons tuned to attributes changed by the adaptation stimulus (Webster, 2015). Adaptation to features processed in lower levels, like tilt (Mathôt and Theeuwes, 2013) or contrast (Gardner et al., 2005), shows purely retinotopic aftereffects, meaning aftereffects are present only at locations exposed to the adapting stimulus but not transferred to non-adapted locations. Neurons in higher cortical areas have larger receptive field sizes (Van Essen and

Anderson, 1995; Suzuki et al., 2005), therefore aftereffects are at least partially transferred to non-adapted retinal locations, like it has been shown for adaptation to complex facial features (Zimmer and Kovacs, 2011). For this face aftereffect (FAE), it has also been shown that the effect size decreases in case of simultaneous presentation of conflicting stimuli (Afraz and Cavanagh, 2008). For distortion adaptation with natural stimuli also higher cortical levels are involved, since it has been shown that distortion adaptation aftereffects are transferred to non-adapted locations (Habtegiorgis et al., 2017). The presence of multiple opposing aftereffects in our experiment again suggests involvement of lower areas, where different neuron populations are able to adapt differently for different retinal locations. The question arises whether adaptation is aggravated in case of simultaneous adaptation with two opposing stimuli. This could be seen in a smaller effect size when comparing aftereffects in our experiment to a condition with only one adaptation stimulus. If we take the change in angle of perceived motion direction as a direct measurement for perceived skew distortion, meaning the skew angle θ corresponds to ΔPSE, the effect size in our experiment is comparable to the previous study showing global adaptation aftereffects (Habtegiorgis et al., 2017).

The motion direction aftereffect is known to be retinotopic, also with locally opposing aftereffects (Wenderoth and Wiese, 2008). So the results of our experiment could be explained by adaptation to changed motion direction alone. But the natural image sequence used in this experiment as adaptation stimulus contains a variety of motion as well as form features. It is well-known that form adaptation influences motion perception and vice versa (Winawer et al., 2008; Mather et al., 2012; Pavan et al., 2013). So the change of orientation content by distorting the adapting stimulus can induce motion direction aftereffects. At the same time, the altered motion direction statistics of the natural image sequences can influence the perceived skew after adaptation. Both types of aftereffects, change of perceived skew as well as motion direction, are known to occur for skew distorted natural stimuli (Habtegiorgis et al., 2017, 2019). This all suggests that the tested motion aftereffect is a measurement for distortion adaptation. The results show that skew adaptation can take place simultaneously for two stimuli with opposing skew directions and not only with a global homogeneous aftereffect.

Another possible explanation of our results is adaptation to curvature of a three-dimensional surface: Two distorted adaptation stimuli combined could stimulate detectors for curvature of a surface covering the area of both stimulus locations (Suzuki, 2001). Opposite skew distortions, as used in this study, fit to a parallel projection of the undistorted stimulus on two oppositely inclined planes. In this geometrical configuration, the stimuli would then lie on different sides of a three-dimensional object, with the intersection line of the two inclined planes between them. Adaptation to the curvature of the surface would then also lead to a shift of perceived motion direction in opposite directions. There are some reasons why the stimulation of a corresponding surface curvature detector is not guaranteed in our setup: Image skew is ambiguous in the tilt of the three-dimensional-oriented planar surface, the undistorted image is projected on, similar to an ellipse which has two interpretations in 3D (Stevens, 1983). Therefore, a concave as well as convex configuration of planes could distort the two stimuli in the same way. Furthermore, our stimulus setup does not show a continues curvature, meaning the point between the two stimulus locations where the hypothetical surface inclination would change is in fact not part of given visual information. It has been shown that for curvature adaptation such a gap in the adapting stimulus drastically reduced aftereffects (Gheorghiu et al., 2009). For the perception of a surface curvature form motion, there needs to be a change in the second derivative of the optic flow field (Droulez and Cornilleau-Pérès, 1990). But this is not introduced by skew distortions, as it is a linear transformation of spatial coordinates. The orientation of the hypothetical rotated planes could be perceived by motion, but again there is an ambiguity of the plane tilt because of the linearity of the skew transformation (Zhong et al., 2006). Combined, it is not clear which role curvature adaptation plays in the process of adaptation to opposite skew distortions and requires further investigation.

The process revealed by this study is an important part of understanding of how the visual system copes with optically induced distortions. The results show that humans' visual system can reduce the amount of perceived spatially varying distortions by adaptation. Wearers of PALs or VR-glasses benefit from this process by a decrease of problems like discomfort and nausea. In the case of optically induced distortions, additional complexity arises by the fact that varying distortions are in general not spatially distinct and homogeneous but gradually change across the visual field. Also the distortions in the visual field are constantly modulated by eye movements. The distortions are not fixed relative to the retina, as it is the case in this study, but mostly relative to the head and therefore change upon gaze. To reduce the perceived distortions in VR headsets or PALs, aftereffects would thus have to occur not relative to the retinal but the spatial coordinates of an adaptation stimulus. For a single homogeneously distorted adaptation stimulus, the transsaccadic transfer of aftereffects has been shown in retinotopic as well as spatiotopic reference frames (Habtegiorgis et al., 2018a). The spatiotopic adaptation process, in contrast to purely retinotopic adaptation, requires necessarily involvement of high level neurons (Duhamel et al., 1992; Nakamura and Colby, 2002; d'Avossa et al., 2007). Future studies might reveal the presence of this spatiotopic aftereffects after eye movements also for multiple opposing distortions.

DATA AVAILABILITY STATEMENT

The raw data supporting the conclusions of this article will be made available by the authors, without undue reservation.

ETHICS STATEMENT

The studies involving human participants were reviewed and approved by Ethics Committee of the Medical Faculty of the Eberhard Karls Universität Tübingen and the University

Hospital. The patients/participants provided their written informed consent to participate in this study.

AUTHOR CONTRIBUTIONS

All authors developed the study idea and procedure. YS performed the experiment and the analysis. All authors discussed the results and contributed to the final manuscript.

FUNDING

The work was done in an industry-on-campus cooperation of Carl Zeiss Vision International GmbH and the University Tübingen, within the excellence Initiative of the University of the German Research Foundation (DFG). The funder was not involved in the study design, collection, analysis, interpretation of data, the writing of this article or the decision to submit it for publication.

REFERENCES

Afraz, S.-R., and Cavanagh, P. (2008). Retinotopy of the face aftereffect. *Vis. Res.* 48, 42–54. doi: 10.1016/j.visres.2007.10.028

Anstis, S., Verstraten, F. A., and Mather, G. (1998). The motion aftereffect. *Trends Cogn. Sci.* 2, 111–117. doi: 10.1016/S1364-6613(98)01142-5

Apthorp, D., Cass, J., and Alais, D. (2011). The spatial tuning of "motion streak" mechanisms revealed by masking and adaptation. *J. Vis.* 11:17. doi: 10.1167/11.7.17

Bao, M., and Engel, S. A. (2012). Distinct mechanism for long-term contrast adaptation. *Proc. Natl. Acad. Sci. U.S.A.* 109, 5898–5903. doi: 10.1073/pnas.1113503109

Baumann, T. (2010). *Valkaama*. Available online at: http://www.valkaama.com

Blakemore, C., and Campbell, F. W. (1969). On the existence of neurones in the human visual system selectively sensitive to the orientation and size of retinal images. *J. Physiol.* 203, 237–260. doi: 10.1113/jphysiol.1969.sp008862

Brainard, D. H. (1997). The psychophysics toolbox. *Spat. Vis.* 10, 433–436. doi: 10.1163/156856897X00357

Burr, D., and Ross, J. (2008). A visual sense of number. *Curr. Biol.* 18, 425–428. doi: 10.1016/j.cub.2008.02.052

Clifford, C. W. (2002). Perceptual adaptation: motion parallels orientation. *Trends Cogn. Sci.* 6, 136–143. doi: 10.1016/S1364-6613(00)01856-8

Clifford, C. W., Webster, M. A., Stanley, G. B., Stocker, A. A., Kohn, A., Sharpee, T. O., et al. (2007). Visual adaptation: neural, psychological and computational aspects. *Vis. Res.* 47, 3125–3131. doi: 10.1016/j.visres.2007.08.023

d'Avossa, G., Tosetti, M., Crespi, S., Biagi, L., Burr, D. C., and Morrone, M. C. (2007). Spatiotopic selectivity of bold responses to visual motion in human area MT. *Nat. Neurosci.* 10, 249–255. doi: 10.1038/nn1824

Dekel, R., and Sagi, D. (2015). Tilt aftereffect due to adaptation to natural stimuli. *Vis. Res.* 117, 91–99. doi: 10.1016/j.visres.2015.10.014

Droulez, J., and Cornilleau-Pérés, V. (1990). Visual perception of surface curvature. the spin variation and its physiological implications. *Biol. Cybern.* 62, 211–224. doi: 10.1007/BF00198096

Duhamel, J., Colby, C., and Goldberg, M. (1992). The updating of the representation of visual space in parietal cortex by intended eye movements. *Science* 255, 90–92. doi: 10.1126/science.1553535

Ejima, Y., and Takahashi, S. (1984). Facilitatory and inhibitory after-effect of spatially localized grating adaptation. *Vis. Res.* 24, 979–985. doi: 10.1016/0042-6989(84)90074-9

Faubert, J. (2002). "The influence of optical distortions and transverse chromatic aberrations on motion parallax and stereopsis in natural and artificial environments," in *Three-Dimensional Television, Video, and Display Technologies*, eds B. Javidi and F. Okano (New York, NY: Springer-Verlag Berlin Heidelberg), 359–396.

Foster, D. H. (2011). Color constancy. *Vis. Res.* 51, 674–700. doi: 10.1016/j.visres.2010.09.006

Gardner, J. L., Sun, P., Waggoner, R. A., Ueno, K., Tanaka, K., and Cheng, K. (2005). Contrast adaptation and representation in human early visual cortex. *Neuron* 47, 607–620. doi: 10.1016/j.neuron.2005.07.016

Gheorghiu, E. et al. (2009). Multiplication in curvature processing. *J. Vis.* 9:23. doi: 10.1167/9.2.23

Gibson, J. J., and Radner, M. (1937). Adaptation, after-effect and contrast in the perception of tilted lines. I. quantitative studies. *J. Exp. Psychol.* 20:453. doi: 10.1037/h0059826

Habtegiorgis, S. W., Jarvers, C., Rifai, K., Neumann, H., and Wahl, S. (2019). The role of bottom-up and top-down cortical interactions in adaptation to natural scene statistics. *Front. Neural Circ.* 13:9. doi: 10.3389/fncir.2019.00009

Habtegiorgis, S. W., Rifai, K., Lappe, M., and Wahl, S. (2017). Adaptation to skew distortions of natural scenes and retinal specificity of its aftereffects. *Front. Psychol.* 8:1158. doi: 10.3389/fpsyg.2017.01158

Habtegiorgis, S. W., Rifai, K., Lappe, M., and Wahl, S. (2018a). Experience-dependent long-term facilitation of skew adaptation. *J. Vis.* 18:7. doi: 10.1167/18.9.7

Habtegiorgis, S. W., Rifai, K., and Wahl, S. (2018b). Transsaccadic transfer of distortion adaptation in a natural environment. *J. Vis.* 18:13. doi: 10.1167/18.1.13

Jin, D. Z., Dragoi, V., Sur, M., and Seung, H. S. (2005). Tilt aftereffect and adaptation-induced changes in orientation tuning in visual cortex. *J. Neurophysiol.* 94, 4038–4050. doi: 10.1152/jn.00571.2004

Johnson, L., Buckley, J. G., Scally, A. J., and Elliott, D. B. (2007). Multifocal spectacles increase variability in toe clearance and risk of tripping in the elderly. *Invest. Ophthal. Vis. Sci.* 48, 1466–1471. doi: 10.1167/iovs.06-0586

Johnston, A., Arnold, D. H., and Nishida, S. (2006). Spatially localized distortions of event time. *Curr. Biol.* 16, 472–479. doi: 10.1016/j.cub.2006.01.032

Knapen, T., Rolfs, M., and Cavanagh, P. (2009). The reference frame of the motion aftereffect is retinotopic. *J. Vis.* 9:16. doi: 10.1167/9.5.16

Kuhl, S. A., Thompson, W. B., and Creem-Regehr, S. H. (2009). HMD calibration and its effects on distance judgments. *ACM Trans. Appl. Percept.* 6, 1–20. doi: 10.1145/1577755.1577762

Leopold, D. A., Rhodes, G., Müller, K.-M., and Jeffery, L. (2005). The dynamics of visual adaptation to faces. *Proc. R. Soc. B* 272, 897–904. doi: 10.1098/rspb.2004.3022

Lord, S. R., Dayhew, J., Sc, B. A., and Howland, A. (2002). Multifocal glasses impair edge-contrast sensitivity and depth perception and increase the risk of falls in older people. *J. Am. Geriatr. Soc.* 50, 1760–1766. doi: 10.1046/j.1532-5415.2002.50502.x

Mathôt, S., and Theeuwes, J. (2013). A reinvestigation of the reference frame of the tilt-adaptation aftereffect. *Sci. Rep.* 3, 1–7. doi: 10.1038/srep01152

Mather, G., Pavan, A., Bellacosa, R. M., and Casco, C. (2012). Psychophysical evidence for interactions between visual motion and form processing at the level of motion integrating receptive fields. *Neuropsychologia* 50, 153–159. doi: 10.1016/j.neuropsychologia.2011.11.013

Meister, D. J., and Fisher, S. W. (2008). Progress in the spectacle correction of presbyopia. part 1: design and development of progressive lenses. *Clin. Exp. Optomet.* 91, 240–250. doi: 10.1111/j.1444-0938.2007.00245.x

Nakamura, K., and Colby, C. L. (2002). Updating of the visual representation in monkey striate and extrastriate cortex during saccades. *Proc. Natl. Acad. Sci. U.S.A.* 99, 4026–4031. doi: 10.1073/pnas.052379899

Pavan, A., Marotti, R. B., and Mather, G. (2013). Motion-form interactions beyond the motion integration level: evidence for interactions between orientation and optic flow signals. *J. Vis.* 13:16. doi: 10.1167/13.6.16

Saunders, D. R., and Woods, R. L. (2014). Direct measurement of the system latency of gaze-contingent displays. *Behav. Res. Methods* 46, 439–447. doi: 10.3758/s13428-013-0375-5

Schütt, H. H., Harmeling, S., Macke, J. H., and Wichmann, F. A. (2016). Painfree and accurate Bayesian estimation of psychometric functions for (potentially) overdispersed data. *Vis. Res.* 122, 105–123. doi: 10.1016/j.visres.2016.02.002

Stevens, K. A. (1983). Slant-tilt: the visual encoding of surface orientation. *Biol. Cybern.* 46, 183–195. doi: 10.1007/BF00336800

Suzuki, S. (2001). Attention-dependent brief adaptation to contour orientation: a high-level aftereffect for convexity? *Vis. Res.* 41, 3883–3902. doi: 10.1016/S0042-6989(01)00249-8

Suzuki, S., and Cavanagh, P. (1998). A shape-contrast effect for briefly presented stimuli. *J. Exp. Psychol.* 24:1315. doi: 10.1037/0096-1523.24.5.1315

Suzuki, S., Clifford, C., and Rhodes, G. (2005). "High-level pattern coding revealed by brief shape aftereffects," in Fitting the Mind to the World: Adaptation and After-Effects in High-Level Vision, Vol. 2, eds C. W. G. Clifford, and G. Rhodes (Oxford: Oxford University Press), 135–172. doi: 10.1093/acprof:oso/9780198529699.003.0006

Timmis, M. A., Johnson, L., Elliott, D. B., and Buckley, J. G. (2010). Use of single-vision distance spectacles improves landing control during step descent in well-adapted multifocal lens-wearers. *Invest. Ophthalmol. Vis. Sci.* 51, 3903–3908. doi: 10.1167/iovs.09-4987

Uttal, W. R., Spillmann, L., Stürzel, F., and Sekuler, A. B. (2000). Motion and shape in common fate. *Vis. Res.* 40, 301–310. doi: 10.1016/S0042-6989(99)00177-7

Van Essen, D. C., and Anderson, C. H. (1995). "Information processing strategies and pathways in the primate visual system," in *An Introduction to Neural and Electronic Networks*, Vol. 2, eds S. F. Zornetzer, J. L. Davis, C. Lau, and T. McKenna (San Diego, CA: Academic Press), 45-76.

Webster, M. A. (2015). Visual adaptation. *Annu. Rev. Vis. Sci.* 1, 547–567. doi: 10.1146/annurev-vision-082114-035509

Wenderoth, P., and Wiese, M. (2008). Retinotopic encoding of the direction aftereffect. *Vis. Res.* 48, 1949–1954. doi: 10.1016/j.visres.2008.06.013

Winawer, J., Huk, A. C., and Boroditsky, L. (2008). A motion aftereffect from still photographs depicting motion. *Psychol. Sci.* 19, 276–283. doi: 10.1111/j.1467-9280.2008.02080.x

Zhong, H., Cornilleau-Peres, V., Cheong, L.-F., Yeow, G., and Droulez, J. (2006). The visual perception of plane tilt from motion in small field and large field: psychophysics and theory. *Vis. Res.* 46, 3494–3513. doi: 10.1016/j.visres.2006.04.003

Zimmer, M., and Kovacs, G. (2011). Position specificity of adaptation-related face aftereffects. *Philos. Trans. R. Soc. B Biol. Sci.* 366, 586–595. doi: 10.1098/rstb.2010.0265

Conflict of Interest: SW and KR are employees of Carl Zeiss Vision International GmbH, as detailed in the affiliations.

The remaining author declares that the research was conducted in the absence of any commercial or financial relationships that could be construed as a potential conflict of interest.

iScience

CellPress
OPEN ACCESS

Article

Self-motion illusions from distorted optic flow in multifocal glasses

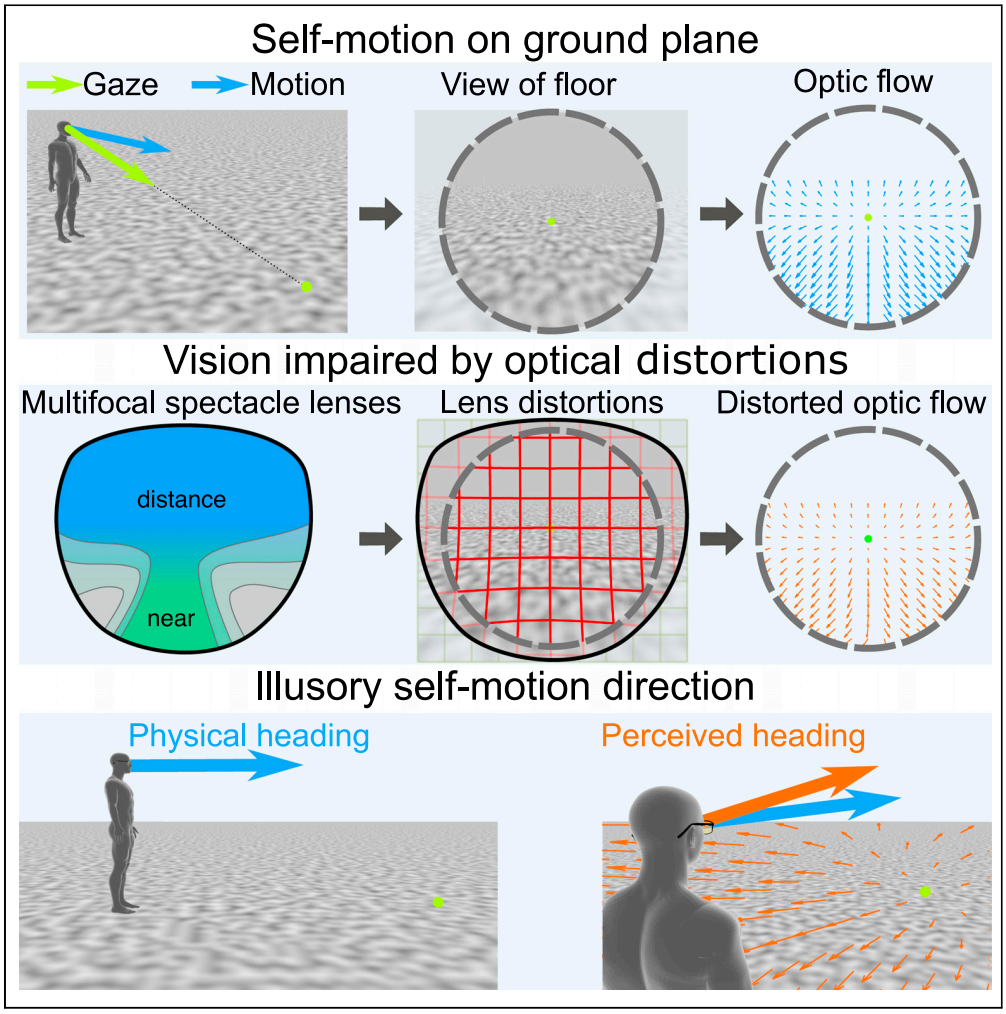

Yannick Sauer,
Malte Scherff,
Markus Lappe,
Katharina Rifai,
Niklas Stein,
Siegfried Wahl

yannick.sauer@uni-tuebingen.de (Y.S.)
malte.scherff@uni-muenster.de (M.S.)

Highlights

Multifocal lenses impair vision of spectacle wearers with gaze-dependent distortions

A model of heading perception from distorted optic flow suggest a misperception

Heading perception was tested with a virtual reality-based simulation of distortions

Distortions lead to gaze direction-dependent illusions in perceived vertical heading

Sauer et al., iScience 25, 103567
January 21, 2022
https://doi.org/10.1016/j.isci.2021.103567

iScience

CellPress
OPEN ACCESS

Article

Self-motion illusions from distorted optic flow in multifocal glasses

Yannick Sauer,[1,4,5,*] Malte Scherff,[2,4,*] Markus Lappe,[2] Katharina Rifai,[1,3] Niklas Stein,[2] and Siegfried Wahl[1,3]

SUMMARY

Progressive addition lenses (PALs) are ophthalmic lenses to correct presbyopia by providing improvements of near and far vision in different areas of the lens, but distorting the periphery of the wearer's field of view. Distortion-related difficulties reported by PAL wearers include unnatural self-motion perception. Visual self-motion perception is guided by optic flow, the pattern of retinal motion produced by self-motion. We tested the influence of PAL distortions on optic flow-based heading estimation using a model of heading perception and a virtual reality-based psychophysical experiment. The model predicted changes of heading estimation along a vertical axis, depending on visual field size and gaze direction. Consistent with this prediction, participants experienced upwards deviations of self-motion when gaze through the periphery of the lens was simulated, but not for gaze through the center. We conclude that PALs may lead to illusions of self-motion which could be remedied by a careful gaze strategy.

INTRODUCTION

With increasing age, accommodation capabilities of the human eye decrease and it becomes harder to focus on nearby objects (Atchison, 1995). Progressive addition lenses (PALs) are a common treatment method using a special kind of spectacle lens design with complex optical properties. PALs have two regions of different optical power for far and near vision (Meister and Fisher, 2008a) (Figure 1A). The far zone in the upper area of the lens corrects far vision, whereas the near zone in the lower area of the lens has additional optical power to reduce accommodative demand when focusing on close objects. Between these two zones, there is a progressive increase in optical power which inevitably produces unwanted astigmatism (Sheedy et al., 2005). This causes blur and skew distortions in the periphery. Thus, the wearers of these lenses have to cope with spatially varying distortions of the visual field. Figure 1B shows a simulation of a progressive addition lens' optical distortions.

When wearers of PALs move their eyes, these distortions are not fixed in the visual field but change with gaze direction. During central view through the upper area of the lens that is designed for far vision, the distortions are visible mainly in the visual field's periphery. Alternatively, gaze direction through the lower left or right area of the lens leads to substantial distortions in the visual field center.

Optical distortions can have negative influences on visual perception, including form, motion, and distance estimations. Many PAL wearers report a perception of unnatural motion of the environment (swim effect) (Meister and Fisher, 2008b), even causing nausea for some of them (Alvarez et al., 2009). A considerable number have problems with tripping while wearing PALs (Johnson et al., 2007; Lord et al., 2002). Because some wearers cannot adapt to the distorted perception, they reject PALs entirely. We wondered whether the difficulties might be related to distortions of the visual motion experienced during locomotion.

Walking through a rigid environment forms moving patterns of light on the retina of the observer. These patterns are called optic flow and they contain information about amplitude and direction of motion relative to the surroundings and about the appearance of the scene (Gibson, 1950). Typically optic flow is described as a two-dimensional vector field, so-called optic flow field, which carries information about the retinal placement and direction of each flow element. The human visual system is able to extract information from optic flow for the control of self-movement (Warren and Hannon, 1988; Lappe et al., 1999;

[1]Institute for Ophthalmic Research, University of Tuebingen, Tuebingen 72076, Germany

[2]Department of Psychology & Otto Creutzfeldt Center for Cognitive and Behavioral Neuroscience, University of Muenster, Muenster 48149, Germany

[3]Carl Zeiss Vision International GmbH, Aalen 73430, Germany

[4]These authors contributed equally

[5]Lead contact

*Correspondence: yannick.sauer@uni-tuebingen.de (Y.S.), malte.scherff@uni-muenster.de (M.S.)

https://doi.org/10.1016/j.isci.2021.103567

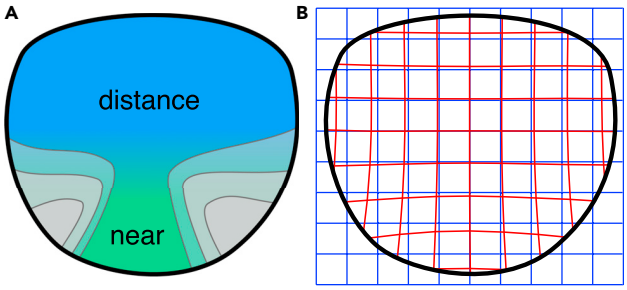

Figure 1. Schematic illustration of a PAL

(A) The lens has a zone optimized for distance vision in the upper and a zone optimized for near vision in the lower part. The gradient of color represents a progressive change of optical power between the two zones. As a side effect, the power gradient leads to astigmatic blur in the left and right periphery, indicated by the gray areas.

(B) PALs distort the visual field of the wearer. The blue mesh represents object points in the visual field. PAL distortions displace the perceived position as illustrated by the red mesh. Prominent distortions are in the lower periphery.

Warren et al., 2001), the perception of the environmental structure (Andersen, 1989), the prevention of collision (Sidaway et al., 1996), and the estimation of traveled distance (Lappe et al., 2007).

For a pure translational motion of the observer, e.g., walking with gaze fixed on the horizon, optic flow consists of a radial pattern expanding from a single point in the direction of the translation, the focus of expansion (FoE). However, such a static gaze is a rare occurrence during self-motion. During walking, humans look around, often at the ground in front, in order to check for obstacles and find good locations for foot placement (Hollands et al., 1995; Patla and Vickers, 1997; Calow and Lappe, 2008; 't Hart and Einhauser, 2012; Matthis et al., 2018), or to adjust gaze toward a new destination when changes on the planned path occur (Hollands et al., 2002). In such cases, rotational eye movements stabilize the gaze on objects in the environment via smooth pursuit (Niemann et al., 1999) or eye rotation reflexes (Miles and Busettini, 1992; Lappe et al., 1998; Angelaki and Hess, 2005; Matthis et al., 2018). Because of the rotation of the eye, the resulting flow structure on the retina is no longer a radial pattern but resembles a spiral with the center near the fovea (Warren and Hannon, 1990; Lappe and Rauschecker, 1995; Lappe et al., 1999). Such patterns, despite lacking retinal motion at the visual field's center, contain a large variety of motion directions at low speed in the parafoveal area. The peripheral visual field, in contrast, features much higher speeds in more radially distributed directions (Calow and Lappe, 2007). The visual system is able to recover from such retinal flow (Warren and Hannon, 1990; Lappe et al., 1999; Bremmer et al., 2010). PAL glasses, however, would produce additional distortions in this pattern, depending on how gaze is directed through the lens.

When a person aims to fixate a point on the floor during walking, various combinations of head and eye movements are suitable to execute this task. One possible way to do so is to keep the head orientation straight in walking direction and direct the eye downward to fixate the ground (Figure 2B, right). Alternatively, one might tilt the head downward while keeping the orientation of the eye straight with respect to the head (Figure 2B, left). Although these two behaviors result in the same structure of optic flow in normal eyes, they lead to different distortions for PAL wearers: When the eye is directed downwards but the head remains level, gaze is through the peripheral, more distorted part of the lens. Therefore, distortion occurs in the center of the visual field. In contrast, when the head, and therefore the PAL glasses, are moved, gaze is directed through the less distorted central area of the PAL and the distortion occurs mainly in the visual periphery.

Distortions alter the optic flow a PAL wearer receives on the retina, possibly resulting in an internal misperception regarding the own movement. Our study aimed to investigate the influence of PAL distortions on heading perception and to determine differences in perception between the central and peripheral views in a typical self-motion scenario. We had two goals. First, we wanted to determine how PAL distortions would be expected to affect heading estimates. For this, we first created PAL distorted flow fields and then used computer simulations of an established model of heading perception in humans to estimate the expected effects on heading. Second, we wanted to determine if PAL distortions lead to misperceptions of self-motion in human observers. For this, we tested heading estimation in human participants in

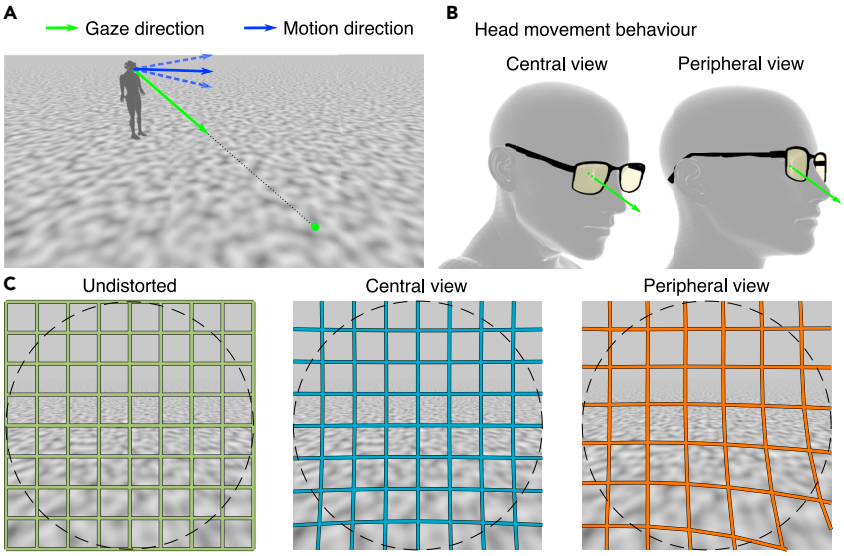

Figure 2. Experimental setup

(A) Visualization of the self-motion scenario used in this study: Gaze (green) is downwards onto the floor and off to the side. Self-motion (blue) consists of a translation over the ground. In experimental conditions, translation could also be slightly downward or slightly upward with respect to the ground (dashed blue lines).

(B) Two different head orientations while fixating a point on the ground. In the central view condition the observer's line of sight is through the center of the lens and the head is tilted downward and to the side. In the peripheral view condition, the head remains at level and gaze is through the periphery of the lens.

(C) The visible scene of the moving environment is the same in all conditions, but distortions, illustrated by colored meshes on top, differ between central view and peripheral view. The dashed circle indicates a circular field of view with radius 50° as presented in the VR experiments.

a virtual reality (VR) simulation of PAL distortions along the axis that provided the strongest predicted misperception in the model simulations.

RESULTS

Simulations of PAL distortions in retinal flow fields

We simulated a translation across a ground plane while fixating a point on the floor next to the path (Figure 2A), a scenario that occurs naturally during walking (Hollands et al., 1995; Patla and Vickers, 1997; Calow and Lappe, 2008; 't Hart and Einhauser, 2012; Matthis et al., 2018). We considered two distortion conditions corresponding to central view and peripheral view through the PAL (Figure 2C). Optic flow fields were calculated for the motion scenario with and without distortions using a ray tracing approach in which for each point in the scene the distorted and undistorted positions in the image plane are calculated followed by calculation of the (distorted) optical motion in the image plane (see STAR Methods).

Panel A in Figure 3 shows an example of a superposition of the peripheral view distorted (orange arrows) on top of the undistorted (green arrows) retinal flow field. In this particular simulation, the direction of self-motion (heading) was to the left. The overall pattern appears very similar in both cases and exhibits the typical spiral flow field structure for the fixation of a ground element (Warren and Hannon, 1990; Lappe and Rauschecker, 1995; Lappe et al., 1999). Differences between the distorted (orange) and undistorted (green) flow can be seen in the lower left area but appear to be rather small. However, panel B shows how the distortion changes direction (angle) and speed (ratio) across the visual field and reveals that there are large areas of systematic differences between the distorted and the undistorted flow. The parafoveal area exhibits directional changes of the flow, clockwise on one side and anti-clockwise on the other side of the fovea, as well as increases and decreases of speed in the upper and lower parafoveal fields. Owing to the typically low flow speeds in this area, even a small distortion may already cause a different flow perception, impacting the spiral structure emerging from the center. Panel C shows the differences in direction and speed in the central view condition. They exhibit a different retinal distribution than in the peripheral

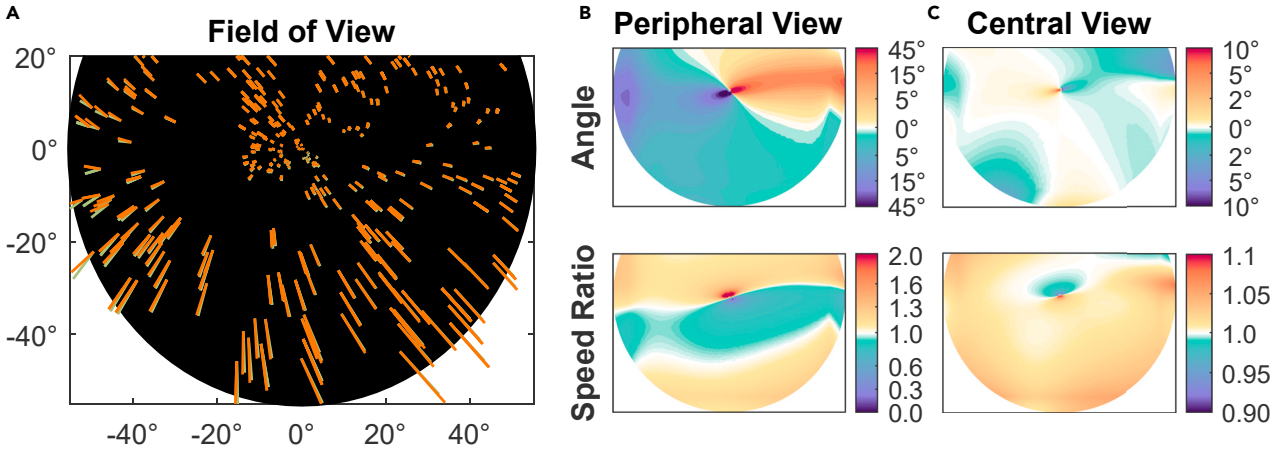

Figure 3. Changes in flow fields because of distortions

(A) Example flow fields used in the simulations for a translation parallel to the ground to the left of the fixation point. Green arrows show the undistorted flow, orange arrows show the flow distorted because of the peripheral view condition.

(B) The top panel shows the angle between flow vectors at all points in the visual field for the peripheral condition. A position colored in the yellow-red spectrum indicates an anti-clockwise turn from an undistorted vector to the distorted vector there. The bottom panel shows changes in speed as the ratio of the speed of the distorted vector to the speed of the undistorted vector. Values greater than 1 indicate an increase in speed at that position.

(C) Directional and speed changes because of the central gaze condition. The color scales are limited because of the undistorted flow in the central area almost vanishing, limiting its validity as a reference there.

view condition and are overall smaller. The quantitative analysis of both distortions shows that they do not act as random noise to the flow field but impose a systematic and continuous pattern of changes to the optic flow field. These systematic differences in flow, though small in value, might lead to misestimations or increased variability in heading estimates. Owing to the complexity of the flow field, however, it is not immediately clear which or how much distortions of self-motion perception may be expected. We therefore used computational modeling to better understand the potential implications of the optic flow distortion.

To estimate whether these distortions might influence heading estimation from retinal flow, we presented distorted flow fields to the method for heading recovery used in an established model of heading perception in humans (Lappe and Rauschecker, 1993; Lappe et al., 1999; Li et al., 2018). This model implements the subspace algorithm for heading estimation (Heeger and Jepson, 1992) that computes a likelihood map of heading space, i.e., a 2D map of potential heading directions in retinal coordinates representing the likelihoods with which each one of them explains a given flow field. Distortions of the flow field might influence the likelihood distribution in this map. Figure 4 shows an example of the likelihood distribution for a distorted flow field using a gray scale to indicate the likelihood of each heading direction. The model selects patches of flow (four of them are shown in the left part of panel A) from the flow field, similar to receptive fields of neurons in the visual motion pathway of the brain (Lappe et al., 1996). It then computes likelihood maps of the heading for each patch. The four small plots on the left of panel B show the likelihoods for the four patches in A. Dark areas indicate the most likely heading. Finally, the individual likelihood maps are averaged to compute a global likelihood map (right plot in panel B), in which the most-likely heading (red dot) is the model's heading estimation for the given flow field.

Because the most likely headings (dark area in Figure 4B) cover the true heading (green dots), the results of the simulation indicate that the heading perceived from this flow field is still close to the true heading. The vertical spread of the dark area indicates that PAL distortions might create uncertainty along a vertical axis because of the corresponding headings mainly differing in the vertical component. In case of an undistorted flow field the likelihood map would contain a single dark spot coinciding with the true heading and be colored white elsewhere.

We tested this prediction in a psychophysical experiment with flow fields including the different types of optical distortions resulting from the two distinct kinds of head orientation behavior, i.e., the central view condition and the peripheral view condition.

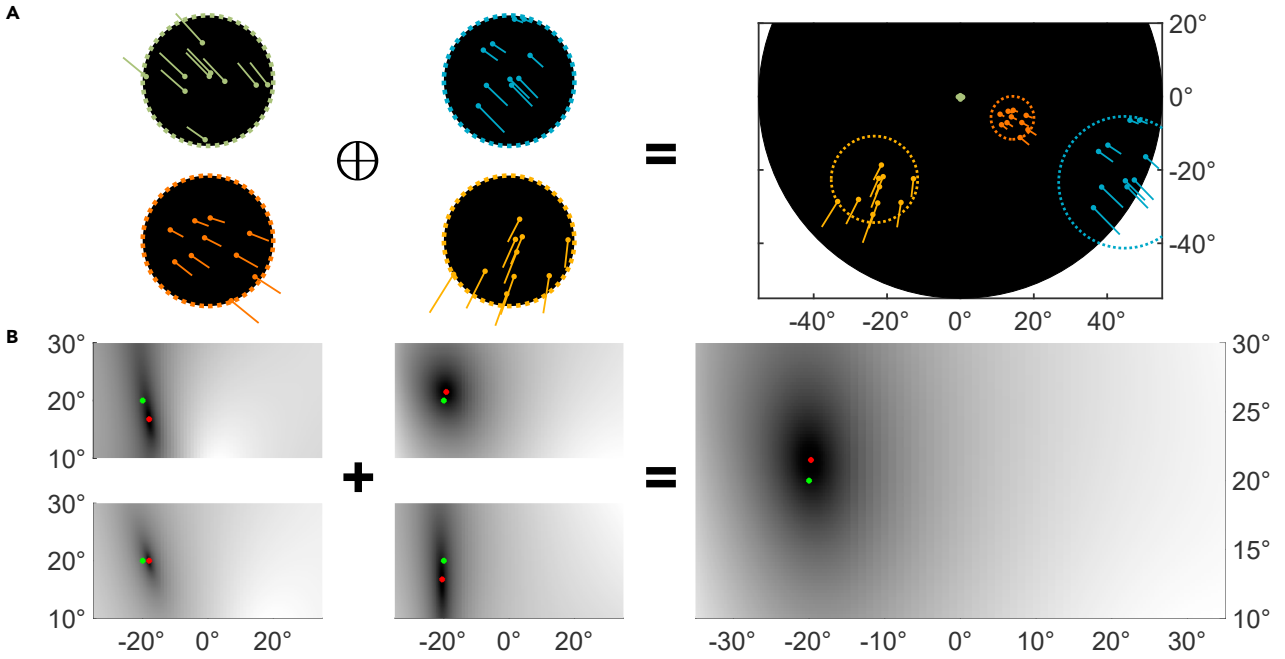

Figure 4. Visual description of the simulation process

The simulation calculates the map of heading likelihoods for a particular flow field with a defined heading and gaze direction: (A) Circular patches (four are shown in this example) were placed randomly inside the visual field with area size proportional to eccentricity. A total of 10 points per patch were selected randomly and their motion vectors were calculated according to the heading and gaze direction. Combining the patches yields the optic flow field for this heading direction (−20°,20°) in the peripheral distortion condition. (B) The likelihoods of all the heading directions, shown in retinal coordinates that are considered as an explanation for the small flow fields are presented as a gray-scale map. The darker a direction is displayed the more likely it is to explain the flow field. The combination of the ratings for the small and locally restricted flow fields yields a global estimate for heading direction. Red dots mark the most likely heading, i.e., the heading, which according to the model, explains the flow field best. The green dots indicate the true heading direction.

Virtual reality experiment on distorted self-motion perception in humans

To study human perception under the influence of PAL distortions in an isolated experimental environment, we developed a simulation of optical distortions in VR (Stein et al., 2021). The PAL distortions of a Zeiss lens design (Carl Zeiss Vision GmbH, Aalen, Germany) were precomputed by ray tracing for different gaze directions. The virtual image was distorted to simulate PAL distortions for either the central view or peripheral view. For comparison, in a third condition the virtual image was undistorted. The self-motion scenario simulated movement across a virtual ground plane while fixating a point on the floor as in Figure 2. The self-motion was either parallel to the ground or contained a small upwards or downwards component between −3.5° and 3.5°. Participants reported their perceived direction of self-motion by indicating their perception of either *sinking in* or *lifting off* in each trial. The three distortion conditions were measured in one session in randomized trial order.

For each subject and each distortion condition, the vertical translation angle perceived as a motion parallel to the floor (point of subjective equality - PSE) was determined by fitting a psychometric function to the subjects' answers depending on the vertical translation angle. Then the difference of PSE between the distorted condition and the undistorted condition was calculated. This relative shift (ΔPSE) provided a measure for the influence of simulated distortions in the two view conditions.

Figure 5 A shows the answers and psychometric fits for all conditions for one example subject. There is a clear shift of the psychometric function in the case of simulated gaze through the periphery of the PAL compared to the undistorted condition. The PSE is 0.73° lower than in the undistorted condition. This subject perceived the translational movements more upwards than in the undistorted condition. In the central view condition, the PSE is similar to that of the undistorted condition. Figure 5B shows the change of PSE in the two distortion conditions relative to the undistorted condition across all subjects. In the peripheral view

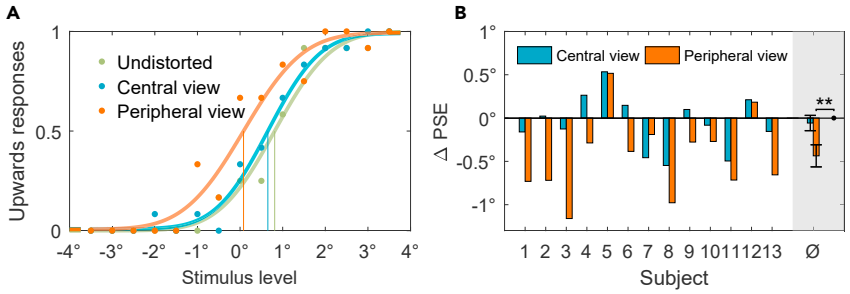

Figure 5. Experimental results

(A) Percentage of upwards responses and psychometric fits for one example subject. The green data points were obtained in the undistorted trials. The blue and orange data points show the answers in the two distortion conditions for simulated central view and simulated peripheral view, respectively. All three datasets were fitted with a psychometric function. The 50% point of the fit function is taken as the point of subjective equality (PSE) (vertical lines).

(B) Difference of the PSEs between the distortion conditions and the undistorted condition for all tested subjects. The rightmost bars are the mean value of Δ PSE with standard deviation as error bars. **p < 0.01.

condition, there is a significant deviation (ΔPSE) from the undistorted condition (t test, $p<0.01$). On average, the angle perceived as a straight movement was 0.43˚ smaller than in the undistorted condition, i.e., the Δ PSE was negative. Thus, in the peripheral gaze condition participants reported a self-motion percept that appeared as if they were slightly lifting up from the ground when in fact the motion was parallel to the ground. For the simulated gaze through the center of the PAL, there is no significant difference between the distorted and undistorted cases.

Model simulation of VR experiment

The results of the VR experiment showed that PAL distortions of the optic flow indeed produced misperception of self-motion along the vertical dimension. We next presented the same vertical heading task to the model in computer simulations to see whether the size of the misperception fitted the distortions of the flow fields. For these simulations, fifty flow fields with different random distributions of flow vectors were calculated for each heading direction. Then, these flow fields were distorted to create individual fields for the different distortion conditions. Next, the most likely heading direction according to the model was calculated using the subspace algorithm. Finally, to recreate the psychophysical procedure, model heading estimates were converted from a direction into upwards and downwards answers, depending on the sign of the vertical component relative to a direction parallel to the ground. In the case that the estimate was parallel to the ground, it was counted both for upwards and downwards answers. For each distortion condition, the percentage of answers upwards was computed for each vertical direction of the stimulus. Then, for each distortion condition, the vertical heading angle perceived as a motion parallel to the floor (PSE) was determined by fitting a psychometric function to the answers using the same fitting procedure as for the experimental analysis. Because the model in the undistorted condition always produced a PSE of 0 (i.e., it recovered the correct heading) the shift in PSE (ΔPSE) corresponds directly to the extracted PSE for the distortion conditions.

For the model simulations, the maximum field of view (FoV) was set to be circular with a radius of 55˚. This matched the specifications of the VR headset we used for the experiment. However, the effective FoV when wearing an HMD is often smaller because parts of the screen are not visible because of individual adjustments in fitting the HMD on the head. Therefore, we also performed the simulation procedure with slightly reduced sizes of the FoV.

Figure 6 shows the PSE for the central and peripheral distortion conditions for effective FoV sizes between 40° and 55° radius.

For FoV sizes between 50° and 55°, the results show a negative PSE value for the peripheral view condition and a small positive value for the central view condition. This is consistent with the experimental findings which showed a significant negative PSE shift for the peripheral view condition and a much smaller PSE shift, not different from zero, for the central view condition.

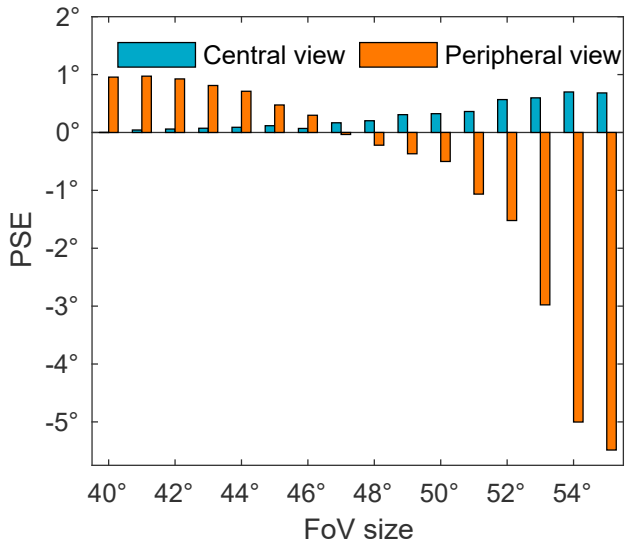

Figure 6. Simulation results

Shift of PSE in the simulation results for the two distortion conditions for different simulated FoV sizes.

Figure 6 furthermore shows that size and direction of the PSE depend on the size of the FoV. For FoVs smaller than 50° the PSE in the central view condition further diminishes while the PSE in the peripheral view condition becomes positive, indicating a self-motion toward the ground. This dependence might be important in explaining individual data in the experiment and in considerations of the field of view in real PAL glasses.

DISCUSSION

Summary of results

We investigated the influence of optical distortions of progressive addition lenses (PALs) on heading perception from optic flow for a translational movement across a ground plane while fixating a point on the floor, a typical walking scenario. We combined simulations of optic flow-based heading estimation and a VR-based psychophysical experiment. We compared two distortion conditions: first gaze through the center of the simulated progressive lens (central view condition) and second gaze through a point in the periphery of the lens (peripheral view condition). These two cases correspond to different combinations of gaze and head orientation. For the first condition, the observer would need to tilt the head downward while looking straight through the lens. For the second condition the head would remain level while the gaze would be directed downwards.

The resulting distortions of the progressive lens vary between the two scenarios because the periphery of the lens type we used induces considerably stronger distortions than the central area. In both experimental data and model simulations, we found that the central view condition produced small, if any, heading errors. The peripheral view condition, in contrast, produced heading estimates that appear as if one would slightly lift up from the ground.

Discrepancies in experimental results

The experimental results had some variation between subjects in effect size as well as sign of Δ PSE, with two of them experiencing a positive shift in heading estimation in both distortion conditions. One might speculate that these variations could be explained by differences in effective FoV in the HMD, because model simulations also showed a dependence of the direction of heading estimate in the peripheral view condition on the size of the FoV. Although the rendered FoV of the HMD nominally spans 107° horizontally and 108° vertically (Musil, 2021), the effective FoV is usually smaller because parts of the screen are not visible. The FoV has a circular shape with a radius in the range of 45°to55°. The specific radius depends on individual factors, like physiological face properties and headset tightness, determining how close the

eyes are to the HMD's lenses. These factors, together with a dependence of perceived heading on FoV might explain individual differences in our experiment.

On the other hand, some subject data do not match the effect of FoV in the model simulation. Although a positive shift of PSE in both distortion conditions fits to simulations with a small FoV, some subjects have a clear negative PSE in the central view condition - a result not predicted by the model. Experiments testing differently sized restricted FoVs are needed to better understand the influence of FoV and to possibly adapt the heading estimation model.

Conclusion for optic flow processing

Participants in psychophysical experiments are able to estimate simulated heading directions from optic flow fields. How well this task is executed is coupled to the quality of the flow presented. Adding random noise to the flow increases the estimation errors (van den Berg, 1992; Foulkes et al., 2013). The PAL distortions, even though their influence on the global flow field pattern is subtle, add a form of noise to the flow fields and induce estimation errors as well. This estimation error is more systematic in the form of a heading bias along the vertical axis, an effect not reported from the addition of random noise to flow fields.

The PAL distortions led to continuous changes of speed and direction of flow field vectors that vary throughout the visual field. Regarding the typical spiral flow field structure, more radial in the periphery but rotational in the central area, the impact of the distortions may differ locally as well. A similar directional change in local flow in the periphery that is nearly unidirectional does not confound the spiral structure as much as such a directional change in local flow that curls around a single point in the center.

In our study, we found changes in heading estimations when the FoV changed in size, showing not only the influence of the extent of the flow field but also the aforementioned local differences in changes of flow structure. We conclude that for modeling heading estimation, it is necessary to consider location dependent flow processing and the presented model is a first step in establishing a simulation of heading estimation for such flow fields based on the local structures.

Practical implications

Heading illusions as shown in this study would put visual perception in conflict with other self-motion perceptions and might relate to the "swim effect" observed in novice wearers of PAL glasses (Meister and Fisher, 2008b) and contribute to discomfort and nausea shown by some PAL wearers (Alvarez et al., 2009). The amount of misperception differed depending on the area of the lens through which gaze was directed. For normal eye movement behavior with constantly changing gaze direction, this can produce motion perception characterized by a continuous change of perceived motion direction. In complicated walking scenarios, e.g., climbing stairs, misperception of heading changing during every eye movement can lead to complications with foot placement and tripping (Johnson et al., 2007), especially considering decreased capabilities of elderly people for heading control from optic flow (Berard et al., 2009).

An illusory, gaze-dependent perception of relative motion of the surrounding area is an often reported side effect for PAL wearers (swim effect) that still is only vaguely described (Han et al., 2003; Alvarez et al., 2009). Quantifying the very discomforting motion illusions by evaluating the distorted optic flow field would be a first step in objectively characterizing the swim effect, and even identifying differences between lenses. A PAL with large differences in the heading estimate for different gaze directions is expected to cause more discomfort. Therefore, optic flow-based analysis of PAL distortions might become a tool for lens design to improve the experience of PAL wearers by presenting distortions for more consistent optic flow perception.

Independent of design, our results suggest an advantage for heading estimation for the central view condition when distortions are mainly in the periphery. Wearers of progressive lenses should rather use the lens' central area while walking to perceive less distorted optic flow in the center of the visual field. This would lead to increased head movements for PAL wearers compared to other people, a change in behavior that was already found in a natural scenario (Rifai and Wahl, 2016).

Variable FoV size has to be considered not only in experimental conditions but also as a practical issue. The part of the visual field covered by a spectacle lens depends on frame size and distance to the eye. For a

typical vertex distance of 12 mm, nodal point of the eye of 7.3 mm (Jones et al., 2016) and lens width between 40 mm and 60 mm, the horizontal FoV ranges between 92° and 115°. Points outside of the spectacle frame are not distorted. As a result there is a frame-dependent border between distorted and undistorted optic flow in the periphery, which might influence heading perception and might be an additional factor for discomfort because of inconsistencies in the optic flow pattern. Although our experiment did not investigate it, the FoV dependency of our simulation results suggest that frame size can also indirectly influence self-motion perception by determining the size of the distorted part of the visual field. To better understand the influence of FoV size, further experiments are needed which test perception for defined restricted areas in the visual field of changing size.

Most wearers of PAL spectacles, even if they initially experience motion misperceptions, adapt to their spectacles over a couple of weeks. Such adaptation plays an important role in the acceptance of progressive lenses. It has been shown that humans can adapt to distortions of the visual field. These include not only local simple geometric transformations (Jin et al., 2005) but also skew distortions as present for progressive lens wearers (Habtegiorgis et al., 2017) and spatially varying distortions (Sauer et al., 2020). Furthermore, skew distortion adaptation aftereffects show trans-saccadic transfer (Habtegiorgis et al., 2018), which is important in the context of distortion changes by eye movements. Aftereffects do not only appear as altered form features, but also in motion perception and even include interactions in which exposure to distorted form also influences motion perception (Rifai et al., 2020). Our experiments were designed to study motion misperceptions that occur during novel wearing of PAL glasses. It might be interesting to see how the adaptation process of PAL wearers can influence heading perception in future experiments.

Outlook

In our simulation, we only considered translational motions as possible candidates for the distorted flow field. However, distortions might also induce misperceptions of rotational motion components. A perceived rotation could describe unnatural motion of the environment, reported by many PAL wearers. Therefore, an extension of our optic flow model to include rotations could help to further understand motion illusions in PAL wearers. Development of a quantification method of distortion-induced motion discomfort based on optic flow could help in the future design of progressive lenses.

Limitations of the study

Because of the limited FoV of the VR headset, our experiment could not fully replicate the distortions visible to PAL wearers. The use of high-FoV headsets in the future could simulate a FoV similar to that covered by real spectacle frames. The measured effect might increase because of more visible distortions in the periphery. Regarding the everyday problems of PAL wearers, not only shifts of the most likely heading, but also other aspects of the optic flow field have to be considered. Distorted vision results in unnatural flow fields, which becomes clear from the heading likelihood maps: the distribution of likely headings is wide with no direction fitting perfectly to the distorted flow field. It is not clear to what extent the widened distribution of heading directions contributes to discomfort of PAL wearers. In addition, when self-motion does not suffice to explain the flow field entirely, illusory movement of the environment might be perceived to account for unexplained flow.

Quantification of the naturalness of distorted optic flow and measurements of the discomfort related to it are needed to cover this aspect. Furthermore, only one type of PAL was tested in this study. Different lenses with corrections for different refractive errors can differ in their distortions and therefore also in their influence on self-motion perception. Other distortions of the optic flow field might also induce horizontal heading illusions. Future studies might concentrate on the differences between different correction power or design parameters influencing the distortions.

STAR★METHODS

Detailed methods are provided in the online version of this paper and include the following:

- KEY RESOURCES TABLE
- RESOURCE AVAILABILITY
  - Lead contact
  - Materials availability

ACKNOWLEDGMENTS

M.L. was supported by the German Research Foundation (952-4-3, DFG La 952-7). This work has received funding from the European Union's Horizon 2020 research and innovation programme under the Marie Skodowska-Curie grant agreement No 734227. This project has received funding from the European Union's Horizon 2020 research and innovation programme under grant agreement No 951910.

AUTHOR CONTRIBUTIONS

Conceptualization, Y.S., M.S., M.L., and K.R.; Methodology, Y.S., M.S., M.L. and N.S.; Software, Y.S. and M.S.; Investigation, Y.S. and M.S.; Writing – Original Draft, Y.S. and M.S.; Writing – Review & Editing, Y.S., M.S., M.L., K.R., N.S. and S.W.; Supervision, M.L. and S.W.

DECLARATION OF INTERESTS

The authors declare that there are no conflicts of interest that could have interfered in the course of this study.

Received: September 14, 2021
Revised: November 3, 2021
Accepted: December 1, 2021
Published: January 21, 2022

REFERENCES

Stein, N., Rifai, K., Wahl, S., and Lappe, M. (2021). Simulating lens distortion in virtual reality. In Proceedings of the 13th International Conference on Disability, Virtual Reality & Associated Technologies (https://miami.uni-muenster.de/Record/1b1fc62f-a70a-4a01-b8d4-40e845ff9f5e/Summary#tabnav).

't Hart, B.M., and Einhauser, W. (2012). Mind the step: complementary effects of an implicit task on eye and head movements in real-life gaze allocation. Exp. Brain Res. *223*, 233–249.

Albright, T.D., and Desimone, R. (1987). Local precision of visuotopic organization in the middle temporal area (MT) of the macaque. Exp. Brain Res. *65*, 582–592.

Alvarez, T.L., Han, S., Kania, C., Kim, E., Tsang, O., Semmlow, J.L., Granger-Donetti, B., and Pedrono, C. (2009). Adaptation to progressive lenses by presbyopes. In 2009 4th International IEEE/EMBS Conference on Neural Engineering (IEEE), pp. 143–146.

Andersen, G.J. (1989). Perception of three-dimensional structure from optic flow without locally smooth velocity. J. Exp. Psychol. Hum. Percept. Perform. *15*, 363–371.

Angelaki, D.E., and Hess, B.J. (2005). Self-motion-induced eye movements: effects on visual acuity and navigation. Nat. Rev. Neurosci. *6*, 966–976.

Atchison, D.A. (1995). Accommodation and presbyopia. Ophthalmic Physiol. Opt. *15*, 255–272.

Berard, J.R., Fung, J., McFadyen, B.J., and Lamontagne, A. (2009). Aging affects the ability to use optic flow in the control of heading during locomotion. Exp. Brain Res. *194*, 183–190.

van den Berg, A.V. (1992). Robustness of perception of heading from optic flow. Vis. Res *32*, 1285–1296.

Bremmer, F., Kubischik, M., Pekel, M., Hoffmann, K.P., and Lappe, M. (2010). Visual selectivity for heading in monkey area mst. Exp. Brain Res. *200*, 51–60.

Calow, D., and Lappe, M. (2007). Local statistics of retinal optic flow for self-motion through natural sceneries. Network *18*, 343–374.

Calow, D., and Lappe, M. (2008). Efficient encoding of natural optic flow. Network *19*, 183–212.

Foulkes, A.J., Rushton, S.K., and Warren, P.A. (2013). Flow parsing and heading perception show similar dependence on quality and quantity of optic flow. Front. Behav. Neurosci. *7*, 49.

Gibson, J.J. (1950). The Perception of the Visual World (Houghton Mifflin).

Habtegiorgis, S.W., Rifai, K., Lappe, M., and Wahl, S. (2017). Adaptation to skew distortions of natural scenes and retinal specificity of its aftereffects. Front. Psychol. *8*, 1158.

Habtegiorgis, S.W., Rifai, K., and Wahl, S. (2018). Transsaccadic transfer of distortion adaptation in a natural environment. J. Vis. *18*, 13.

Han, Y., Ciuffreda, K.J., Selenow, A., and Ali, S.R. (2003). Dynamic interactions of eye and head movements when reading with single-vision and progressive lenses in a simulated computer-based environment. Invest. Ophthalmol. Vis. Sci. *44*, 1534–1545.

Heeger, D.J., and Jepson, A.D. (1992). Subspace methods for recovering rigid motion i: algorithm and implementation. Int. J. Comput. Vis. *7*, 95–117.

Hollands, M.A., Marple-Horvat, D.E., Henkes, S., and Rowan, A.K. (1995). Human eye movements during visually guided stepping. J. Mot. Behav. *27*, 155–163.

Hollands, M.A., Patla, A.E., and Vickers, J.N. (2002). "Look where you're going!": gaze behaviour associated with maintaining and changing the direction of locomotion. Exp. Brain Res. *143*, 221–230.

Jin, D.Z., Dragoi, V., Sur, M., and Seung, H.S. (2005). Tilt aftereffect and adaptation-induced changes in orientation tuning in visual cortex. J. Neurophysiol. *94*, 4038–4050.

Johnson, L., Buckley, J.G., Scally, A.J., and Elliott, D.B. (2007). Multifocal spectacles increase variability in toe clearance and risk of tripping in the elderly. Invest. Ophthalmol. Vis. Sci. *48*, 1466–1471.

Jones, J.A., Edewaard, D., Tyrrell, R.A., and Hodges, L.F. (2016). A schematic eye for virtual environments. In 2016 IEEE Symposium on 3D User Interfaces (3DUI) (IEEE), pp. 221–230.

Lappe, M., and Rauschecker, J.P. (1993). A neural network for the processing of optic flow from ego-motion in man and higher mammals. Neural Comput. *5*, 374–391.

Lappe, M., and Rauschecker, J.P. (1995). Motion anisotropies and heading detection. Biol. Cybern. *72*, 261–277.

Lappe, M., Bremmer, F., Pekel, M., Thiele, A., and Hoffmann, K.P. (1996). Optic flow processing in monkey sts: a theoretical and experimental approach. J. Neurosci. *16*, 6265–6285.

Lappe, M., Pekel, M., and Hoffmann, K.P. (1998). Optokinetic eye movements elicited by radial optic flow in the macaque monkey. J. Neurophysiol. *79*, 1461–1480.

Lappe, M., Bremmer, F., and van den Berg AV, A. (1999). Perception of self-motion from visual flow. Trends Cogn. Sci. *3*, 329–336.

Lappe, M., Jenkin, M., and Harris, L.R. (2007). Travel distance estimation from visual motion by leaky path integration. Exp. Brain Res. *180*, 35–48.

Li, L., Ni, L., Lappe, M., Niehorster, D.C., and Sun, Q. (2018). No special treatment of independent object motion for heading perception. J. Vis. *18*, 19, 1–16.

Longuet-Higgins, H.C., and Prazdny, K. (1980). The interpretation of a moving retinal image. Proc. R. Soc. Lond. B Biol. Sci. *208*, 385–397.

Lord, S.R., Dayhew, J., Howland, A., and Howland, A. (2002). Multifocal glasses impair edge-contrast sensitivity and depth perception and increase the risk of falls in older people. J. Am. Geriatr. Soc. *50*, 1760–1766.

Matthis, J.S., Yates, J.L., and Hayhoe, M.M. (2018). Gaze and the control of foot placement when walking in natural terrain. Curr. Biol. *28*, 1224–e5.

Meister, D.J., and Fisher, S.W. (2008a). Progress in the spectacle correction of presbyopia. part 1: design and development of progressive lenses. Clin. Exp. Optom. *91*, 240–250.

Meister, D.J., and Fisher, S.W. (2008b). Progress in the spectacle correction of presbyopia. part 2: modern progressive lens technologies. Clin. Exp. Optom. *91*, 251–264.

Miles, F.A., and Busettini, C. (1992). Ocular compensation for self-motion. Visual mechanisms. Ann. N. Y Acad. Sci. *656*, 220–232.

Musil, R. (2021). HMD Geometry Database — Collected Geometry Data from Some Commercially Available VR Headsets (https://risa2000.github.io/hmdgdb/).

Niemann, T., Lappe, M., Büscher, A., and Hoffmann, K.P. (1999). Ocular responses to radial optic flow and single accelerated targets in humans. Vis. Res *39*, 1359–1371.

Patla, A.E., and Vickers, J.N. (1997). Where and when do we look as we approach and step over an obstacle in the travel path? Neuroreport *8*, 3661–3665.

Rifai, K., and Wahl, S. (2016). Specific eye–head coordination enhances vision in progressive lens wearers. J. Vis. *16*, 5.

Rifai, K., Habtegiorgis, S.W., Erlenwein, C., and Wahl, S. (2020). Motion-form interaction: motion and form aftereffects induced by distorted static natural scenes. J. Vis. *20*, 10.

Sauer, Y., Wahl, S., and Rifai, K. (2020). Parallel adaptation to spatially distinct distortions. Front. Psychol. *11*, 544867.

Schütt, H.H., Harmeling, S., Macke, J.H., and Wichmann, F.A. (2016). Painfree and accurate bayesian estimation of psychometric functions for (potentially) overdispersed data. Vis. Res *122*, 105–123.

Sheedy, J.E., Campbell, C., King-Smith, E., and HAYES, J.R. (2005). Progressive powered lenses: the minkwitz theorem. Optom. Vis. Sci. *82*, 916–922.

Sidaway, B., Fairweather, M., Sekiya, H., and Mcnitt-Gray, J. (1996). Time-to-collision estimation in a simulated driving task. Hum. Factors *38*, 101–113.

Warren, W.H., and Hannon, D.J. (1988). Direction of self-motion is perceived from optical flow. Nature *336*, 162–163.

Warren, W.H., and Hannon, D.J. (1990). Eye movements and optical flow. J. Opt. Soc. Am. A. *7*, 160–169.

Warren, W.H., Kay, B.A., Zosh, W.D., Duchon, A.P., and Sahuc, S. (2001). Optic flow is used to control human walking. Nat. Neurosci. *4*, 213–216.

STAR★METHODS

KEY RESOURCES TABLE

REAGENT or RESOURCE	SOURCE	IDENTIFIER
Software and algorithms		
MATLAB (R2020a)	MathWorks	RRID: SCR_001622
Unity (2019.4)	Unity Technologies	
Subspace algorithm	Heeger and Jepson (1992)	https://doi.org/10.1007/BF00128130
Model for heading estimation	This paper	https://github.com/MalteScherff/Self-motion-illusions-from-distorted-optic-flow-in-multifocal-glasses

RESOURCE AVAILABILITY

Lead contact

Further information and requests for resources should be directed to and will be fulfilled the lead contact, Yannick Sauer (yannick.sauer@uni-tuebingen.de).

Materials availability

This study did not generate new unique reagents.

Data and code availability

Experimental data and simulation results reported in this paper will be shared by the lead contact upon request. The model simulation code is accessible on github.com. Any additional information required to reanalyze the data reported in this paper is available from the lead contact upon request.

METHOD DETAILS

Ray tracing optical distortions

The lens design used for this study is a progressive addition lens (PAL) without optical correction in the far zone and with addition power 2dpt in the near zone. To simulate the distortions of this lens we calculated the projection of points on a virtual image plane in front of the lens onto the image plane behind the lens. The points on the virtual image plane with fixed distance d in front of the lens were defined on an equidistant grid. For each point (x,y) the perceived distorted position (x_d, y_d) through the lens is calculated by ray tracing. Figure 1 B shows an example of an undistorted image grid and a distorted image grid.

As a mathematical description of the distortion, we define a function $\mathcal{F}$, which transforms a point (x,y) in the undistorted image plane to the point (x_d, y_d) in the distorted image, i.e. the point at which it would appear when looking through the lens.

$$\begin{pmatrix} x_d \\ y_d \end{pmatrix} = \begin{pmatrix} \mathcal{F}_x(x,y) \\ \mathcal{F}_y(x,y) \end{pmatrix} \quad \text{(Equation 1)}$$

The two components of $\mathcal{F}$ and their derivatives were interpolated from a 21×21 ray traced grid using 2D linear interpolation in Matlab (The Mathworks Inc, Natick, MA, USA). Individual transformation functions were prepared based on individual distortion grids for the gaze directions tested in this study. In the central view condition, the simulated gaze during ray tracing was through the center of the PAL. For the peripheral view condition, the simulated gaze crossed the lens at 20° vertically downwards and ±20° horizontally.

Simulation of heading estimation

Our model simulations follow the subspace algorithm (Heeger and Jepson, 1992) as implemented in the population heading map model (Lappe and Rauschecker, 1995; Lappe et al., 1996). Here we describe how this model is applied to distorted flow. We begin by describing how the distorted flow field is calculated for a given heading and gaze direction and then describe the process and simulation for recovering heading from such a distorted flow field.

Calculation of the distorted optic flow field. The undistorted optic flow vector arising from a static three-dimensional point $\boldsymbol{P}=(X,Y,Z)$ due to the movement of a monocular observer is described as

$$v(\boldsymbol{P}) = \frac{1}{Z}\begin{pmatrix} -f & 0 & x \\ 0 & -f & y \end{pmatrix}\boldsymbol{T} + \begin{pmatrix} (xy)/f & -(f+x^2/f) & y \\ f+y^2/f & -(xy)/f & -x \end{pmatrix}\boldsymbol{\Omega} = \begin{pmatrix} \dot{x} \\ \dot{y} \end{pmatrix}, \qquad \text{(Equation 2)}$$

where $\boldsymbol{T}=(T_X,T_Y,T_Z)^\top$ depicts the observer's translation and $\boldsymbol{\Omega}=(\Omega_X,\Omega_Y,\Omega_Z)^\top$ the rotation of the eye. This equation is the time derivative of the perspective projection

$$pr(\boldsymbol{P}) = f(X/Z, Y/Z) = (x,y)$$

onto an image plane placed perpendicular to the line of sight in distance f and is used regularly to describe optic flow (Longuet-Higgins and Prazdny, 1980; Heeger and Jepson, 1992; Lappe and Rauschecker, 1995). Wearing PALs alters the path the light takes in the projection onto the image plane. To account for such effects we included distortions via the aforementioned functions $\mathcal{F}$ into the projection. Taking the derivative with respect to time of this new type of projection

$$pr_d(\boldsymbol{P}) = \begin{pmatrix} \mathcal{F}_x(pr(P)) \\ \mathcal{F}_y(pr(P)) \end{pmatrix} = \begin{pmatrix} \mathcal{F}_x(x,y) \\ \mathcal{F}_y(x,y) \end{pmatrix}$$

results in the following equation for distorted optic flow,

$$v_d(\boldsymbol{P}) = \begin{pmatrix} \dot{x}_d \\ \dot{y}_d \end{pmatrix} = \begin{pmatrix} \frac{\partial \mathcal{F}_x}{\partial x} & \frac{\partial \mathcal{F}_x}{\partial y} \\ \frac{\partial \mathcal{F}_y}{\partial x} & \frac{\partial \mathcal{F}_y}{\partial y} \end{pmatrix}\begin{pmatrix} \dot{x} \\ \dot{y} \end{pmatrix}. \qquad \text{(Equation 3)}$$

Equations 2 and 3 were used to calculate the flow vector for a point $\boldsymbol{P}$ on the ground plane at image plane position $pr(\boldsymbol{P})$ for the undistorted and $pr_d(\boldsymbol{P})$ for the distorted projection.

Heading estimation. The subspace algorithm (Heeger and Jepson, 1992) computes the likelihood of a set of candidate heading directions, the heading space, as a least-squares residual value for each of the candidate directions for a given flow field. This value describes how incongruous a particular direction is with the flow field. Finding the minimum in the residual surface of the heading space leads to the most suitable heading direction to explain the given flow field. In the model, the flow field is split into smaller, locally restricted patches that are evaluated separately. Finding the minimum of the sum of the emerging residual surfaces increases the robustness and uniqueness of the estimation.

A schematic illustration of the simulation process for a single flow field distorted due to the peripheral gaze condition can be seen in Figure 4. The flow field consists of four randomly placed patches, each containing 10 flow vectors (Figure 4A). The residual surfaces are calculated per patch and displayed after a logarithmic transformation for better discriminability (Figure 4B, left). Every single patch carries enough information for running the subspace algorithm and estimate the most likely heading for these flow vectors. Those headings are marked with red dots in the residual surfaces. The full model sums up all the residual surfaces and estimates the heading direction based on the summed residual landscape (Figure 4B, right).

The subspace algorithm finds the best-matching heading for a flow field that consists of observer translation and gaze rotation. It can be constrained to search only for combinations of gaze rotations that result from fixations of environmental objects or for gaze rotations that are free of torsion (Lappe and Rauschecker, 1995). In our simulations we included only the latter constraint.

For application of the subspace algorithm we needed to select points on the ground plane for which the flow vectors were calculated to constitute the flow field. For this, random locations for the centers of 50 patches in the visual field were selected and the size (area) of each patch set according to the following equation

$$A = (1.04^\circ + 0.61\varepsilon)^2 \qquad \text{(Equation 4)}$$

with ε being the respective center point's eccentricity. This increase in patch size with eccentricity is based on similar findings in the visual system of primates and is well matched to the natural statistics of optic flow fields (Albright and Desimone, 1987; Calow and Lappe, 2007, 2008). Then, ten locations were chosen randomly inside each patch. At each location, the optic flow vector was calculated according to Equations

2 and 3, assuming a point P on the ground plane that is projected onto this location, a translation T as predefined for the simulation, and a rotation $\boldsymbol{\Omega}$ that nullifies the optic flow at the fixation point in the undistorted condition to simulate the tracking motion. Combining all of these vectors from within all patches results in the full flow field.

Simulation procedure. Aiming to simulate self-motion estimations based on optic flow we established the scene by placing a virtual monocular observer on a plane consisting of single points. Gaze was directed 20° downwards onto the fixation point from a simulated eye height of 1.8 m. Translation was initialized 20° to the left and to the right of that point and parallel to the floor with an added vertical heading angle between −3.5° and 3.5° in steps of 0.5°. Rotation was calculated such that the gaze remains on the fixation point. To include the distortions we used the aforementioned functions $\mathcal{F}$.

Candidate and heading directions were defined in retinal coordinates, relative to the gaze direction. Hence $(0°, 20°)$ describes the translation parallel to the floor toward the fixation point and was set to be the center of the set of candidate directions. That heading space covered an area of $70° \times 20°$ in which all directions sampled in 0.25° steps horizontally and vertically were tested for their compatibility with the flow fields. This included all heading directions that were actually used in flow field calculations.

The maximum simulated FoV was set to be a circular area with radius 55° in accordance to the specifications given by the VR-headset manufacturer. To explore differences in heading estimations based on different FoV sizes we further defined a set of effective FoV sizes to range from a FoV with radius 40° up to one with radius 55°. These simulations used only patches of the flow field for which all the locations of the vectors in a patch are within the effective FoV.

Overall the complete simulation consisted of 50 separate runs, each containing the evaluation of flow fields that resulted from 90 combinations of heading directions and distortion conditions.

Experimental methods

To study human perception under the influence of PAL distortions in an isolated environment, we developed a simulation of optical distortions in VR. In a psychophysical experiment the self-motion scenario of moving along a virtual ground plane was recreated. PAL distortions were presented in two different conditions representing the two different directions of gaze through the progressive lens. The vertical heading perception of subjects was tested with a direction discrimination task.

Participants. Thirteen subjects (seven female and six male) aged between 21 and 28 years (mean = 24.0 years) participated in the study. None of the participants reported any ocular complication or any medical condition that would affect their normal vision or their motion judgements. There was no prior history of epilepsy or motion sickness.

Ethics. The study adhered to the tenets of the Helsinki Declaration (2013). The ethics authorisation to perform the measurements was granted by the Medical Faculty Human Research Ethics Committee from the University of Tuebingen. Prior to data collection, the experiment was explained in detail to the participants, and written informed consent was collected from each participant.

Distortion simulation in VR. The aforementioned ray-tracing function for an optical lens was be used in our VR framework to simulate the influence of optical distortions in a virtual environment. The distortion simulation was implemented in the game engine Unity (Unity Technologies, CA, USA) as a post processing shader (a program part manipulating the rendered image), which geometrically transforms the rendered image according to the mathematical transformation defined before. The pixel transformation is implemented as a fragment shader. For a pixel position in the output texture, the corresponding position in the input texture is needed. The inverse transformation function $\mathcal{F}^{-1}$, i.e., the mapping from distorted image to undistorted image, is used for this process. $\mathcal{F}^{-1}$ is approximated using a 2D polynomial fit of the ray traced distortion data: In Matlab, two functions were fitted, for the x and y component of $\mathcal{F}$, so that ${\mathcal{F}_x}^{-1}(x_d,y_d) = x$ and ${\mathcal{F}_y}^{-1}(x_d,y_d) = y$, where (x,y) are the defined object points for ray tracing and (x_d,y_d) corresponding distorted points, as perceived through a progressive lens.

Before applying the function, the Unity texture coordinates $(u,v) \in [0,1] \times [0,1]$ had to be scaled and shifted to points (x,y) in the corresponding image plane considering the virtual cameras horizontal and vertical FoV. The center of the rendered left and right eye image textures are not exactly the center of visual field, corresponding to the center of the ray tracing simulations. This vertical and horizontal displacement is accessible from the projection matrices of the left and right eye virtual cameras in Unity. The coordinates (x,y) were shifted by this displacement (Δ_x, Δ_y) so that the origin (0,0) corresponds to the center of the simulated distortion mesh

$$\begin{pmatrix} x \\ y \end{pmatrix} = \begin{pmatrix} 2(u-0.5)\tan\left(\frac{\mathrm{FoV_{hor}}}{2}\right) \\ 2(v-0.5)\tan\left(\frac{\mathrm{FoV_{ver}}}{2}\right) \end{pmatrix} - \begin{pmatrix} \Delta_x \\ \Delta_y \end{pmatrix} \quad \text{(Equation 5)}$$

To determine the corresponding pixel position in the undistorted image (x,y), the inverse transformation is applied to (x_d,y_d):

$$(x,y) = \mathcal{F}^{-1}(x_d, y_d) \quad \text{(Equation 6)}$$

The image plane coordinates (x,y) are now mapped back to texture coordinates (u,v) of the original undistorted texture:

$$u = \frac{x+\Delta x}{2\tan\left(\frac{\mathrm{FoV_{hor}}}{2}\right)} + 0.5 \quad \text{(Equation 7)}$$

$$v = \frac{y+\Delta y}{2\tan\left(\frac{\mathrm{FoV_{ver}}}{2}\right)} + 0.5 \quad \text{(Equation 8)}$$

Unity then automatically interpolated the value of the pixel (u_d,v_d) in the output texture from pixels (u,v) in the input texture. This results in the distorted image.

The shader-based coordinate scaling and pixel transformation was validated by comparing the rendered output with a distorted texture precomputed in using the same transformation function.

Stimulus creation and VR setup. The virtual environment for the experiment was implemented using Unity and presented to participants using an HTC Vive Pro Eye VR headset (HTC Corporation, Taoyuan, Taiwan). The manufacturer claims a FoV of the VR headset of 110°, although the effectively visible FoV is usually smaller, depending on the individual subject's eye position and placement of the headset on the head. Optic flow was induced by a moving virtual ground plane with a perlin noise texture. The background above the horizon was uniformly gray. To present the same optic flow to each subject, the virtual ground plane was fixed relative to the subject's view with the virtual eye height of 1.8 m. The direction of the virtual camera was 20° downwards and 20° left or right (randomized between subjects) relative to the direction of motion. The subject's virtual position relative to the floor and motion direction are illustrated in Figure 2. Position and orientation tracking of the VR headset was turned off for this experiment, in order for the presented stimulus not to be influenced by a change of position or orientation of the subject. Apart from the ground plane, only a dot was shown in the center of the visual field as a fixation target.

Procedure. Subjects were introduced to the experiment procedure before putting on the VR headset. They performed the experiment in a seated position with their head placed on a chin rest to maintain a stable head position. At the beginning of a trial, only a centered dot as fixation target was visible, while the ground plane was not shown yet. Subjects were instructed to fixate the fixation target. Compliance was controlled by the eye tracker of the Vive Pro Eye headset. Subjects pressed a key on a keyboard to start the trial. The motion phase of the trial started only if gaze was within 2° to the fixation target. After the keypress, the ground plane faded in within 0.2s while the fixation point faded out. The fade out of the fixation point ensured that subjects could perform involuntary tracking motion during the later presented flow (Miles and Busettini, 1992; Lappe et al., 1998; Angelaki and Hess, 2005). Then the actual motion started. It simulated a 0.3s translation over the ground plane at a speed of $2\mathrm{ms}^{-1}$ with a vertical component (heading angle) between −3.5° and 3.5° in steps of 0.5°.

Afterward, the ground plane disappeared and subjects reported their perceived vertical heading direction by pressing the 'up' key on the keyboard when they felt lifting up and the 'down' key when they felt sinking. The next trial started after the subjects gave their response. In one session, all three distortion conditions - undistorted, central view, and peripheral view - were presented. All motion directions were performed 12 times for all distortion conditions leading to 540 trials in total. The order of presented distortions, as well as heading angles, was randomized.

QUANTIFICATION AND STATISTICAL ANALYSIS

To measure the influence of the distortions on heading perception, the vertical translation angle perceived as a motion parallel to the floor was determined for each of the three distortion conditions. For each subject and each distortion condition, first, the percentage of answers upwards was computed depending on the vertical angle of the simulated motion relative to the ground plane.

These datasets were then fitted with a cumulative normal distribution function with free but equal asymptotes using Psignifit (Schütt et al., 2016). The 50% point of the fit function was used as the point of subjective equality (PSE). It corresponds to the vertical motion angle that is perceived as a movement parallel to the floor by the subject in the specific condition.

To identify the influence of the simulated distortions, we compared the PSEs in the two distorted conditions to the undistorted condition by calculating the difference ΔPSE. As statistical analysis, one-sample *t*-tests were used with ΔPSE to test the presence of a significant shift of perceived heading.

scientific reports

Check for updates

OPEN

An objective measurement approach to quantify the perceived distortions of spectacle lenses

Yannick Sauer[1,2,4]✉, David-Elias Künstle[1,3,4]✉, Felix A. Wichmann[1] & Siegfried Wahl[1,2]

The eye's natural aging influences our ability to focus on close objects. Without optical correction, all adults will suffer from blurry close vision starting in their 40s. In effect, different optical corrections are necessary for near and far vision. Current state-of-the-art glasses offer a gradual change of correction across the field of view for any distance—using Progressive Addition Lenses (PALs). However, an inevitable side effect of PALs is geometric distortion, which causes the *swim effect*, a phenomenon of unstable perception of the environment leading to discomfort for many wearers. Unfortunately, little is known about the relationship between lens distortions and their perceptual effects, that is, between the complex physical distortions on the one hand and their subjective severity on the other. We show that perceived distortion can be measured as a psychophysical scaling function using a VR experiment with accurately simulated PAL distortions. Despite the multi-dimensional space of physical distortions, the measured perception is well represented as a 1D scaling function; distortions are perceived less with negative far correction, suggesting an advantage for short-sighted people. Beyond that, our results successfully demonstrate that psychophysical scaling with ordinal embedding methods can investigate complex perceptual phenomena like lens distortions that affect geometry, stereo, and motion perception. Our approach provides a new perspective on lens design based on modeling visual processing that could be applied beyond distortions. We anticipate that future PAL designs could be improved using our method to minimize subjectively discomforting distortions rather than merely optimizing physical parameters.

The natural decline in the eye's accommodative capabilities makes it progressively harder to focus on close objects. This natural aging process results in the eye's lens becoming less flexible, losing its ability to change shape. Approximately 2 billion people worldwide suffer from this condition, termed *presbyopia*[1,2]; without optical correction, all adults would experience blurry close vision starting in their 40s.

Presbyopes can use reading glasses for sharp near vision, which have to be taken off for looking at distant objects—in the case of preexisting corrections, this requires constant switching between two pairs of glasses. The convenient solution combines both lenses: the near correction at the bottom and the far correction at the top of each lens[3]. Those so-called bifocal lenses, however, cannot offer correction for intermediate distances and show a visible, distracting border at the transition between both lens areas. This edge in the lens is also considered to create a stigma of glasses for "old people". An obvious refinement is a smooth transition between the near and far areas by gradually changing the curvature of the lens surface. These Progressive Addition Lenses (PALs) became available in the second half of the 20th century through technical advances in manufacturing technologies[4,5]. Today, PALs are the state-of-the-art lens in presbyopia correction.

Even though there has been great progress in improving PALs, the gradual increase in optical correction between far and near areas will always lead to unwanted optical errors, so-called aberrations. This causes blur or degradation of sharpness in some areas of the lens. Another aberration is geometric distortion, a variation in the magnification across the visual field, leading straight lines to appear curved when looking through the lens (Fig. 1). Sadly, for PALs, it is physically impossible to reduce aberrations to zero, as stated by the Minkwitz theorem[6–8]. What lens designers and manufacturers can do, however, is to *change the distribution of aberrations* in the field of view—attempting to find subjectively more benign patterns of aberrations across the visual field.

[1]University of Tübingen, Tübingen, Germany. [2]Carl Zeiss Vision International GmbH, Aalen, Germany. [3]Tübingen AI Center, Tübingen, Germany. [4]These authors contributed equally: Yannick Sauer and David-Elias Künstle. ✉email: yannick.sauer@uni-tuebingen.de; david-elias.kuenstle@uni-tuebingen.de

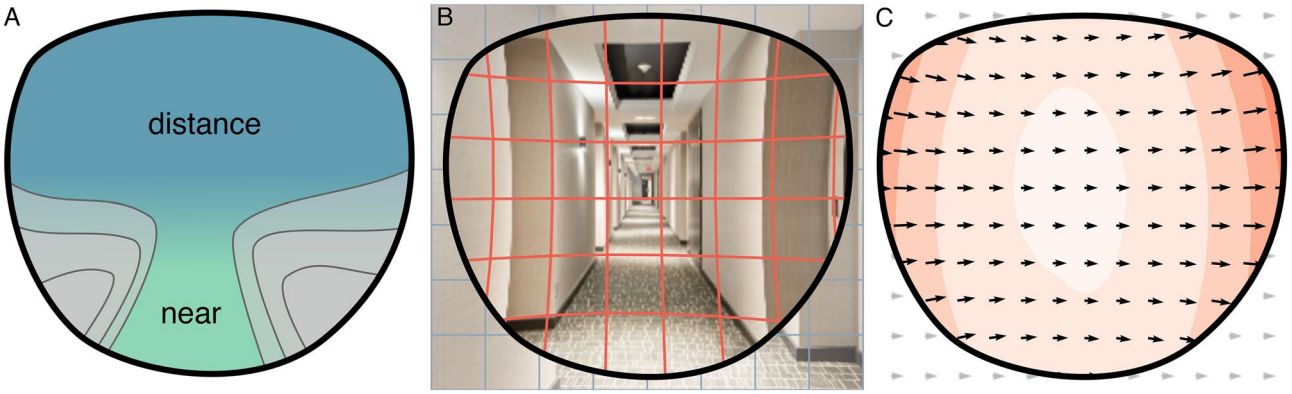

Figure 1. Progressive Addition Lenses (PALs). (**A**) The upper lens area is designed for far vision, with an optical power fitting the far refraction of the wearer. The optical power increases vertically towards the near area, which offers additional power for focusing close objects. The gradient in power will always lead to lateral astigmatism. (**B**) Optical distortions of PALs change the size and orientation of objects. Vertical and horizontal edges in a typical indoor environment appear curved. (**C**) Perceived motion during a horizontal head movement. The retinal motion pattern—optic flow—is altered by optical distortions. Points in the visual field move along curved trajectories instead of straight lines. Lens distortions increase towards the periphery leading to an increase in optic flow speed (illustrated by the heat map in the background). The unnatural distorted optic flow pattern can be perceived as an unstable movement of the environment (swim effect).

This flexibility in shifting the aberrations to different areas in PAL design is used to develop specific PALs for tasks like driving or office work. Such PALs show reduced blur in task-relevant areas, inevitably accompanied by increased blur in other areas, however.

How to optimize the design for distortions *in general* is an open question, however, because their influence on visual perception is poorly understood. The swim effect, a phenomenon of unnatural or unstable perception of the environment during head or eye movements, causing instability, dizziness, tripping, and nausea[8–11], is at least partly caused by geometric distortions. It is unclear how those effects scale with the physical distortion of the lens and its distribution across the visual field.

Understanding and quantifying the influence of distortions on human perception can—in future applications—enable PALs with reduced distortion-induced discomfort. To our knowledge, this study presents the first rigorous measurements of perceived distortions of PALs.

The main influence on PAL distortions is the optical correction in the far and near area, the optical power measured in diopters. The correction in the far area, the spherical power *Sph*, can be positive or negative (correction for hyperopia or myopia, respectively); in the near area, the additional power *Add* usually increases with the age of the wearer, since the eye can accommodate less and less by itself. The optical power changes progressively from the upper far area to the near area below, allowing vision at intermediate distances. Depending on the sign of *Sph*, the general shape follows a pincushion or barrel distortion[12], i.e., curving straight lines more inwards or outwards. Additionally, distortions show asymmetry between near and far areas, influenced by *Sph* and *Add*. Relating *Sph* and *Add* to perceived distortion builds a foundation for understanding PAL-induced discomfort.

Our suggested measurement is a psychophysical scale, quantifying the relative change of perceived distortion for different combinations of *Sph* and *Add*. This scale indicates how much distorted a lens feels if *Sph* or *Add* changes by a certain amount of diopters. We present distortions of PALs of different near and far correction in a virtual reality (VR) simulation. Aberrations of ophthalmic lenses have been studied previously using simulations in screen-based or VR set-ups[13–16], which allow greater control over the stimulus while, in the case of VR, still allowing natural behavior. In our experiment, subjects can move freely in a virtual indoor environment, inducing distorted motion perception under natural self-motion. To study the influence of geometric distortions independent from other typical aberrations of PALs, we simulate only geometric distortions, not the blur caused by other lens aberrations.

Each trial consecutively presents three out of eleven simulated PAL distortions of various *Sph* and *Add*. Subjects responded which distortions appeared more similar (1 & 2 or 2 & 3). This ordinal data is used to fit the subject's perceptual distortion scale with ordinal embedding methods[17]. Unlike other studies about PAL distortions, our embedding method results in an objective scaling function, which can quantify the relative influence of different lens parameters.

In contrast to screen-based distortion studies ([18–23]), VR technology allows considering stereo and motion perception like the swim effect. It minimizes the lab-to-reality gap—increases ecological validity[24]—by recreating actual lens distortions in realistic environments in which observers can move and experience visual consequences of their own actions.

In summary, we measure the perception of geometric distortions of PALs in a realistic VR environment with natural head movements—decoupled from other typical optical aberrations. Using an ordinal comparison-based experimental paradigm in combination with an analysis by an embedding algorithm, we derive their perceptual scales individually for every observer. Our statistical modeling predicts perception across subjects well, allowing

a potential application of our method for improving spectacle lenses by reducing perceived lens distortions for a generic observer.

Methods

Subjects

Subjects wearing spectacle lenses might already be habituated to certain distortions over the often long time having worn them. Thus only emmetropic subjects were included in the experiment to exclude this as a possible confounding factor; we assessed acuity of all subjects with the 6/6 Snellen chart. Seven male and seven female participants (mean age 24.6 years; SD 4.0 years) were confirmed not to have any known ocular diseases. One of the male subjects decided to discontinue the experiment because of VR sickness; therefore, the results of 13 subjects were analyzed. The study followed the principles of the Declaration of Helsinki and was approved by the ethical board committee of the University of Tübingen (439/2020BO). Informed consent was obtained from all participants before the measurements.

Stimuli

Subjects looked through simulated spectacles in a 3D-modelled hallway using an XTAL VR headset (VRgineers Inc, Prague, Czech Republic). The headset's horizontal FoV of 140 degree allows realistic simulation of spectacle lens distortions, affecting the part of the FoV covered by real spectacle lenses. The virtual environment was designed to replicate a scenario where distortions are visible clearly for PAL wearers: an indoor environment with many horizontal and vertical edges, shown in Fig. 2.

Distortions of ten different PALs were included in the experiment. The far refraction ranged from −5 dpt to 5 dpt in steps of 2.5 dpt. For each of those five *Sph* values, two lenses with *Add* power 1 dpt and 3 dpt were used. All 10 lenses had the same PAL design (ZEISS Smart Life). An additional undistorted condition was included for reference. The distortions were precalculated using ray tracing based on the lens surface data provided by the manufacturer[25]. The precalculated distortions are represented as horizontal and vertical displacement of image plane coordinates; the displacement vectors are stored pixel-wise as two color channels of a texture. In the Unity game engine, the texture is used as an input to transform the rendered image by performing a coordinate transformation in a fragment shader. The procedure is performed independently for left and right eye cameras. In our experiment, the same *Sph* and *Add* corrections were used for both eyes, resulting in horizontally mirrored distortions.

Similar to the edge of a spectacle frame, we show an ellipse-shaped mask in the FoV that separates the distorted "lens area" from the undistorted periphery. The XTAL VR headset has an FoV larger than typical spectacle lenses, which makes it possible to simulate a typical inner frame size of 54 mm by 28 mm with an ellipse of 116° inner width and a height of 80°. This frame ellipse was rendered on the image for each eye. The monocular FoV is limited in the nasal direction to 45°. Therefore, the ellipse is cut off in the nasal direction. The combined binocular perception shows a full ellipse. The ellipse thickness was 2° in visual angle.

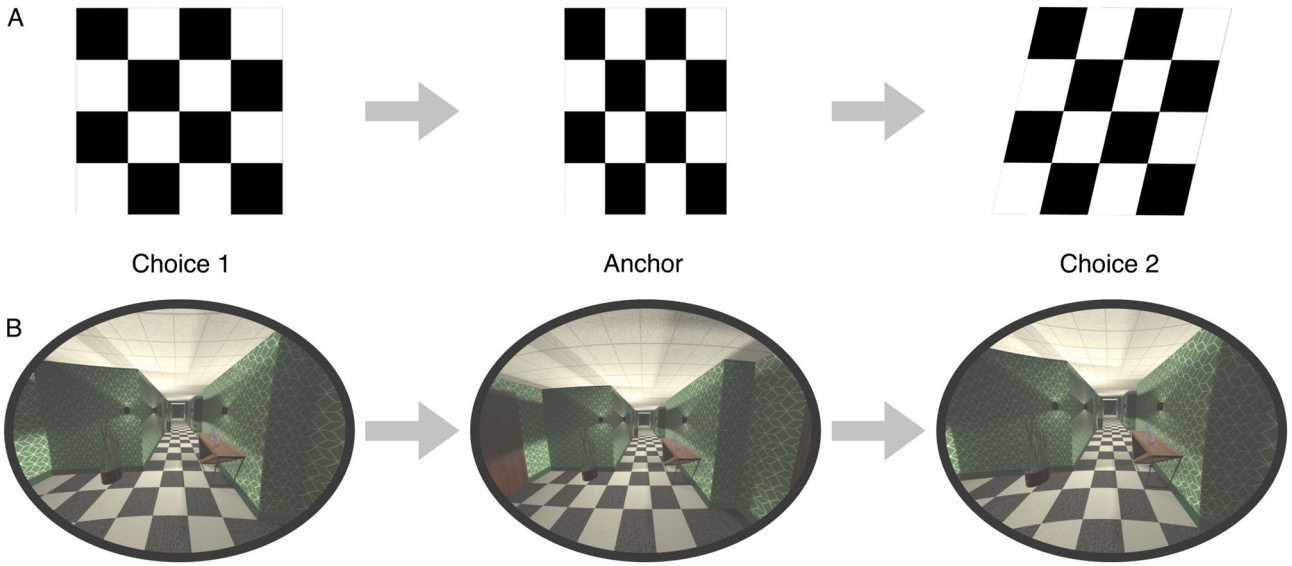

Figure 2. The triplet paradigm of the experiment presents three distortion stimuli consecutively in each trial: choice 1, anchor, and choice 2. The task for subjects was to answer if the first distortion (choice 1) or the last distortion (choice 2) is more similar to the second distortion (anchor). This task is equivalent to asking which of the two transitions between distortions seems smaller. (A) The checkerboard pattern with simple distortion transformations demonstrates the task during the initial training phase. (B) The experiment simulated PAL distortions in a virtual indoor environment. While the different distortions were presented, subjects could look around freely. Distorted motion perceived during dynamic behavior is expected to cause an unnatural or unstable perception of the environment.

Experiment procedure

The experiment used a triplet paradigm, presenting three distortion stimuli in each trial. The three distortions—choice 1, anchor, and choice 2—were all sampled from the predefined set of 11 stimuli (10 distortions and undistorted). Presentation time for each distortion stimulus was 2 s. Between stimuli, a 0.2 s transition was fading the image first to black and then to the next stimulus. Subjects had to judge the similarity of perceived distortions. They answered with a button press on a controller, which distortion—choice 1 or choice 2—appeared more similar to anchor. An alternative but equivalent instruction asks for the smaller transition: from choice 1 to the anchor or from the anchor to choice 2. In the experiment, both variants were used with the subjects.

Subjects were familiarised with this experiment procedure in multiple training phases. To clarify the experimental paradigm, in the first phase, stimuli were only checkerboard patterns distorted with clearly distinct transformations to make it easy for subjects to distinguish the distortions. One example is shown in Fig. 2. In phase two, the stimuli showed the 3D environment of the main experiment but with trivial distortion combinations (including easy-to-perceive distortions of lenses with *Sph* 8 dpt or 5 dpt together with clearly less distorted lenses). During those two training phases, a green or red colored background at the end of each trial gave feedback to the subjects if their answer was as expected (choosing the two strongly distorted or the two clearly less distorted lenses as more similar).

In the last training phase, the distortion combinations were similar in difficulty to the main experiment. No feedback was given after the subject's answer. This training phase ensured that all subjects had learned the triplet task and were familiar with the magnitude of (real-world) lens distortions used in the subsequent experiment.

The experiment was performed in a seated position while wearing the VR headset. Subjects could move and look around freely. To induce the swim effect, subjects were encouraged to move their head. This was done by tracking head movements during training phases 2 and 3 and only continuing the trials when subjects moved their head.

The perceived differences between some distortion stimuli can be small, possibly causing frustration. To increase motivation, the experiment included 20% of trivial trials, where one or two of the stimuli were exaggeratedly distorted (*Sph* 8 dpt) and the other was slightly or not distorted. Additionally, these trivial trials provide some baseline validation of subject performance because the misfitting stimulus of the three distortions is obvious and should never be chosen when following the experiment instructions correctly. In total, every subject did 413 trials, of which 83 were trivial. Each triplet combination of the 11 stimuli was presented twice, with flipped order of choice 1 and choice 2 in the second presentation. The trial order was randomized. Subjects could repeat the presentation of a trial any number of times if they felt too uncertain to respond, which might be necessary when there is a great similarity between choice 1 and choice 2 (the number of repetitions per subject can be found in Supplementary Fig. S1 online).

During the experiment, headset tracking data was recorded for subsequent analysis of head movement behavior. The SteamVR 2.0 tracking system (Valve Corporation, HTC)[26] was used with four base stations located around the participants' seating positions. Gaze data were captured with 120 Hz sampling frequency using the VR headset's included video-based eye tracker, accessed via the VRGineers XTAL Unity Plugin (version 2.08) and VRGineers XTAL runtime 3.0.0.77. For calibration, the manufacturer's 5-point calibration was used.

Data analysis

Psychophysical scale

The subject's perceived distortion was estimated from their trial responses (choice 1 or 2 is more similar to anchor) using so-called ordinal embedding methods[17]. These methods estimate a psychophysical scale that assigns coordinates to each stimulus so their distances agree with the subject's similarity judgments. Specifically, we used the *Soft Ordinal Embedding* (SOE)[27] algorithm, implemented in the *cblearn* Python package. The dimensionality of the scale has a great influence on how well the subjects' responses are represented in general. We chose the lowest dimensional scale that still is a good predictor of unseen triplet responses. This predictive accuracy is approximated with a cross-validation procedure[28]. The robustness of our scale can be approximated by repeated estimates on resampled sets of responses (bootstrapping); low spread across scale samples indicates that the scale is determined well by the responses.

The perceived distortions in a scale are only a relative measure and not an absolute value—to compare scales between subjects or to create an "average observer" scale; we aligned all scales using generalized Procrustes analysis[29]. This method minimizes the Euclidean distance between scales by iterative similarity transformations (translation, scaling, and flipping in our case) towards the mean scale. After alignment, we shifted all scales such that the origin—on average—corresponds to the undistorted lens (*Sph* 0 dpt and *Add* 0 dpt). Accordingly, the average scaling value of the distorted lens *Sph* 5 dpt *Add* 3 dpt has a distance 1 to the origin.

Head movement and gaze behavior

From tracking data of headset position and gaze direction, the individual behavior during the experiment was analyzed. Since the experiment was performed in a seated position, relevant head movements are mainly rotations. We analyzed the changes in head direction by transforming the tracked headset orientation into yaw, pitch, and roll angles (Tait-Bryan angles with order y-x-z) as illustrated in Fig. 4A. The movement velocity was computed independently for each rotation component. We calculated the mean velocity for each subject over each trial to illustrate changes in motion behavior over time. Aggregated velocity can be used to compare strategies between subjects.

Eye tracking in the VR headset is implemented independently for the left and right eye. First, the combined binocular eye gaze direction was calculated as the average of both eyes' direction vectors for each gaze sample. We compared gaze behavior between subjects by the area covered in the visual field. To do so, the binocular gaze

samples were transformed to longitude and latitude coordinates in the FoV. Then, a heatmap of individual gaze distribution was calculated with a Kernel Density Estimator of bandwidth 2 degrees as a verified upper bound of eye-tracker precision. We then calculated the solid angle of the 5% percentile, meaning the area in the heatmap, which includes 95% of the distribution's mass.

Results

A one-dimensional scaling function models perception of PAL distortions

Although physical descriptions of PAL distortions require many parameters, the perception of lenses can deviate from this parametrization. In our experiment, we use PALs of different *Sph* and *Add*, which influence the physical distortions differently: *Sph* influences more the overall shape and strength of distortions, while *Add* introduces more asymmetry in the distortion pattern. Multidimensional perception of these multidimensional distortions seems plausible. Any low-dimensional scale provides insights into which lens parameters dominate our perceived similarity of lens distortions and whether these parameters are the same in all persons. We measured individual scales of 13 subjects from triplet responses of 11 lenses of varied *Sph* and *Add*; lenses that are judged as more similar in the responses appear closer in the scale. Indeed, all subject scales are one-dimensional (Fig. 3) and show a comparable influence of *Sph* interacting with *Add*. Additional dimensions do not increase the predictive accuracy for all subjects (see Supplementary Fig. S5). This may be regarded as surprising, given the two varied lens parameters *Sph* and *Add* and their non-linear spatial effect on distortions. Apparently, the human visual system perceives the complex PAL distortions along a single dimension only.

The perceived distortion monotonically increases with both *Sph* and *Add*. For negative *Sph* values, an increase in *Add* leads to less perceived distortions (closer to undistorted), implying a compensation of perceived distortions; for positive *Sph*, an increase in *Add* only increases perceived distortions further. All in all, if *Sph* is strong compared to *Add*, the shape of distortions is mainly influenced by the sign of *Sph*, leading to either pincushion or barrel distortions, which cause different perception as proven by the change of sign of perceived distortions (with undistorted at 0). The relation between perceived distortions and *Sph* can be modeled with an exponential fit of $a + b \cdot c^{\mathrm{Sph}}$ for each value of *Add*, shown in Fig. 3 (right), illustrating a higher rate of increase for positive *Sph* compared to negative *Sph*. Fits between *Add* 1 and *Add* 3 mainly differ in the offset a and slope b, but barely in the base c. Close to *Sph* 0, the exponential fits show a similar rate of increase for *Sph* and *Add*. With higher correction values for *Sph*, the relative influence of *Add* decreases, indicating that for high-power lenses, *Sph* dominates distortions. The individual deviations from this exponential model do not have to be due to perceptual differences or measurement accuracy alone but can also be explained by behavior—if the distortion is perceived locally, it makes a difference where the subject looks through the lens and how they move.

Head and gaze tracking reveals subjects' different behavior

From reports about the swim effect—an unnatural and unpleasant percept of PAL distortions during motion—we expected that especially dynamic behavior might lead to a heightened perception of distortions and thus help subjects in discriminating the stimuli. In fact, we introduced subjects to this idea by explaining the possibility of distortions becoming apparent more clearly during self-motion. Furthermore, during the training phase of the experiment, head movement was actively enforced by our experimental design. To analyze the participants' motor behavior in more detail regarding which kind of behavior they would choose to discriminate distortions, the tracking data of head and eye movements was analyzed. This allows for identifying the strategies subjects followed to distinguish distortions and test for the possible influence of behavior on the perception of distortions.

Results of the head tracking show that subjects followed two different strategies: one group of 7 subjects performed continuous head movements, usually a nodding movement (pitch oscillation like in Fig. 4B and C,

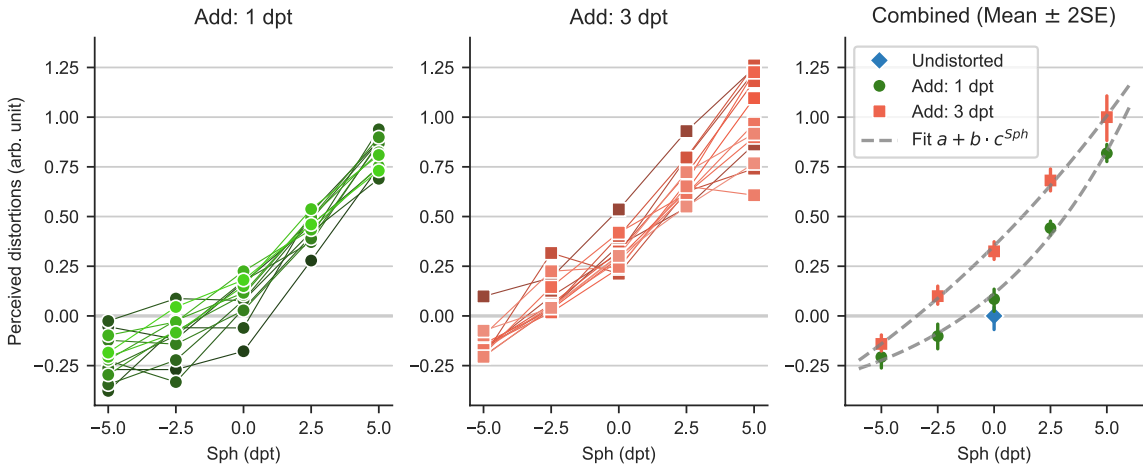

Figure 3. Psychophysical scaling functions of "perceived distortion" depending on the *Sph* and *Add* power of the simulated PALs. The lines in the left and middle plots show individual subjects, while the right plot shows their mean and standard error along an exponential function fit.

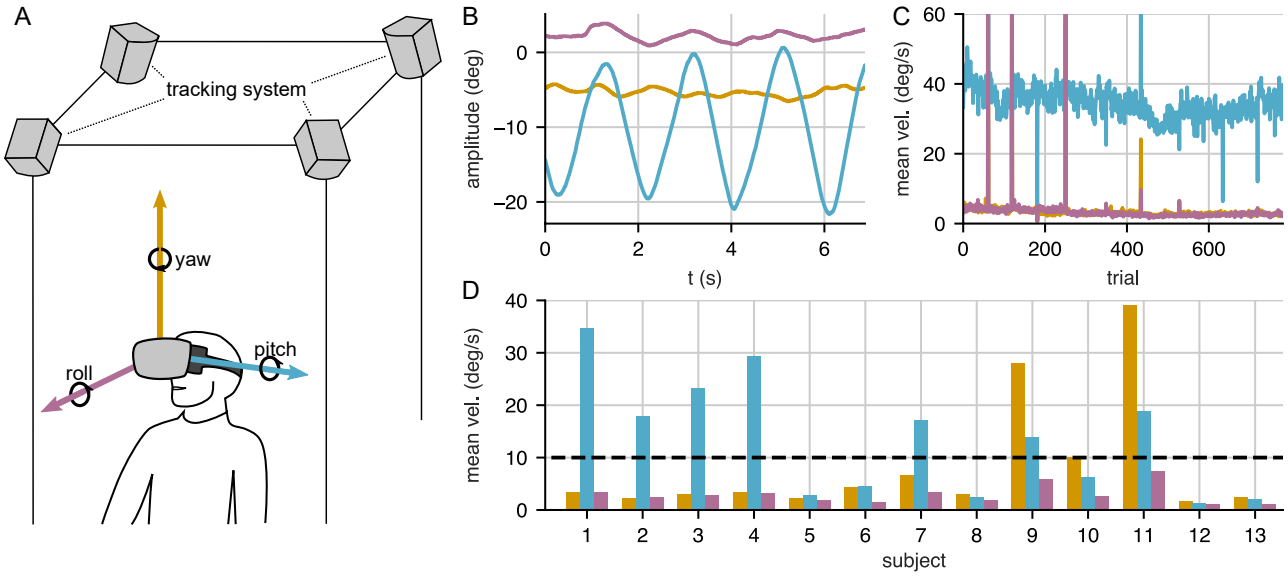

Figure 4. Head movements analyzed from VR headset tracking data (**A**) Tracking setup and definition of head rotation angles. Yaw, pitch, and roll were computed from the tracked orientation of the VR headset. (**B**) The three head rotation angles during one example trial. This example subject performed a continuous pitch movement (head nodding), while the roll and yaw angles stayed relatively stable. (**C**) The mean rotational velocities were calculated for each head rotation component over individual trials. Data is shown for one example subject that consistently followed the same head movement behavior. (**D**) The overview of mean angular velocities for all participants shows different head movement strategies: Some observers did not move their head, while others performed mainly a nodding (pitch) or mainly a horizontal movement (yaw).

some also yaw movements, while the other group of 6 subjects did not move their head or stopped after a few trials. Since subjects usually followed the same movement type throughout the experiment (head movement over time can be found in Supplementary Fig. S2), we calculated the mean velocity over the whole experiment as shown in Fig. 4D.

We grouped subjects in dynamic and static observers based on their mean head movement velocity. If the mean velocity of any of the three rotation components was higher than the defined threshold of $10° \, s^{-1}$ the subject was classified as dynamic observer; otherwise as static observer. The mean roll rotation velocity never was higher than the threshold. Dynamic subjects primarily performed horizontal (yaw) or vertical (pitch) movements. The rotation velocity threshold was chosen in agreement with the examiners' observation during the experiment. The static observers had to rely only on static distortion features in the scene for their comparison judgment. During the training phase, head movements were enforced; consequently, dropping this strategy during the main experiment either indicates that the movement does not convey relevant cues for the observers or that the non-moving observers were less motivated to perform well. We compared the consistency of dynamic and static observers regarding embedding accuracy and catch-trial performance. Accuracy counts the number of triplets that agree with the estimated embedding and thus measures the general coherence of responses; responses to catch-trials, however, should be unambiguous, and any error indicates a lack of concentration. There is a significantly better embedding accuracy ($p < 0.05$) as well as performance in the catch trials ($p < 0.01$) for more *static* observers using the Mann-Whitney U rank test (see Fig. 5). Consequently, it is unlikely that static observers were less motivated. Instead, for those subjects, dynamic features contributed less to the perception of distortions. This result contrasts with the expectation that especially dynamic behavior, associated with the swim effect, would give a clear cue for distinguishing distortions and more reliable results from dynamic observers.

The distribution of gaze in the FoV for the individual subjects is shown in Fig. 6. The gaze was mainly oriented along the center vertical axis, with variations in the latitude between individual observers. Some subjects show a high spread in gaze direction, while others stay in a more defined area of the FoV. This is reflected by the gaze area measure calculated from the individual gaze distributions. This finding suggests that some subjects, with a small gaze area, continuously fixated on the same part of PAL distortions, while others looked more at different parts of the distortion pattern. Next, we want to test if the described differences in behavior also influence the scaling of perceived distortions.

Distortion perception may not be determined by overt behavior

PAL distortions cause a complex, spatially varying transformation of the visual space, altering static and dynamic features and therefore the perception of shape, distance, and motion. Our behavior, however, influences which visual features we perceive; for example, head movements introduce perceived motion. If the various aspects of distortion perception scale differently with the PAL distortion components, then this should be revealed by differences in the scaling function between subjects of different behavior. Especially the difference between static and dynamic observers should show how the swim effect, associated with dynamic situations, contributed to

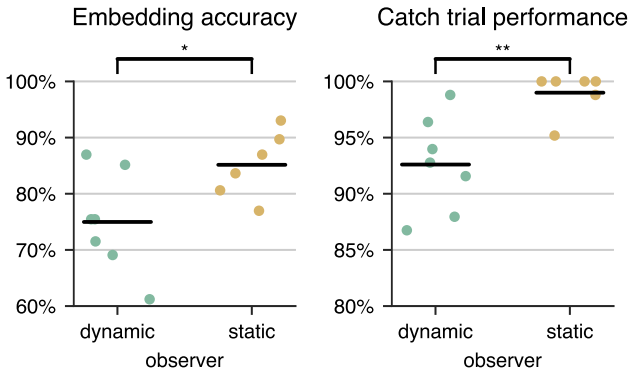

Figure 5. Difference in embedding accuracy and performance in the trivial catch trials between dynamic observers (head movements) and static observers (no head movements).

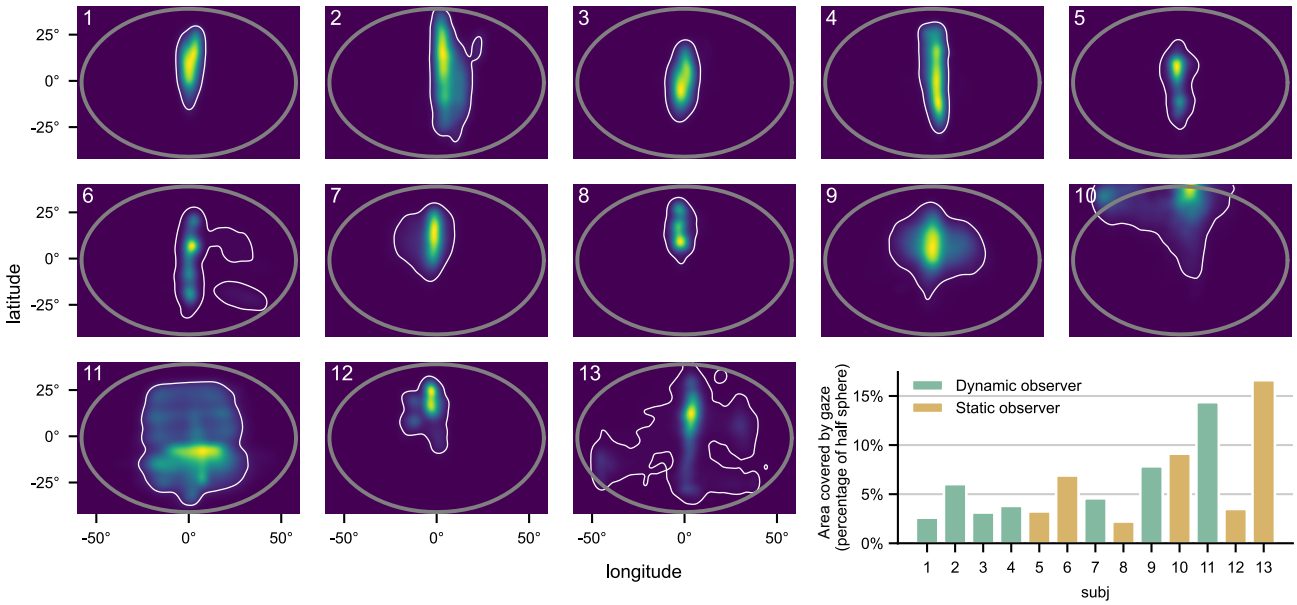

Figure 6. Individual gaze distribution of all observers with Gaussian kernel smoothing. Binocular gaze samples (in head-relative coordinates) of the whole experiment were combined to calculate the gaze distribution in the observers' FoV. The grey ellipse represents the virtual frame size, which was visible as a black border during the experiment. The white contour encompasses 95% of the gaze distribution mass. The area enclosed by this contour for individual subjects is shown in the bar diagram as percentage of the half-sphere area.

distortion perception. But also, different gaze strategies might cause differences in perceived distortion and thus in the recovered perceptual scales. Eye tracking results revealed differences in the spread of gaze. A wider area of gaze implies that subjects see a higher variability in distortions.

To statistically evaluate this possible influence of behavior on the scaling function, we used a linear model to predict perceived distortions depending on *Sph*, *Add*, and head and gaze behavior. For the two head-movement groups, we introduced a categorical variable in the model; gaze spread is modeled by the area in the field of view, covered by gaze (according to 95% KDE distribution mass, see Fig. 6). The model's fixed effects include *Sph*, *Add*, head-movement group, gaze area, and all their interactions. The preceding Procrustes analysis aligned the subjects' individual scales already by shifting and scaling so that random effects for slope or intercept do not have to be considered in the linear model.

To fit the linear model, we used `statsmodels`'s `ols` function in Python. *Sph* and *Add* both show significant effects on perceived distortions ($p < 0.001$). No other effects or interactions are significant. The differences in head movement and gaze behavior did not lead to significantly different perceptions of distortions, which indicates that perceptual effects of both static and dynamic features scale similarly with the amount of PAL distortions.

This result is, from a practical point of view, very good news: It implies that the general scaling of distortion perception is similar for all observers, independent of their specific and often idiosyncratic head and eye movements; different behavior does not lead to differently perceived distortions, which in turn allows a general quantification of perceived distortions for a specific PAL.

A non-linear fit of scales predicts perception of PAL distortions

Only if we can make predictions about the distortion perception of unmeasured subjects—based on scales measured from other subjects— is there a possibility that perception models can actually be used to improve lens designs beyond individual designs. We assessed the predictive ability of three differently complex regression models in a leave-one-subject-out procedure: the models are trained on all but one subject's scaling functions and subsequently tested on the omitted subject. We found that the perception of most subjects follows the same regularities, well captured by an exponential model.

The assessed models include the exponential fit from Fig. 3 along with baseline and ceiling performance models to provide a reference. The baseline model is a linear regression, and the ceiling model is a random forest regressor[30], known for excellent out-of-the-box performance in non-linear problems. R^2 scores in Fig. 7 show an overall high predictability in all but the baseline model, indicating that most of the subjects' scales can be predicted accurately. Inspecting the scales with lowest R^2 scores (compare Supplementary Fig. S4), we see some individual differences. In the extremes, subject 1 shows a noticeably higher influence of *Add* and a more pronounced flattening in negative *Sph*, while the *Add* parameter has almost no influence in the scale of subject 13. The responses of subjects 4 and 11 during the experiment seem less consistent, resulting in higher variations of the scaling estimates. For these subjects, the collection of additional trials might improve the agreement with other subjects and, therefore, improve predictability.

For most subjects, the exponential and random forest models substantially increase prediction over the linear model, again underlining the non-linear influence of *Sph* and *Add*. The random forest, however, can use its greater flexibility with only one subject to predict the scale better—an exponential model actually seems to describe the relationship between perceived distortions and lens parameters very well.

General discussion

We performed a VR experiment to determine a psychophysical scale of perceived optical distortions of PALs. Distortions were simulated in VR based on precalculated ray tracing of real PAL designs. A triplet paradigm was used to retrieve ordinal data of the relative perceived distance of distortions. The approach was tested with a set of PALs of varying *Sph* power (far correction) and *Add* power (near correction). In our explorative study, observers could move their heads and eyes freely to induce the perception of unnatural motion (swim effect) associated with the distortions of progressive lenses.

The scaling functions retrieved by fitting the ordinal data show a similar trend for all observers: perceived distortions increase with spherical power. For positive *Sph*, increasing the *Add* power results in stronger distortions. In contrast, the positive *Add* power in combination with negative *Sph* power reduces the perceived distortions (closer to undistorted), suggesting an advantage for short-sighted PAL wearers. For very high or very low *Sph*, the relative influence of *Add* on perceived distortions seems less relevant; close to *Sph* 0, *Add* and *Sph* seem to have a similar influence on perceived distortions. The relationship is very well modeled by a simple exponential function.

Behavior measurements of head and eye movements show that observers followed different strategies in the experiment. The most apparent strategy difference is the head movement behavior, which also leads to differences in the performance in catch trials. Some subjects moved their head continuously (nodding or shaking motion) while others kept their head stable, despite being instructed in the training of the experiment to perform head movements. This indicates that some observers might be less sensitive to perceive distortions from optic flow. This also agrees with the experience of PAL wearers: some individuals are more sensitive to the swim effect than others[11]. A speculative explanation would be that subjects who relied on head movements perceive the influence of distortions on optic flow more clearly and might suffer more from the swim effect.

However, no influence was found by head movement or gaze behavior for the psychophysical scaling function. We conclude that the global distortion pattern, not only the local distortions, influences the perception of

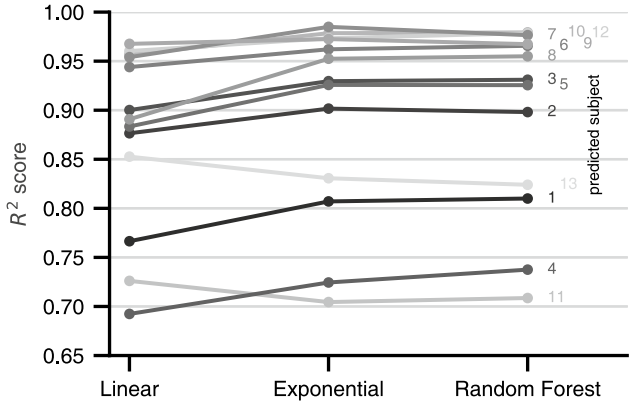

Figure 7. Performance in predicting a subject's perceived distortion with models that are trained on the remaining subjects' scales along *Sph* and *Add*. The linear and random forest models indicate baseline and ceiling performance. Exponential functions of *Sph*, grouped by same *Add*, predict similarly well as the much more general random forest model.

distortions with static and dynamic features. For our virtual scene, distortions perceived from static or dynamic features scale similarly to the PAL parameters. Additionally, the scales generalize well to new observers, confirming that our psychophysical scale can be used as an objective quantification method for PAL distortions. The remaining differences between subjects' scaling functions (for example, differences in the relative influence of *Add* power) could result from individual differences in perception or behavior. We suggest follow-up experiments focusing on increased stimulus and behavioral control. One aspect of our experiment that would be worth investigating in a more controlled setting is the significance of binocular vision for the swim effect. VR technology offers the opportunity to control binocular vision, which helps in investigating the influence of distortions on depth and surface curvature perception. It might be vital to perform binocular tests to ensure suitable participant recruitment. In any of those potential follow-up experiments, an increased number of participants would provide valuable information to identify potential patterns in the perception of observer groups, which could be included in our perceived distortion model.

Further research should investigate static versus dynamic effects in detail as well as extend our inquiry to other lens aberrations. Our study concentrates on the influence of distortions on perception. For real PALs, spherical, astigmatic, and higher-order aberrations negatively impact vision. The possible influence of those aberrations and the interaction with distortion perception could be studied in future experiments by including realistic blur in our VR simulation[31]. In more realistic viewing conditions, PAL wearers will adapt their behavior to gaze through the clear areas of the lens[32]. This development of a "head-mover" behavior[33] should not be confused with the dynamic movement strategy of one part of our subjects. In our experiment, the subjects' behavior reflects their strategy to distinguish differences in the distortions, while in everyday life, PAL wearers would likely follow an approach that minimizes discomfort. The gaze distribution would be determined by the current activity. For instance, during walking, the gaze would be directed downwards. In that sense, our results for behavior do not reflect the influence of PALs in everyday life but individual strategies for distinguishing between distortions.

Conclusion

In this study, we introduced a new measurement method for determining a psychophysical scale of optical distortions. Our measurements show a high agreement between subjects, allowing predictions of PAL distortion perception in general. These results reveal the potential of using psychophysical methods for understanding the swim effect and could help to improve future optical designs of PALs. As stated by the Minkwitz theorem, a total reduction of aberrations in the lens is impossible. Design choices for a given correction power can only change the spatial distribution of aberrations. Choosing a design with a lower amount of perceived distortions can contribute to reducing distortion-related discomfort for PAL wearers and increase satisfaction. To quantify different designs for their perceived distortion, it is required to repeat our experiment to measure perception not only depending on the correction power (*Sph* and *Add*) but directly on parameters describing the possible differences in PAL designs for a given correction. With a model based on the results of this suggested experiment, an arbitrary PAL design could be quantified for perceived distortions purely based on ray-traced distortion data without testing it in an additional experiment. As a completely new approach to lens design, this perception-focused optimization might lead to a realignment of current lens design processes.

Data availability

The dataset generated during this study as well as the analysis code is available on GitHub (https://github.com/ZeissVisionScienceLab/PAL-distortion-scaling).

Received: 10 October 2023; Accepted: 12 February 2024
Published online: 17 February 2024

References

1. Fricke, T. R. *et al.* Global prevalence of presbyopia and vision impairment from uncorrected presbyopia: Systematic review, meta-analysis, and modelling. *Ophthalmology* **125**, 1492–1499 (2018).
2. Charman, W. N. Developments in the correction of presbyopia i: Spectacle and contact lenses. *Ophthal. Physiol. Opt.* **34**, 8–29 (2014).
3. Letocha, C. E. The invention and early manufacture of bifocals. *Surv. Ophthalmol.* **35**, 226–235 (1990).
4. Pope, D. R. Progressive addition lenses: History, design, wearer satisfaction and trends. In *Vision science and its applications*, NW9 (Optica Publishing Group, 2000).
5. Sullivan, C. M. & Fowler, C. W. Progressive addition and variables focus lenses: A review. *Ophthal. Physiol. Opt.* **8**, 402–414 (1988).
6. Minkwitz, G. Über den flächenastigmatismus bei gewissen symmetrischen asphären. *Opt. Acta Int. J. Opt.* **10**, 223–227 (1963).
7. Sheedy, J. E., Campbell, C., King-Smith, E. & Hayes, J. R. Progressive powered lenses: The Minkwitz theorem. *Optometry Vis. Sci.* **82**, 916–922 (2005).
8. Meister, D. J. & Fisher, S. W. Progress in the spectacle correction of presbyopia. Part 1: Design and development of progressive lenses. *Clin. Exp. Optomet.* **91**, 240–250 (2008).
9. Sauer, Y. *et al.* Self-motion illusions from distorted optic flow in multifocal glasses. *Iscience* **25**, 103567 (2022).
10. Johnson, L., Buckley, J. G., Scally, A. J. & Elliott, D. B. Multifocal spectacles increase variability in toe clearance and risk of tripping in the elderly. *Investig. Ophthalmol. Vis. Sci.* **48**, 1466–1471 (2007).
11. Alvarez, T. L. *et al.* Adaptation to progressive lenses by presbyopes. in *2009 4th International IEEE/EMBS Conference on Neural Engineering*, 143–146 (IEEE, 2009).
12. Jalie, M. Modern spectacle lens design. *Clin. Exp. Optom.* **103**, 3–10 (2020).
13. Marin, G., Terrenoire, E. & Hernandez, M. Compared distortion effects between real and virtual ophthalmic lenses with a simulator. in *Proceedings of the 2008 ACM Symposium on Virtual Reality Software and Technology*, VRST '08, 271-272 (Association for Computing Machinery, New York, NY, USA, 2008).
14. Rodríguez Celaya, J. A., Brunet Crosa, P., Ezquerra, N. & Palomar, J. A virtual reality approach to progressive lenses simulation. in *XV Congreso Espanol de Informatica Grafica* (2005).

15. Nießner, M., Sturm, R. & Greiner, G. Real-time simulation and visualization of human vision through eyeglasses on the gpu. in *Proceedings of the 11th ACM SIGGRAPH International Conference on Virtual-Reality Continuum and its Applications in Industry*, 195–202 (2012).
16. Barbero, S. & Portilla, J. Simulating real-world scenes viewed through ophthalmic lenses. *J. Opt. Soc. Am. A* **34**, 1301–1308 (2017).
17. Haghiri, S., Wichmann, F. A. & von Luxburg, U. Estimation of perceptual scales using ordinal embedding. *J. Vis.* **20**, 14 (2020).
18. Watson, A. *Digital Images and Human Vision* (Bradford Bks (MIT Press), 1993).
19. Charrier, C., Maloney, L. T., Cherifi, H. & Knoblauch, K. Maximum likelihood difference scaling of image quality in compression-degraded images. *J. Opt. Soc. Am. A* **24**, 3418 (2007).
20. Ponomarenko, N. *et al.* Tid 2008-a database for evaluation of full-reference visual quality assessment metrics. *Adv. Mod. Radioelectron.* **10**, 30–45 (2009).
21. Chandler, D. M. Seven challenges in image quality assessment: Past, present, and future research. *ISRN Signal Process.* **2013**, 1–53 (2013).
22. Koenderink, J., Valsecchi, M., van Doorn, A., Wagemans, J. & Gegenfurtner, K. Eidolons: Novel stimuli for vision research. *J. Vis.* **17**, 7–7 (2017).
23. Sauer, Y., Wahl, S. & Rifai, K. Parallel adaptation to spatially distinct distortions. *Front. Psychol.* **11**, 544867 (2020).
24. Brunswik, E. Representative design and probabilistic theory in a functional psychology. *Psychol. Rev.* **62**, 193–217 (1955).
25. Rojo, P., Royo, S., Ramírez, J. & Madariaga, I. Numerical implementation of generalized Coddington equations for ophthalmic lens design. *J. Mod. Opt.* **61**, 204–214 (2014).
26. Sitole, S. P., LaPre, A. K. & Sup, F. C. Application and evaluation of lighthouse technology for precision motion capture. *IEEE Sens. J.* **20**, 8576–8585 (2020).
27. Terada, Y. & Luxburg, U. Local ordinal embedding. In *International Conference on Machine Learning*. pp 847–855 (2014).
28. Künstle, D.-E., von Luxburg, U. & Wichmann, F. A. Estimating the perceived dimension of psychophysical stimuli using a triplet accuracy and hypothesis testing procedure. *J. Vis.* **22**, 5 (2022).
29. Gower, J. C. Generalized procrustes analysis. *Psychometrika* **40**, 33–51 (1975).
30. Breiman, L. Random forests. *Mach. Learn.* **45**, 5–32 (2001).
31. Sauer, Y., Wahl, S., Habtegiorgis, S. W. Realtime blur simulation of varifocal spectacle lenses in virtual reality. In SIGGRAPH Asia. in *Technical Communications, SA '22 (Association for Computing Machinery* 2022 (New York, NY, USA, 2022).
32. Rifai, K. & Wahl, S. Specific eye-head coordination enhances vision in progressive lens wearers. *J. Vis.* **16**, 5–5 (2016).
33. Hutchings, N., Irving, E. L., Jung, N., Dowling, L. M. & Wells, K. A. Eye and head movement alterations in naïve progressive addition lens wearers. *Ophthalmic Physiol. Opt.* **27**, 142–153 (2007).

Acknowledgements

Funded by the Deutsche Forschungsgemeinschaft (DFG, German Research Foundation) under Germany"s Excellence Strategy - EXC number 2064/1 - Project number 390727645. This work was supported by the German Federal Ministry of Education and Research (BMBF): Tübingen AI Center, FKZ: 01IS18039A, and by the Open Access Publishing Fund of the University of Tübingen. The authors thank Carl Zeiss Vision International GmbH for providing the PAL distortion data used in the study and the International Max Planck Research School for Intelligent Systems (IMPRS-IS) for supporting David-Elias Künstle. Preliminary parts of this work have been presented as a poster at the Annual Meeting of the Vision Science Society 2023.

Author contributions

All authors contributed to the idea and design of the study. Y.S. implemented the VR experiment and performed the data collection. D.K. implemented the ordinal embedding analysis tool. F.W. and S.W. were involved in planning and supervising the work. Y.S. and D.K. together analyzed the data and took the lead in writing the manuscript. All authors were involved in the interpretation of results and contribution to the manuscript.

Funding

Open Access funding enabled and organized by Projekt DEAL.

Competing interests

The study was part of the industry-on-campus cooperation between the University of Tübingen and Carl Zeiss Vision International GmbH. Two authors, Yannick Sauer and Siegfried Wahl, are Carl Zeiss Vision International GmbH employees. All other authors declare that they do not have any competing interests.

Additional information

Supplementary Information The online version contains supplementary material available at https://doi.org/10.1038/s41598-024-54368-3.

Correspondence and requests for materials should be addressed to Y.S. or D.-E.K.

Supplementary Material

An objective measurement approach to quantify the perceived distortions of spectacle lenses

Yannick Sauer[1], David-Elias Künstle[2], Felix A. Wichmann[3], and Siegfried Wahl[4]

[1,2,3,4]University of Tübingen
[1,4]Carl Zeiss Vision International GmbH
[2]Tübingen AI Center
[1,2]These authors contributed equally to this work.

A Individual subject data

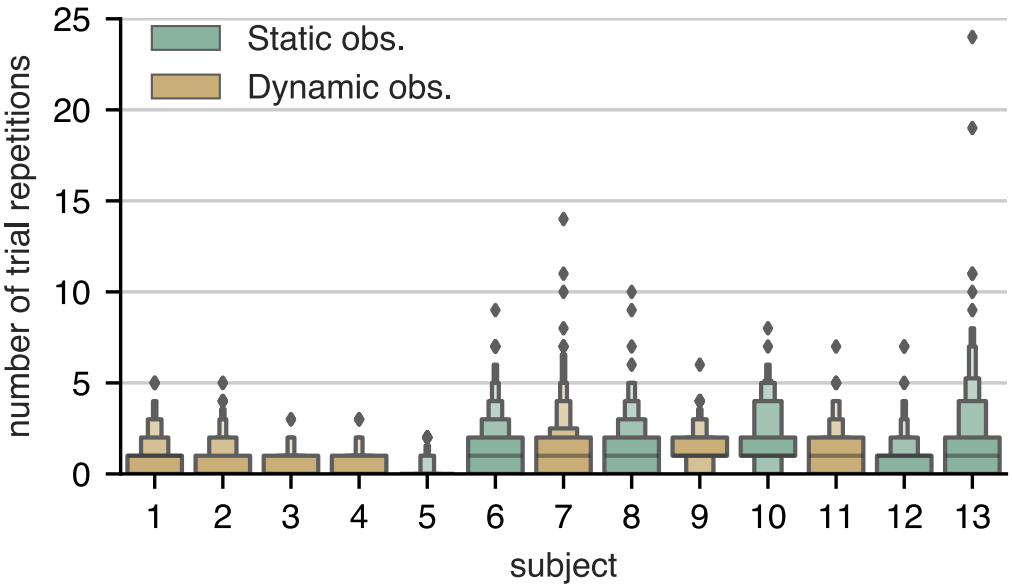

Figure S1: Individual distributions of number of repeated trials per subject.

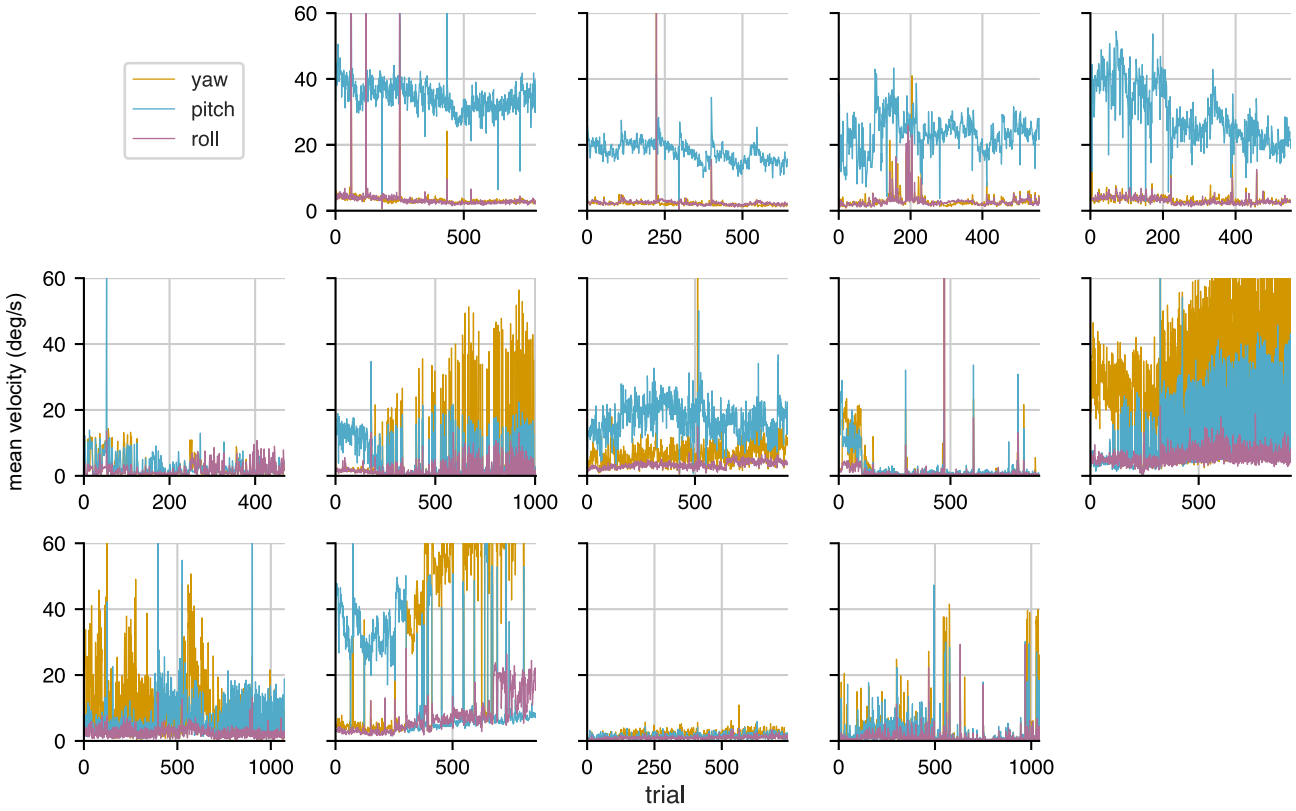

Figure S2: Individual head-movement components for each subject over all trials.

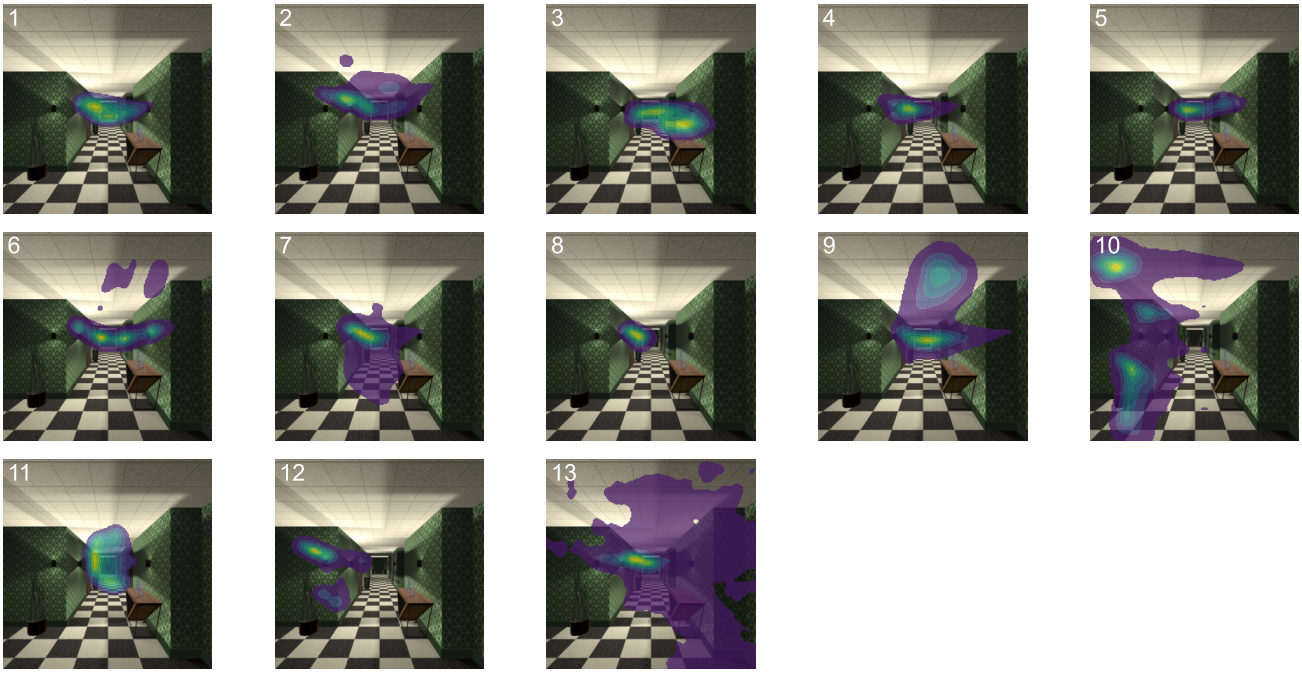

Figure S3: Individual gaze distribution in the scene. The gaze target in the 3D scene is determined by head position and gaze direction. During runtime, the intersection point of the binocular gaze vector and the 3D environment was calculated using a ray cast originating at the headset position. Those 3D points were recorded additionally to all gaze vector samples. From the 3D points we can analyse the 3D gaze distribution in the scene. For visualization, an image of the scene from a fixed viewpoint (the seating position of subjects in the scene) is overlayed with the 3D gaze samples mapped into the scene for the defined viewpoint and smoothed using a Gaussian kernel.

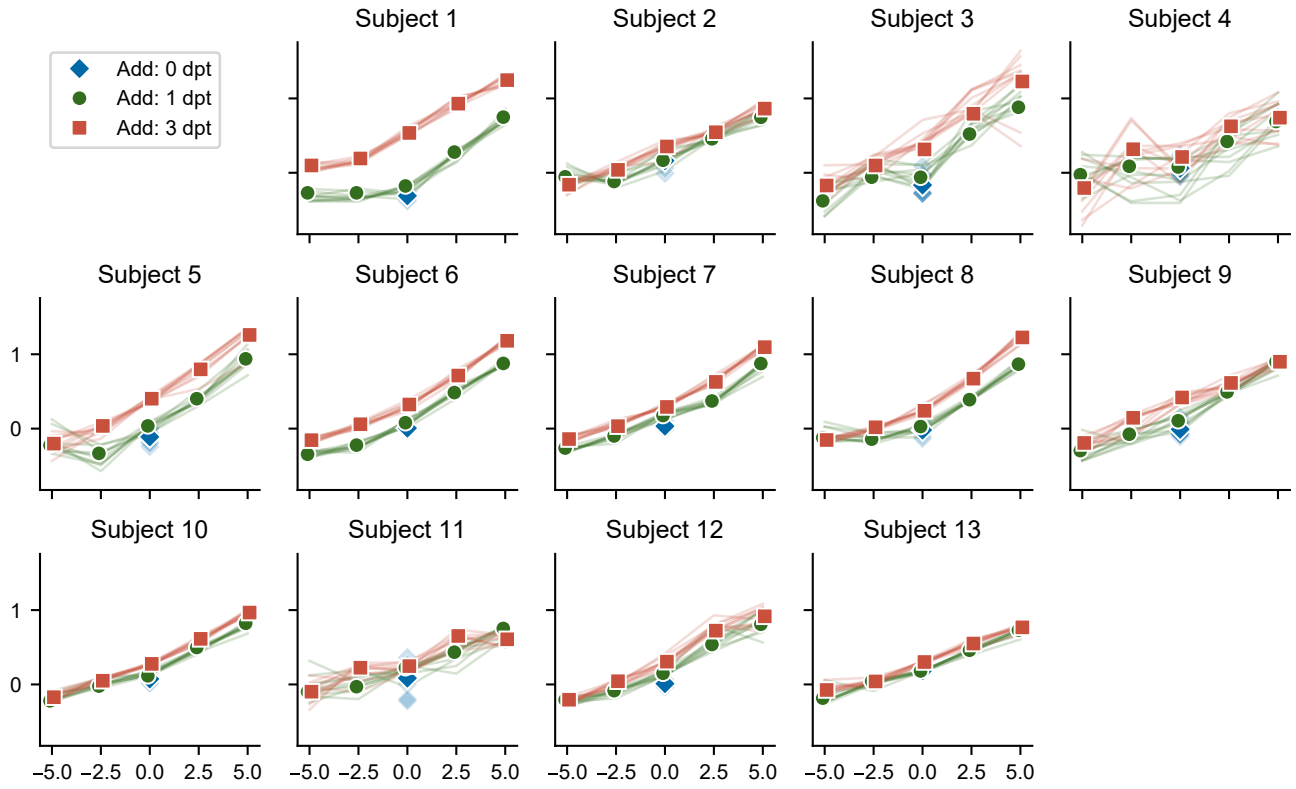

Figure S4: Scales per subject (opaque markers) with bootstrapped variants (transparent markers and lines). The bootstrapped variants are scale estimates based not on all triplets but a random subset of 95% to increase variability. These resamples ought to test the stability of the estimate by simulating how much the scale estimates would change if different triplet questions were asked. For most subjects, these bootstrapped scales are very close to the scale of all triplets, indicating that collecting additional trials would not substantially change the estimate.

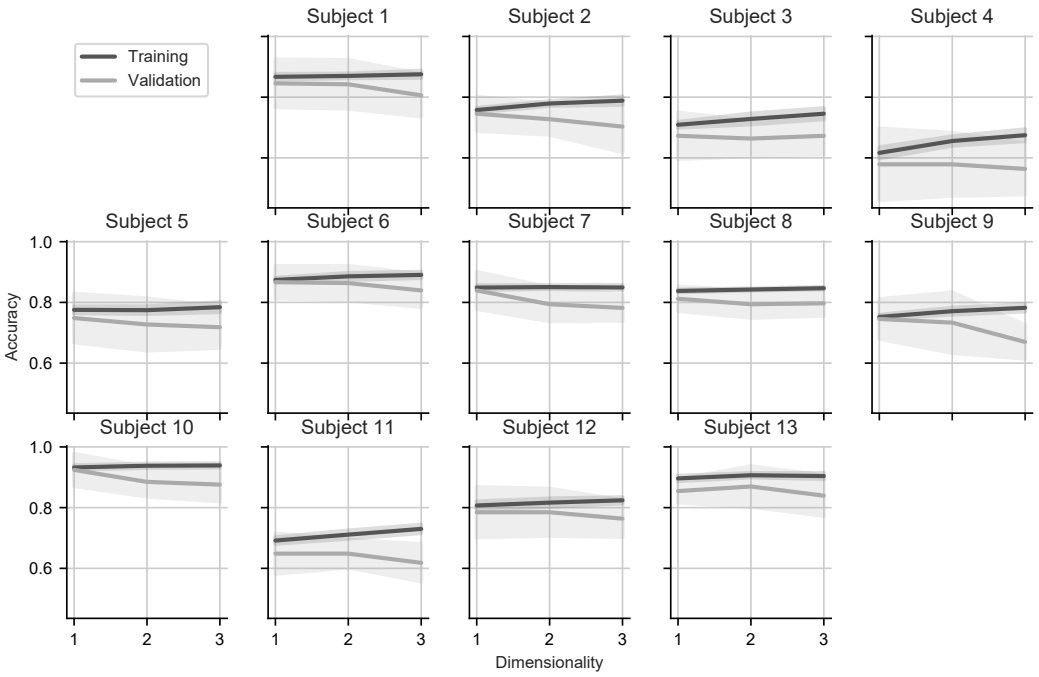

Figure S5: Embedding accuracy depending on embedding dimensionality. Accuracy is the proportion of trials where the response can be predicted from the scale, which was fitted with different dimensionality. The embedding accuracies for all subjects do not increase with the dimensionality, which indicates that a 1D scale already fits the responses sufficiently.
The line and bands show the accuracy mean and standard deviation of 10 so-called cross-validation splits, where the scale was fitted on 90% of the trials ("Training") and validated on the remaining 10% trials. The accuracy of the validation trials ought to approximate the predictive performance for unseen responses. Additionally, the validation accuracy can be understood as an indicator of how consistently subjects respond—subjects 4 and 11 show more inconsistencies than the others.

B Stimuli

Figure S6: Virtual indoor environment used for the psychophysical experiment in the game engine Unity.

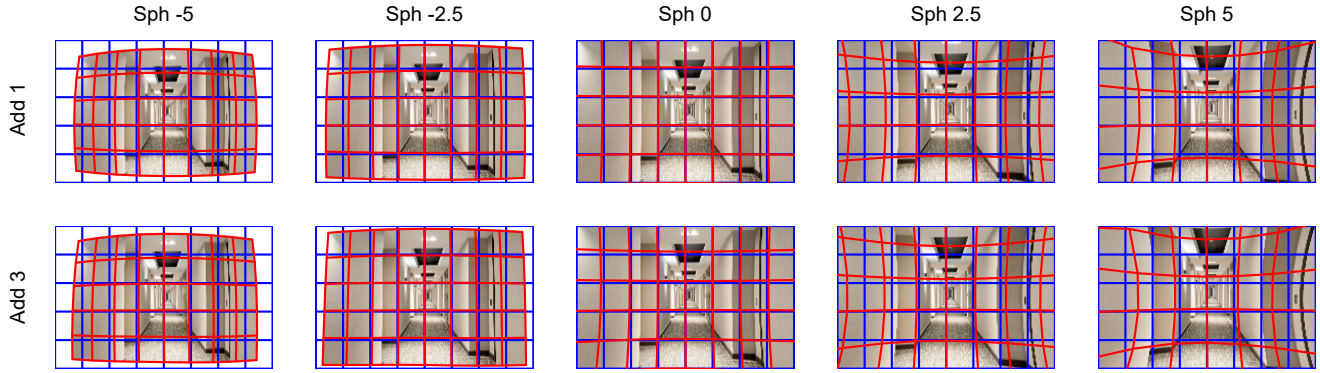

Figure S7: Overview of all ten distortions used in the experiment. The far correction power *Sph* varied between −5 dpt to 5 dpt and the additional power for near vision was 1 dpt or 3 dpt.